

University of Windsor

Scholarship at UWindor

Electronic Theses and Dissertations

Theses, Dissertations, and Major Papers

2009

Effect of one and two stiffeners on residual stresses of ship hull

Sara Kenno
University of Windsor

Follow this and additional works at: <https://scholar.uwindsor.ca/etd>

Recommended Citation

Kenno, Sara, "Effect of one and two stiffeners on residual stresses of ship hull" (2009). *Electronic Theses and Dissertations*. 8098.

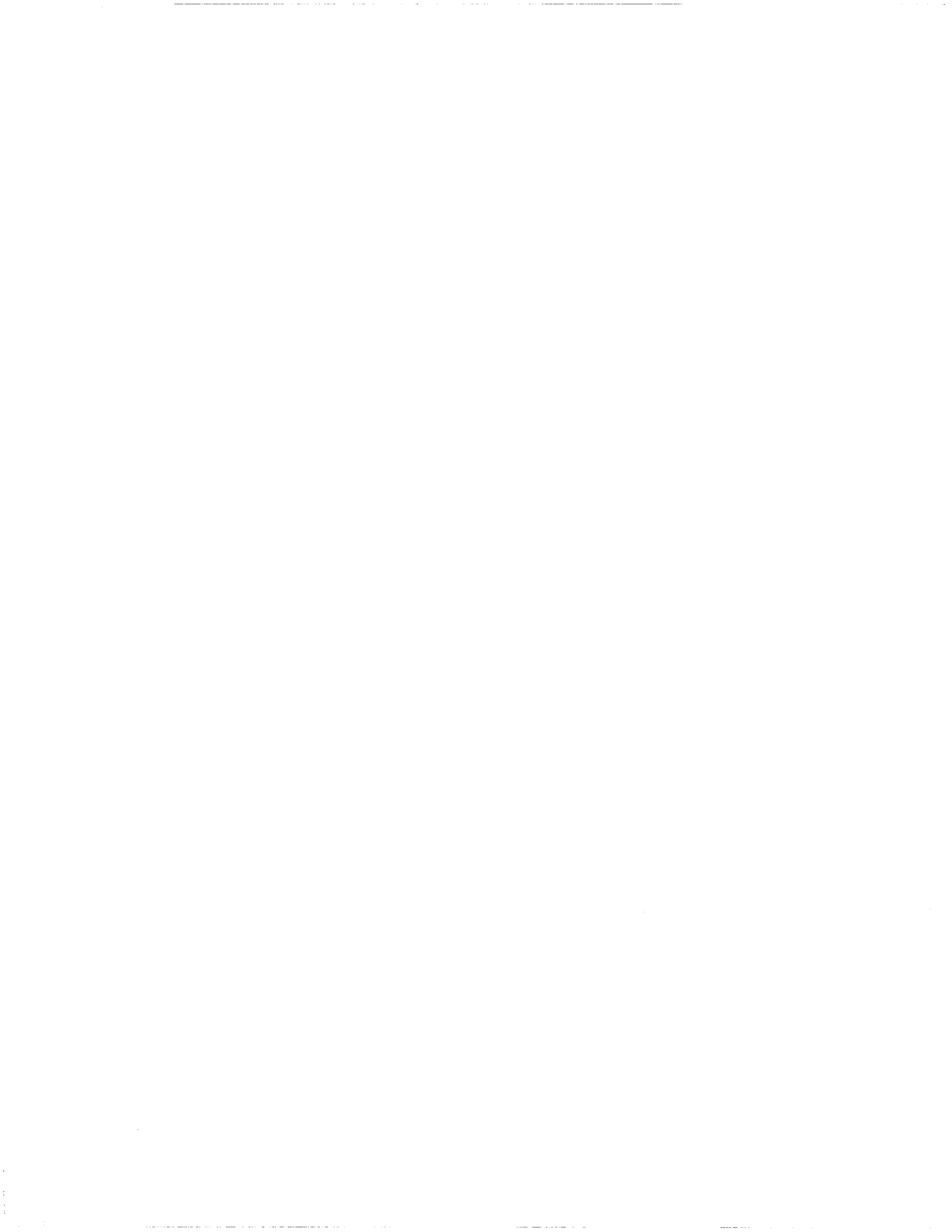
<https://scholar.uwindsor.ca/etd/8098>

This online database contains the full-text of PhD dissertations and Masters' theses of University of Windsor students from 1954 forward. These documents are made available for personal study and research purposes only, in accordance with the Canadian Copyright Act and the Creative Commons license—CC BY-NC-ND (Attribution, Non-Commercial, No Derivative Works). Under this license, works must always be attributed to the copyright holder (original author), cannot be used for any commercial purposes, and may not be altered. Any other use would require the permission of the copyright holder. Students may inquire about withdrawing their dissertation and/or thesis from this database. For additional inquiries, please contact the repository administrator via email (scholarship@uwindsor.ca) or by telephone at 519-253-3000ext. 3208.

NOTE TO USERS

This reproduction is the best copy available.

UMI



Effect of One and Two Stiffeners on Residual Stresses of Ship Hull

by

Sara Kenno

A Thesis

Submitted to the Faculty of Graduate Studies
through Civil and Environmental Engineering
in Partial Fulfillment of the Requirements for
the *Degree of Master of Applied Science* at the

University of Windsor

Windsor, Ontario, Canada

2009

© 2009 Sara Kenno



Library and Archives
Canada

Published Heritage
Branch

395 Wellington Street
Ottawa ON K1A 0N4
Canada

Bibliothèque et
Archives Canada

Direction du
Patrimoine de l'édition

395, rue Wellington
Ottawa ON K1A 0N4
Canada

Your file *Votre référence*
ISBN: 978-0-494-57581-9
Our file *Notre référence*
ISBN: 978-0-494-57581-9

NOTICE:

The author has granted a non-exclusive license allowing Library and Archives Canada to reproduce, publish, archive, preserve, conserve, communicate to the public by telecommunication or on the Internet, loan, distribute and sell theses worldwide, for commercial or non-commercial purposes, in microform, paper, electronic and/or any other formats.

The author retains copyright ownership and moral rights in this thesis. Neither the thesis nor substantial extracts from it may be printed or otherwise reproduced without the author's permission.

In compliance with the Canadian Privacy Act some supporting forms may have been removed from this thesis.

While these forms may be included in the document page count, their removal does not represent any loss of content from the thesis.

AVIS:

L'auteur a accordé une licence non exclusive permettant à la Bibliothèque et Archives Canada de reproduire, publier, archiver, sauvegarder, conserver, transmettre au public par télécommunication ou par l'Internet, prêter, distribuer et vendre des thèses partout dans le monde, à des fins commerciales ou autres, sur support microforme, papier, électronique et/ou autres formats.

L'auteur conserve la propriété du droit d'auteur et des droits moraux qui protègent cette thèse. Ni la thèse ni des extraits substantiels de celle-ci ne doivent être imprimés ou autrement reproduits sans son autorisation.

Conformément à la loi canadienne sur la protection de la vie privée, quelques formulaires secondaires ont été enlevés de cette thèse.

Bien que ces formulaires aient inclus dans la pagination, il n'y aura aucun contenu manquant.


Canada

AUTHOR'S DECLARATION OF ORIGINALITY

I hereby certify that I am the sole author of this thesis and that no part of this thesis has been published or submitted for publication.

I certify that, to the best of my knowledge, my thesis does not infringe upon anyone's copyright nor violate any proprietary rights and that any ideas, techniques, quotations, or any other material from the work of other people included in my thesis, published or otherwise, are fully acknowledged in accordance with the standard referencing practices. Furthermore, to the extent that I have included copyrighted material that surpasses the bounds of fair dealing within the meaning of the Canada Copyright Act, I certify that I have obtained a written permission from the copyright owner(s) to include such material(s) in my thesis and have included copies of such copyright clearances to my appendix.

I declare that this is a true copy of my thesis, including any final revisions, as approved by my thesis committee and the Graduate Studies office, and that this thesis has not been submitted for a higher degree to any other University or Institution.

ABSTRACT

Failure of ship hulls may be a result of a combination of factors. Residual stress caused by welding of the stiffeners on to the steel plates is one of the contributing factors to the failure. This analysis was completed for a more in-depth look at the residual stress distribution found at a typical weld-stiffener connection of ship hulls. Three specimens were built to represent small segments of an actual ship hull. The sizing of the specimens was designed so they could be accommodated at the test facility available at the Canadian Neutron Beam Centre in the Chalk River Laboratories. The specimens were made out of 9.53 mm thick plate of 350 WT grade structural steel stiffened by L127x76.2x9.53 stiffeners. The non-destructive neutron diffraction method was used to collect strain data at locations within the volume of the specimens. The method of neutron diffraction uses the crystal lattice of the sample material as an internal strain gauge. The test results were analyzed to determine the distribution of the residual stress in the parent steel plate and the effect the welding of the stiffeners has on the residual stress field. This thesis presents the three-dimensional residual stress for the parent plate and specimens with one and two stiffeners obtained from this study.

DEDICATION

To my wonderful Parents, Sisters, and Ryan

ACKNOWLEDGEMENTS

I would like to express my gratitude to all those who gave me the opportunity to complete this thesis. I am deeply indebted to my supervisor, Dr. S. Das, whose help, stimulating suggestions, and encouragement helped me during my research and the writing of this thesis. I would like to thank my co-advisor, Dr. J. B. Kennedy, for his guidance and support. Many thanks to my thesis committee members, Dr. M.K.S. Madugula, Dr. N. Kar, and Dr. James Huang for their collaboration and direction.

I want to especially thank Dr. David Stredulinsky and the Department of National Defence for giving me approval and direction to commence this thesis and to complete the research with the guidance on welding and ship structures.

I would like to thank everyone at the Canadian Neutron Beam Centre in the Chalk River Laboratories for their expertise and assistance with this experiment. I would especially like to thank Dr. Ronald Rogge, Dr. Michael Gharghour, Mr. Ronald Donaberger, and Mr. John Fox for their help and extreme patience while I was completing my experiments.

Thanks to my parents who always encourage everything I do, especially school endeavours. Thanks to my sisters who keep me sane and are always there backing me. And to Ryan who always wants what is best for me and supports me in so many ways.

TABLE OF CONTENTS

Author's Declaration of Originality	iii
Abstract	iv
Dedication	v
Acknowledgements	vi
List of Tables	ix
List of Figures	x
1 Introduction	1
1.1 General	1
1.2 Residual Stress	1
1.3 Residual Stress Tests	1
1.4 Methodology	2
1.5 Objectives	2
1.6 Organization	2
2 Literature Review	3
2.1 Introduction	3
2.2 Computer Modelling	4
2.3 Destructive Test Methods	5
2.4 Semi-destructive Test Methods	9
2.5 Non-Destructive Test Methods	15
2.6 Neutron Diffraction	20
2.7 Chalk River Laboratories, Atomic Energy of Canada Limited Facility	36
3 Material Properties and Welding Specifications	39
3.1 Material Properties	39
3.2 Mechanical Properties of Material	39

3.3	Welding Specifications	40
4	Test Method and Test Results	44
4.1	Test Matrix	44
4.2	Test Set-up	48
4.3	Stress-free Reference Samples and Nickel Calibration	50
4.4	Residual Stress Mapping	51
4.4.1	Neutron Diffraction Method	52
4.4.1.1	Specimen 1	53
4.4.1.1.1	Normal Stress for Specimen 1	53
4.4.1.1.2	Transverse Stress from Specimen 1	57
4.4.1.1.3	Longitudinal Stress from Specimen 1	60
4.4.1.2	Specimen 2	63
4.4.1.2.1	Normal Stress for Specimen 2	64
4.4.1.2.2	Transverse Stress for Specimen 2	67
4.4.1.2.3	Longitudinal Stress for Specimen 2	69
4.4.1.3	Specimen 3	74
4.4.1.3.1	Normal Stress for Specimen 3	76
4.4.1.3.2	Transverse Stress for Specimen 3	77
4.4.1.3.3	Longitudinal Stress for Specimen 3	79
5	Summary and Conclusions	82
5.1	Future Work	83
	Appendix A – Raw Data and Checks	84
	Appendix B - Permissions	87
	References	102
	Vita Auctoris	107

LIST OF TABLES

Table 3-A: Chemical Composition of Material	42
Table 3-B: Mechanical Properties of Material	42
Table 3-C: Welding Specifications	43
Table 4-A: Test Matrix	44
Table 4-B: Set-up Specifications	50
Table 0-A : Sample of raw data from computer	86

LIST OF FIGURES

Figure 2.1: FE representation of the specimen (Hu, et al., 1998)	6
Figure 2.2: Residual stress distribution obtained from tests (a) Distance from edge of plate (mm) vs Stress at plate (MPa); (b) Distance from edge of flange (mm) vs Stress at flange (MPa); (c) Distance from junction of plate and web (mm) vs Stress at web (MPa) (Hu, et al., 1998)	7
Figure 2.3: The stress maps measured with the contour method and neutron diffraction (Prime, et al., 2004)	9
Figure 2.4: Comparison of experimental and simulation residual stresses (Cho, et al., 2004)	12
Figure 2.5: Residual stresses in the welded specimens (Weng, et al., 1992)	14
Figure 2.6: Surface residual stress distributions of (a) RS1 – 1.4 kJ/mm, no restraint, (b) RS2 – 1.4 kJ/mm, with restraint, (c) RS3 – 1.7 kJ/mm, no restraint (Gao, et al. 1997)	17
Figure 2.7: Test specimen with a typical crack and residual stress distribution (Rörup, 2005)	18
Figure 2.8: Analysis of the weld-induced residual stresses in the longitudinal direction (Rörup, 2005)	19
Figure 2.9: Lattice spacing with incident (ki) and refracted (kf) beam (Hutchings, et al., 2005)	21
Figure 2.10: Lattice planes (Hutchings, et al., 2005)	21
Figure 2.11: Cross-sectional (Y-Z) details of the multipass weld runs used to make the butt joints in the 8mm and 12mm thick plates of RQT701 steel - (a) 8 mm plate thickness with low heat input (1 kJ/mm), (b) 8 mm plate thickness with high heat input (3 kJ/mm), (c) 12 mm plate thickness with low heat input, and (d) 12 mm plate thickness with high heat input (James, et al., 2006)	25
Figure 2.12: Specimen - 12 mm thick, overmatched weld metal at low heat input 1 kJ/mm (a) Longitudinal (x) stress profile at four depths (b) Transverse (y) stress profile at	

four depths (c) Through-thickness (z) stress profile at four depths (James, et al., 2006)	26
Figure 2.13: Pseudo-strain measured by ND and SD across the weld, (PM = parent material, HAZ = heat affected zone, WM, weld material) (Paradowska, et al., 2006)	27
Figure 2.14: Pseudo-strain measured by ND and SD through the thickness (Paradowska, et al., 2006)	27
Figure 2.15: Location of deep-hole drilling measurements on the 100 mm thick plate specimen (Wimpory, et al., 2003)	29
Figure 2.16: Transverse stresses in the 100 mm T-plate - ND measurement on a 12.5 mm slice and DHD measurement (Wimpory, et al., 2003)	30
Figure 2.17: Longitudinal stresses in the 100 mm T-plate obtained by ND on a 12.5 mm slice and by DHD (Wimpory, et al., 2003)	30
Figure 2.18: Three-dimensional stresses 10mm from surface of side B—flat butt weld (Pearce, et al., 2006)	31
Figure 2.19: The direction of the measurements (transverse x, normal y, longitudinal would be z) using neutron diffraction on the single bead-on-plate (Price, et al., 2006)	32
Figure 2.20: Change in stress in fully restrained specimen in comparison to unrestrained specimen (Price, et al., 2006)	33
Figure 2.21: Longitudinal stress derived from measurements of {110}, {002} and {112} reflections in the high strength steel SNC631 as a function of position through the weld (Holden, et al., 2006)	35
Figure 2.22: Centerline longitudinal strain measured in the two as-welded 12-mm-thick plates using neutrons and synchrotron X-rays (Ganguly, et al., 2006)	36
Figure 2.23: Layout of the Chalk River Laboratories (Canada, 2008)	37
Figure 2.24: L3 Spectrometer at Chalk River Laboratories (Canada, 2008)	38
Figure 3.1: Material samples for metallurgical testing	40
Figure 3.2: Stress-Strain Curve	41
Figure 4.1: Specimen 1 (a) Photo (b) Sketch	45

Figure 4.2: Specimen 2 (a) Photo (b) Sketch	46
Figure 4.3: Specimen 3 (a) Photo (b) Sketch	47
Figure 4.4: Tilted telescope aligned to y-centre	49
Figure 4.5: Level telescope aligned to x-centre	49
Figure 4.6: Stress-free reference samples	51
Figure 4.7: Nickel-reference sample in cadmium container	52
Figure 4.8: Detail for measurement points for Specimen 1	53
Figure 4.9: Normal stress at various depths in transverse (T or Y) direction (line 1-2)	55
Figure 4.10: Normal stress at various depths in longitudinal (L or Z) direction (line 1-3)	55
Figure 4.11: 3-D view of normal stress distribution in transverse (T or Y) direction	56
Figure 4.12: 3-D view of normal stress distribution in longitudinal (L or Z) direction	56
Figure 4.13: Transverse stress at various depths in transverse (T or Y) direction (line 1-2)	58
Figure 4.14: Transverse stress at various depths in longitudinal (L or Z) direction (line 1-3)	59
Figure 4.15: 3-D view of transverse stress distribution in transverse (T or Y) direction (line 1-2)	59
Figure 4.16: 3-D view of transverse stress distribution in longitudinal (L or Z) direction (line 1-3)	60
Figure 4.17: Longitudinal stress at various depths in transverse (T or Y) direction (line 1-2)	61
Figure 4.18: Longitudinal stress through depth in longitudinal (L or Z) direction (line 1-3)	62
Figure 4.19: 3-D view of transverse stress distribution in transverse (T or Y) direction (line 1-2)	62
Figure 4.20: 3-D view of transverse stress distribution in longitudinal (L or Z) direction (line 1-3)	63
Figure 4.21: Detail for measurement points for Specimen 2	64

Figure 4.22: Measurement spacing in the transverse direction (mm)	65
Figure 4.23: Normal stress at various depths in transverse (T or Y) direction (at $z = 0$ mm, line 3-4)	66
Figure 4.24: Normal stress at various depths in transverse (T or Y) direction (at $z = 133$ mm, line 5-6)	67
Figure 4.25: Transverse stress at various depths in transverse (T or Y) direction (at $z = 0$ mm, line 3-4)	68
Figure 4.26: Transverse stress at various depths in transverse (T or Y) direction (at $z=133$ mm, line 5-6)	69
Figure 4.27: Longitudinal stress at various depths in transverse (T or Y) direction (at $z = 0$ mm, line 3-4)	71
Figure 4.28: Longitudinal stress at various depths in transverse (T or Y) direction (at $z = 133$ mm, line 5-6)	71
Figure 4.29: 3-D view of longitudinal stress distribution in transverse (T or Y) direction (at $z = 0$ mm, line 3-4)	72
Figure 4.30: 3-D view of longitudinal stress distribution in transverse (T or Y) direction (at $z = 133$ mm, line 5-6)	72
Figure 4.31: All stresses @ Transverse=-10 mm, Normal = 8.9 mm (line 1-2)	73
Figure 4.32: Detail for measurement points in Specimen 3	74
Figure 4.33: Measurement spacing in the transverse direction (mm)	75
Figure 4.34: Normal Stress at various depths in transverse (T or Y) direction (line 2-1-3)	78
Figure 4.35: Transverse Stresses though the depth in transverse (T or Y) direction (line 2-1-3)	79
Figure 4.36: Longitudinal stress at various depths in transverse (T or Y) direction (line 2-1-3)	81
Figure 4.37: 3-D view of longitudinal stress distribution in transverse (T or Y) direction (line 2-1-3)	81

Figure 0.1: Integrated intensity check – good raw data	84
Figure 0.2: Full Width Half Maximum (FWHM) check – good raw data	84
Figure 0.3: Lattice strain check - good raw data	85
Figure 0.4: Example of good raw data with φ peak counts, $\varphi = -89.89^\circ$	85

1 Introduction

1.1 General

Failure of ship hulls is often a result of a combination of factors. Residual stress caused by welding of the stiffeners on to the steel plates is one of the contributing factors to the failure. This study was completed for a more in-depth look at the residual stress distribution found at a typical weld-stiffener connection of ship hulls. The results show the effect of one and two stiffeners and stop and start in the welding process on the residual stress distributions. Three specimens were built to represent small segments of an actual ship hull. The methods and practices used by ship builders have also been studied and followed in the preparation of the specimens.

1.2 Residual Stress

Residual stresses are a result of processes that either modify the shape of the metal or introduce a temperature gradient, such as welding. Welding produces residual stresses primarily due to the differences in the amount the weld metal shrinks as it cools and hardens to the ambient temperature. Welding often induces a steep gradient of residual stresses that are highly unpredictable due to many factors such as complex thermal profile, material behaviour, and joint configuration. In order to produce acceptable results, numerous locations on the specimen must be measured for strain. Once the strain components are collected the elastic strain equations are used to calculate the stress values. (Withers, et al., 2001)

1.3 Residual Stress Tests

There are numerous methods available for determining residual stresses. The methods available for testing can be broken down into the following categories: (i) computer modelling, (ii) destructive, (iii) semi-destructive, and (iv) non-destructive. These methods will be discussed in depth in Chapter 2.

1.4 Methodology

Three specimens were made to obtain detailed information on the residual stresses induced from the welding process of the stiffeners in a typical ship structure. The first specimen was a plain plate with no stiffeners. The second specimen had one stiffener welded on the parent plate. The third specimen had two stiffeners welded on the base plate, 250 mm on centre. All residual stress data collection was completed at the Canadian Neutron Beam Centre of the Chalk River Laboratory facilities in Chalk River, ON, Canada.

1.5 Objectives

The objectives of this study are as follows:

- To determine the residual stress distribution created in the parent plate from its manufacturing rolling process
- To determine the residual stress distribution in the parent plate induced by the welding process of welding one stiffener
- To determine the residual stress distribution caused by one stiffener on the welding of the subsequent (second) stiffener
- To determine the residual stress distribution caused by the stop and start of the welding process during a welding pass

1.6 Organization

Chapter 1 introduces the thesis by providing background information on the subject and the objectives of the thesis. Chapter 2 presents the literature review on the subject of residual stress testing methods and the work completed in this area to date. Chapter 3 organizes the information on the material used and the welding method and data. Chapter 4 presents the data and discusses the results found during testing. Chapter 5 provides a summary of the work completed and the recommendations and plans for upcoming research.

2 Literature Review

2.1 Introduction

Residual stresses are caused by thermomechanical processing of steel. These processes either alter the shape of the metal or induce a temperature gradient which generates residual stress. Processes that alter the physical shape include machining, forging, rolling, drawing, etc. The welding, casting, and quenching processes introduce a temperature gradient to the metal.

Residual stresses develop in welded structures primarily as the result of differences in the amount the weld metal shrinks as it cools and hardens to the surrounding temperature. Residual stresses are highly unpredictable and often non-uniform. The residual stress distribution will also change depending on the restrictions of the parent plate. In order to produce acceptable results, several locations on the specimen must be measured for strain, since a steep gradient in strain may be produced by residual stresses.

Residual stresses are usually calculated from the elastic strain values. The elastic strain measured is either the existing strain or the change in strain when residual stresses are released. The elastic strain values are converted to stress values using the elastic strain constants. Hooke's Law and Young's Modulus are applicable here when calculating the stress values. Residual stresses developed during the welding process are macrostresses (Type I) that are continuous from grain to grain and from phase to phase. (Hutchings, et al., 2005)

The method for measuring residual stress and the locations and number of measurements depend on the expected stress field. Preliminary tests may be required for a better estimate of the residual stress field. The chosen method also may depend on the nature of the specimen, for example, if the specimen is too large to move and measure in a laboratory, the measurements need to be carried out using portable measurement devices in the field.

A scaled version of the actual specimen may be used for determining the residual stress distribution. However, it must be large enough to avoid improper readings, when a

laboratory test method is chosen. Generally, the rule that is followed is that the length and width of the plate should be at least three times the plate thickness (Hutchings, et al., 2005).

There are various methods available for measuring the residual stresses. These methods are divided into three major categories: (i) destructive, (ii) semi-destructive, and (iii) non-destructive. Discrepancies exist among these different types of test methods. This is because a steep gradient of stress exists in the steel and because the test volume required for the different types of test methods vary as well.

The required test area or volume must be less than 1 mm^2 or 1 mm^3 , respectively, to produce an accurate image of the stress field. The peak stress values may be missed if the test areas are too large for the very sharp stress gradients. Thus, the test area or volume size must be optimized for the best data collection with the minimal number of measurements taken, to detect the peak stresses and their values. (Hutchings, et al., 2005)

The type of test chosen may produce different types of errors. These errors are due to material characteristics of the steel such as, crystallographic texture, phase composition, grain size, and plastic strain.

The following sections will outline a method of testing and discuss previous work completed using that method.

2.2 Computer Modelling

The residual stress distribution is also determined using numerical methods such as finite element (FE) method. ABAQUS (Simulia, 2008), which is a commercially available general purpose FE code, often used to determine the residual stress distribution in solids and structures (Prime, et al., 2004). ABAQUS can be used to model the behaviour of solids under externally applied loads and body forces, such as due to residual stress. ABAQUS is used for three-dimensional models subject to static and dynamic loading patterns. Other FE codes such as ADINA (Hu, et al., 1998) and ANSYS (Cho, et al., 2004) are also available and used for determining residual stresses.

2.3 Destructive Test Methods

Destructive test method is the most commonly used technique for determining residual stress distribution in steel structures. This is because the method is convenient and simple. Destructive methods are basically stress relaxation techniques, where the residual stress within a finite element (very small volume) is released and the change in strain is measured. As a result of destructive testing, the specimen becomes inoperative and therefore, there must be enough material to test and destroy.

Destructive tests produce optimal results when the nature of the stress field and the estimate for magnitude of stress gradient are known. The stress field determined can be triaxial, biaxial, or uniaxial producing a stress gradient that is three, two, or one-dimensional, respectively. The magnitude of the stress gradient affects the sample volume of residual stress measured along that gradient.

The most widely used form of destructive testing is the sectioning method. The sectioning method uses strain gauges to read the initial strain values. The material is then removed around the gauges and the final strain readings are taken. The strain due to residual stress in the metal is the difference between the initial and final strain values. The methods of removal include milling, sawing, grinding, drilling, and lathe turning. Numerous sections and readings may be taken however; assumptions must be made to factor in the stress previously released in the preceding sections. The method of metal removal can introduce high stress levels at the surface of the material and must be accounted for. The surface stresses introduced in this method can be minimized or even be removed by using electrochemical methods. Some metal removal methods reduce the residual stress by introducing heat which consequently anneals the specimen. Chemical or electrolytic polishing is one type of material removal sectioning processes that does not introduce additional residual stresses into the metal.

Recent interest has been in another form of destructive testing called the contour method. In this method, an electro-discharge machine cuts the severely restrained specimen using a flat cut. The specimen deforms across the cross-section as the residual stresses relax. The deviations of the contours are measured using laser scanning. The laser scanning results and

computer analysis determine the out-of-plane stresses. This method provides a two-dimensional stress field normal to the cut and is best used for measuring the longitudinal stress in a weld. The method is generally used when the stress levels are low and the specimens are smaller in overall size and cross-sectional area.

Hu and Jiang (1998) conducted laboratory tests to determine the ultimate strength of stiffened panels with varying amounts and types of damage. Then they compared the residual stress test results with the results obtained from nonlinear finite element analysis. The metal used in the specimens was hot-rolled 350 WT steel (CSA, 2004). The length of all the specimens was 2000 mm (Figure 2.1). The stiffeners were tee sections with flange dimensions of 103.9 mm x 8.1 mm and web dimensions of 136.8 mm x 6.2 mm. The base plate was 500 mm wide and 9.7 mm thick. Coupon test data indicted a yield strength of 425 MPa for the plate, 411 MPa for the web, and 395 MPa for the flange. The residual stresses were found in the longitudinal direction (Figure 2.1) using the sectioning method. Figure 2.2 shows the residual stress distributions obtained in the longitudinal direction.

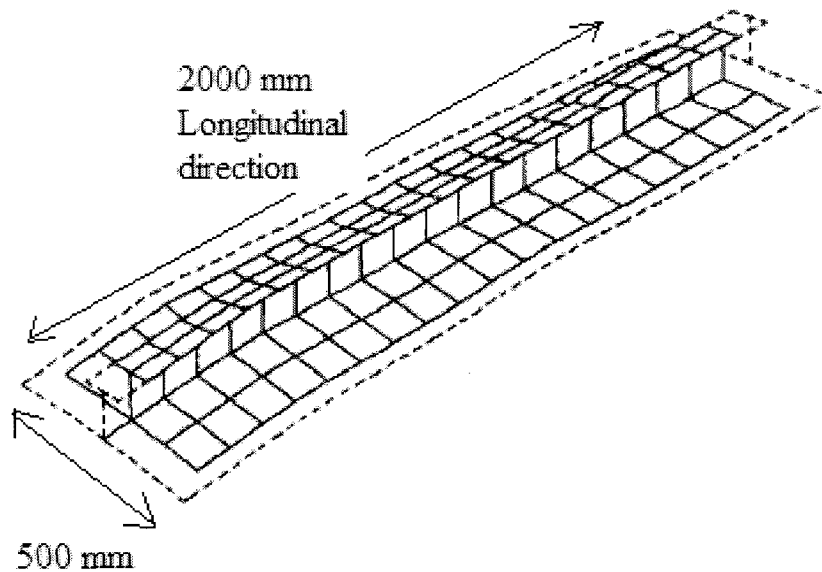


Figure 2.1: FE representation of the specimen (Hu, et al., 1998)

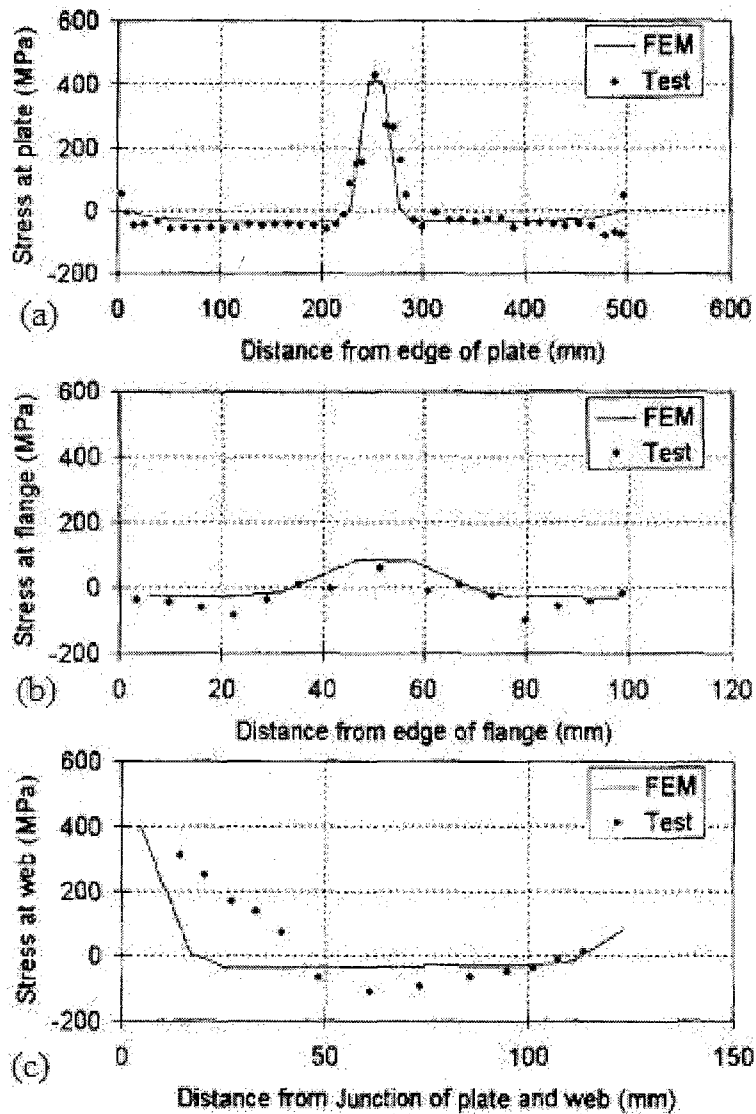


Figure 2.2: Residual stress distribution obtained from tests (a) Distance from edge of plate (mm) vs Stress at plate (MPa); (b) Distance from edge of flange (mm) vs Stress at flange (MPa); (c) Distance from junction of plate and web (mm) vs Stress at web (MPa) (Hu, et al., 1998)

The nonlinear finite element models were developed using code ADINA (ADINA R & D, 2008). A four-node quadrilateral shell element was used to simulate the plate and stiffeners. The residual stress due to welding was simulated using a thermal stress application. The FE models and the laboratory tests provided similar stress patterns. However, the magnitude varied since the actual welding processes were not as closely monitored. The longitudinal

stress values were tensile near the weld with a steep conversion to compressive stress away from the weld (Figure 2.2 (a)). The maximum value of stress was almost equal to the tensile yield stress of the metal. The results from the FE method and the physical tests are compared in Figure 2.2. The FE analysis indicated that the behaviour of a stiffened panel is greatly affected by the degree and location of the residual stresses from welding.

Prime et al. (2004) used the contour method with laser scanning to measure residual stresses normal to the cross-section that is, the longitudinal stress component of residual stresses. The specimens were ferritic steel BS 4360 grade 50D (ASTM, 2007) with minimum yield strength of 355 MPa. The plate was flame-cut to a size of 1000 mm x 150 mm x 12.5 mm with an 8 mm U-groove at the centre. A 12-pass weld was made in the groove using Tungsten Inert Gas (TIG) and metal active gas (MAG) wire for the welding process. The plate was clamped for all passes except the last two, resulting in a 7° bend in the plate from the weld line. The plate was then cut into 200 mm wide strips from the centre of the plate for testing. The 200 mm specimens were measured using the contour method and neutron diffraction. A comparison between two contour methods using the higher resolution non-contact laser surface contouring method and using the conventional touch probe machine, (typically using a Coordinate Measuring Machine (CMM)) were undertaken. The stress distribution from the contour methods were finally determined using FE code, ABAQUS. The results between the two contours methods showed a good agreement. However, higher resolution was possible with the laser scanning, which is the best choice for more moderate variations in stress profiles. They also used the neutron diffraction method to measure the stress distribution. The comparison between the neutron diffraction results and the contour methods showed a good agreement as well. The results obtained from the neutron diffraction method and the laser surface contouring method are shown in Figure 2.3.

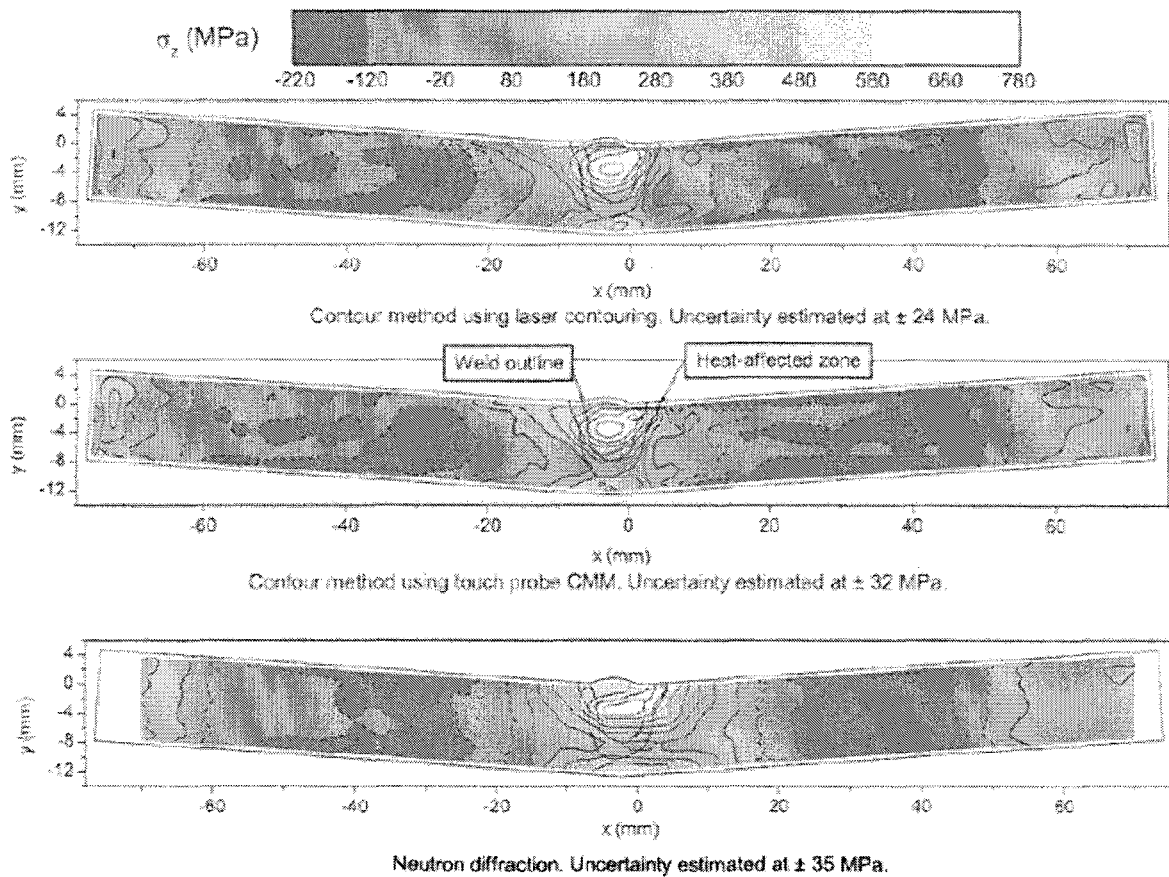


Figure 2.3: The stress maps measured with the contour method and neutron diffraction (Prime, et al., 2004)

2.4 Semi-destructive Test Methods

Semi-destructive test methods are commonly used when the integrity of the specimen need to be kept intact. Majority of the semi-destructive methods are stress relaxation techniques, similar to the destructive methods. These methods do not completely destroy the component but still inflict minimal damage to the surface of the specimen. Examples of semi-destructive test methods are: hole-drilling, ring coring, trepanning, indentation, and spot annealing methods.

The most commonly used semi-destructive method is the hole-drilling method which uses either shallow holes or deep holes. The method uses strain gauges to measure the change in the surface strain caused by residual stresses which are released when a hole is drilled in the surface. The remaining material then readjusts to reach equilibrium. Another method called

the ring coring method is similar to the hole-drilling method, except a ring is drilled around the strain gauge and a cylinder of metal is isolated around the gauge of strain-free material. The depth of the measurement in both methods is roughly equal to the diameter of the hole. The most accurate results are obtained at a depth of half the diameter. (Hutchings, et al., 2005)

Since the stress is assumed constant over the entire area, these methods should not be used where the stress gradient is high. Local plastic yielding occurs during the drilling process; therefore, areas where the stresses are greater than one-third the yield strength must be avoided. The drilling also causes strain hardening in the area around the hole and can cause an error of up to 70 MPa (10 ksi). The thickness of the measured specimen must be at least four times the hole diameter and the holes must be spaced at least eight times their diameter to obtain accurate results. (Totten, et al., 2002)

Wilken (1976) examined the use of the hole-drilling method in comparison with the splitting-up (sectioning) method. The hole-drilling method is a semi-destructive method and thus, useful for in-service structures. In comparison with the splitting-up method, the hole-drilling method was found to be much easier to apply and yielded similar results. However, the hole-drilling method requires the use of complicated mathematical computations and makes several assumptions which may be incorrect. The assumptions are:

1. The stress is uniform across the whole thickness of the sheet.
2. The plate is unlimited in all directions.
3. The validity of Hooke's law.
4. The constant nature of residual stresses in the region of the measuring point.
5. The avoidance of plastic deformation at the edge of the drilled hole, affected by placing the measuring sensor at a certain distance from it.

The accuracy of the hole-drilling method was first compared to the splitting up (sectioning) method on plated I-girders welded in various sequences. The results obtained from the two methods were considered accurate within reasonable error limits and proved the validity of

the hole-drilling method. Then hole-drilling experiments were carried out on the welds of the longitudinal frame of a ship. Compressive residual stresses were found in the webs and high tensile residual stresses were found in the flange near the weld. The ship was in service for 18 months and no cracks had developed at the time when the hole-drilling procedure was conducted. Since this research was conducted in the 70s, the use of finite element method was not common practice and thus, it was not used.

Several ships experienced catastrophic failures in the 1940s. Therefore, Meriam et al. (1946) conducted several tests on actual ship subassemblies to determine a method of measurement of residual stresses from welding. Strain gauges were used and holes were drilled around the gauge to remove the plug of metal containing the gauge. Two measurements were taken: (i) after the welding process and (ii) after the drilling. All strains measured were assumed to be elastic and elastic equations were used to convert the measured strain values to stress. Due to the nature of the equipment available at the time, the shortest length gauge was 6 mm (¼ in); consequently the steep nature of the stress near the weld was averaged over the area and precise values were not available. This method only allowed measurement of surface stresses and no stress measurements through the thickness of the plate were undertaken. All stresses were assumed as to average over the plate thickness, and therefore, remain constant through the thickness. The final results found using this method were satisfactory with an error of ± 13.8 MPa (± 2000 psi).

Cho et al. (2004) compared the residual stresses due to welding process and due to post-weld heat treatment using FE code, ANSYS (ANSYS, 2008), and the hole-drilling method. The type of metal used was SM400B (A131 Gr. 50) with a yield stress of 294.2 MPa, a Young's Modulus of 210.8 GPa, and a Poisson's ratio of 0.3, all at 20°C. A ten pass regular butt weld, a twelve pass K-type butt weld, and a nine pass V-type weld were analyzed using the FE method. The ten pass butt weld produced a minimum residual stress of -267 MPa (compression) and a maximum value of 333 MPa (tension). Following the post-weld heat treatment the maximum residual stress found was 38 MPa. The K-type weld produced a range of residual stresses from -300 MPa to 316 MPa which were reduced to a 39 MPa maximum following the heat treatment. The V-type weld produced a minimum residual stress of -239 MPa and a maximum value of 265 MPa, which were reduced to -34.2 and 30.7

MPa, respectively following the heat treatment. The welding process was simulated in ANSYS with the time for the heat transfer analysis for each weld pass as the total weld length (varies) divided by the welding velocity (20 cm/min). The hole-drilling method of measuring surface residual stresses was used on the butt weld and the results were consistent. A post-weld heat treatment was programmed for the K- and V-type welds and produced a significant drop (85%) in residual stress values. The results for the ten pass regular butt weld are compared in Figure 2.4.

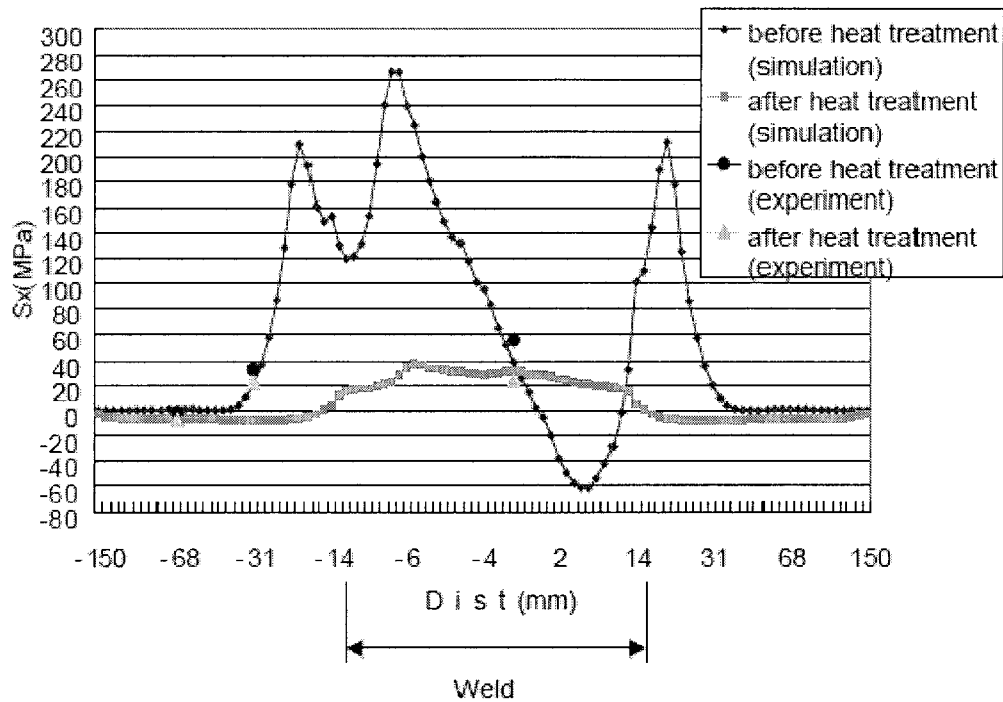


Figure 2.4: Comparison of experimental and simulation residual stresses (Cho, et al., 2004)

Somerville et al. (1977) measured distortions and residual stresses in stiffened panels. The panels were constructed of various sizes and welded with varying sizes and spacing of stiffeners. Two types of steel were used: mild steel (yield stress = 262 MN/m² or 262 MPa) and 'B' quality steel (yield stress = 355 MPa). They studied the contraction of the stiffener weld as it cools and the compressive stresses that develop in the plate. They measured surface strains using dial gauges. The stiffeners caused limited or no access to some areas. Thus, modifications in measurement techniques were made using indents instead of drilled

holes. The results of these tests provided a very rough estimate of the residual stress field and the distortion effects. The lack of equipment available at the time of testing provides little correlation with the results achieved from more recent experiments.

Weng and Lo (1992) used the hole-drilling method of ASTM E837 (ASTM, 2008) to measure the residual stresses in welded structures and compared the results to those found using the sectioning method. Since hole-drilling creates local plasticity due to stress concentration in the metal, calibration tests were performed to determine calibration coefficients. The ASTM E837 method provides calibration coefficients but only when stress values are less than 50% of the yield stress. Twelve specimens were produced using A36 and A572 grade 50 structural steel (ASTM, 2007) plates of thicknesses 15 mm and 32 mm. Residual stresses were measured in three different types of joints: butt, tee, and corner. The welding was completed using the submerged arc welding (SAW) method. The diameter of the drill used was 1.57 mm, and the maximum depth of the hole is 1.2 times the diameter, as specified in ASTM E837, roughly equal to 1.88 mm. The hole-drilling method, therefore, could only measure surface stresses and not the internal stresses. Also, due to the nature of the strain gauges and hole-drilling technique, the residual stresses were measured only to the edge of the weld and the stresses within in the weld and welded part could not be measured. The residual stress near the weld was found to be from 84% to 100% (312 MPa to 377 MPa) of the yield stress and therefore, required the recalculated calibration coefficients for the local plasticity from drilling the holes. For surface stress measurements, the hole-drilling method was found to have similar results to those found using the sectioning method. The results are shown in Figure 2.5, and each graph contains a diagram of the specimen and testing axes. The results are plotted by distance from welded edge (mm) versus the residual stress (MN/m^2). Figure 2.5 (a) shows the residual stress values found in both the x-direction (transverse) and y-direction (longitudinal) of the butt-welded joint. The longitudinal stress distribution on the butt-welded joint shows a tensile stress peak at the weld and at the edge of the plate. Figure 2.5 (b) shows the residual stress values (MN/m^2) for the tee joint plotted against the distance from the welded edge (mm). The stress distribution was calculated at various depths (A, B, C, D, E) and in both the x-direction (transverse) and y-direction (longitudinal). Figure 2.5 (c) shows the residual stress in the x-direction (transverse) and y-direction (longitudinal) on the corner welded plate.

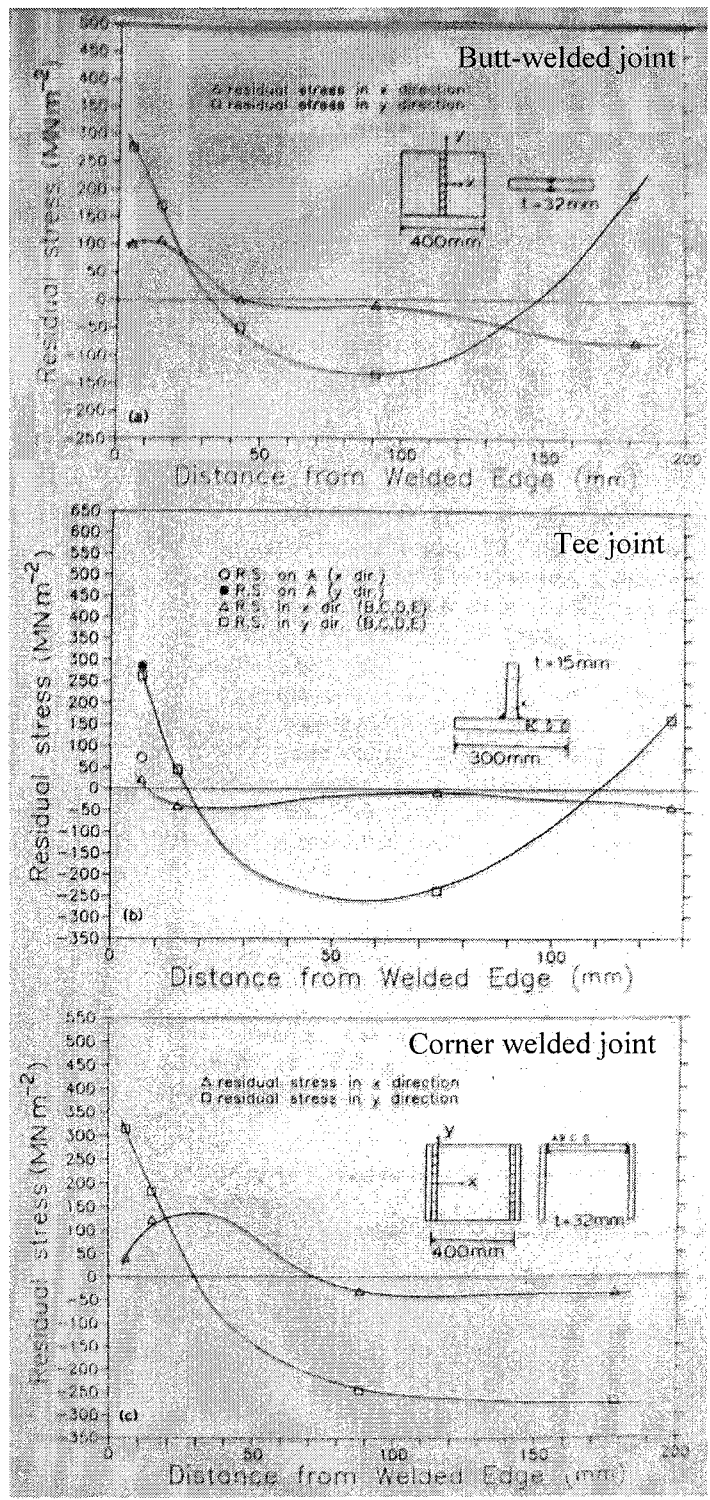


Figure 2.5: Residual stresses in the welded specimens (Weng, et al., 1992)

2.5 Non-Destructive Test Methods

Non-destructive test methods produce no permanent physical damage to the specimen or structure. The most common methods are X-ray diffraction, the magnetic Barkhausen noise technique, and neutron diffraction, which will be discussed in a later section.

X-ray radiation was discovered in 1896, and used for residual strain determination 20 years later when Bragg's equations were formulated. X-ray has minimal capability of penetrating the crystalline structures of typical engineering materials. The penetration path length is adjustable by appropriate selection of specific x-ray energies and wavelengths, but is still limited to a few tens of microns. X-rays are diffracted by the cloud of electrons surrounding the nucleus of the sample material. Recently, with the introduction of third-generation synchrotron sources, which provide higher x-ray energies, there are no absorption edges and the attenuation length increases noticeably with increasing energy. This combined with the relatively high x-ray intensities that they produce leads to path length of centimetres in steel (Krawitz, 2001).

The magnetic Barkhausen noise technique is used in ferromagnetic metals to measure the number and magnitude of sudden magnetic reorientations made by expansion and contraction of the magnetic fields. The stresses are measured by the inductive measurement of a noise-like signal, generated when a magnetic field is applied to the metal. However, the depth of measurement only varies between 0.01 and 1.5 mm. The depth possible depends on frequency range of Barkhausen noise signal analyzed and the conductivity and permeability of the sample material.

Gao et al. (1998) tested three welded HSLA-100 (ASTM, 2007) steel plate specimens with WIC joint configuration using standard X-ray diffraction to determine the residual stress fields. The plates were 19 mm thick and were heat-treated, quenched, hardened to produce yield strengths between 690 MPa and 830 MPa. All specimens were preheated to 50°C then gas metal arc welding (GMAW) was used with MIL-120S-1 welding consumables. The first specimen was welded with no restraints on its edges and with a heat input of 1.4 kJ/mm. The second specimen was restrained and was subjected to the same heat input as the first

specimen (1.4 kJ/mm). The third specimen was not restrained and welded with a higher heat input of 1.7 kJ/mm.

The X-ray diffraction measurements were acquired using with a portable apparatus. Subsurface measurements were achieved using electropolishing, removing 50 μm layers between each reading. X-ray diffraction can only measure approximately several microns deep into most engineering materials. The residual stress measurements were taken in the longitudinal, transverse, and 45° directions from the weld bead. The longitudinal stress component is in the direction of the weld, the transverse stress component is perpendicular to the weld direction, and the 45° direction bisects these two stress components. The results from these experiments show that welding heat input has a significant effect on the residual stress values. A higher heat input produces less residual stress. The decrease is a result of a slowed cooling rate, which causes a restriction in shrinkage and phase transformations. They also found that the restraining of the specimen also has a considerable effect on the residual stress field. It was found that additional tensile residual stresses may be introduced due to the restraint. However, phase transformations may occur during restraint and produce compressive stresses. The measurements obtained using the X-ray diffraction technique show similar stress fields as previously established (Weng, et al., 1992 and Hu, et. al., 1998). The longitudinal surface stresses were tensile near the weld and compressive away from the weld. At the surface of the plate, the transverse stresses were compressive near the weld and increased to tensile stresses as the distance from the weld increases. The stresses measured at 45° from the weld were found to be values within the envelope of the longitudinal and transverse stresses. The results are shown in Figure 2.6 for all three specimens for the three different directions of surface residual stresses. Figure 2.6 (a) shows the first specimen that was welded with the low heat input (1.4 kJ/mm) and no end restraints. Figure 2.6 (b) shows the residual stress in the second specimen, with the low heat input (1.4 kJ/mm) and end restraints, plotted against the distance from the weld. Figure 2.6 (c) shows the residual stress values of the third specimen, with high heat input (1.7 kJ/mm) with end restraints, plotted against the distance from the weld.

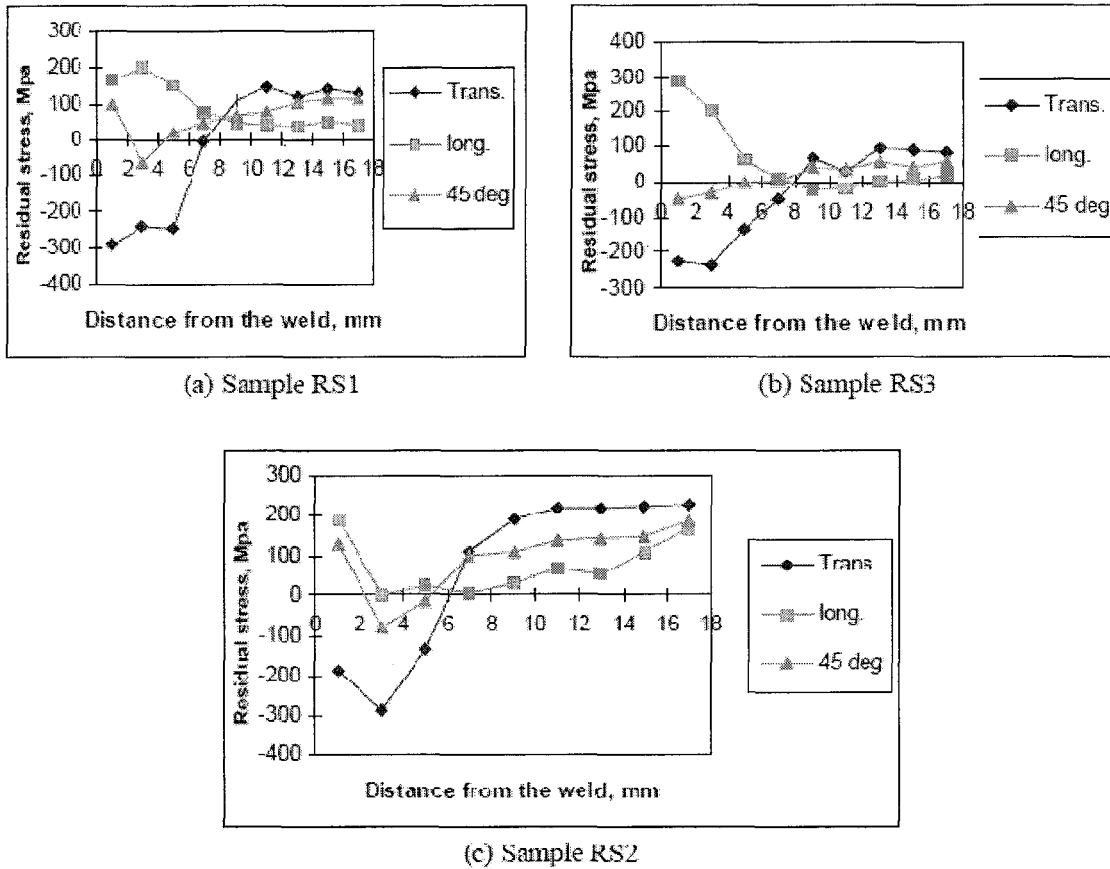


Figure 2.6: Surface residual stress distributions of (a) RS1 – 1.4 kJ/mm, no restraint, (b) RS2 – 1.4 kJ/mm, with restraint, (c) RS3 – 1.7 kJ/mm, no restraint (Gao, et al. 1997)

Gauthier et al. (1998) studied the use and validity of the magnetic Barkhausen noise (MBN) method. The MBN method uses the theory that a ferromagnetic material, such as structural steel, when undergoing a change in magnetization will produce noise in the form of voltage pulses, which are induced in a coil, set near the specimen. The MBN signal increases with the presence of tensile stresses and decrease in the presence of compressive stresses therefore, provides an accurate picture of the residual stress field. The specimen used was an L-shaped cold-formed steel beam with a yield stress of 466 MPa and an elastic modulus of 203 GPa. The results were compared with the cutting and sectioning method, the hole drilling method, and X-ray diffraction method. All these methods provided comparable results. The MBN method requires very close ($\sim 0.1\mu\text{m}$) proximity to the specimen and the stress measurements in the corner of the specimen are not accurate. Therefore, the use of this

method in measuring stresses at the welds of stiffeners does not produce acceptable results since sharp gradients in stresses present in the measurement area.

Rörup (2005) tested a 550 mm x 120 mm x 12.5 mm 355 MPa steel plate with 150 mm x 30 mm x 12.5 mm plate longitudinal stiffeners welded on both surfaces of the plate using a two pass fillet weld, as shown in Figure 2.7. The plates were all saw cut from one larger plate. The specimen was loaded with two constant compressive cyclic load ranges, 140 N/mm² or 180 N/mm². The test showed that after the initiation of the fatigue crack, perpendicular to the stiffener, the crack growth rate increases under the compressive loading cycle followed by a sudden deceleration or stop in propagation in the crack.

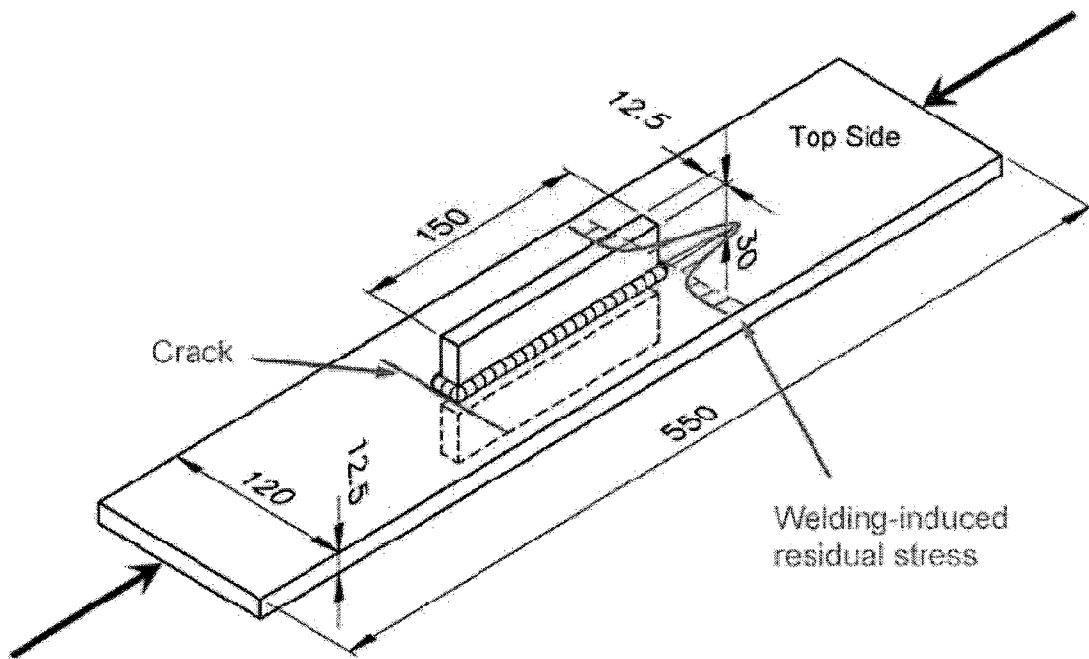


Figure 2.7: Test specimen with a typical crack and residual stress distribution (Rörup, 2005)

The initial residual stresses were measured using both the X-ray diffraction method and the hole drilling method. The stresses were found to be lesser on the surface of the plate where the stiffener was welded later. The redistributed stress field at the crack tip due to the cyclic loading were measured using the neutron diffraction and X-ray diffraction methods for comparison. These results were then compared with the FE model and analysis as shown in

Figure 2.8. The residual stress was modeled in the FE analysis using heat flux input. The FE analysis predicted similar stress values as was found in the physical experiments. The residual stresses due to the welds influenced the fatigue life of the plate under a compressive cyclic load. The fatigue life of the stiffened panel increased due to the crack propagation phase of the loading. At the weld toe and the crack tip, the residual stresses are in tension. With the introduction of the cyclic compressive loading, the crack propagates in the compressive residual stress region. The crack as it expands, moves the tensile stress region forward as it loses strength, which in turn causes the crack growth to slow or stop completely.

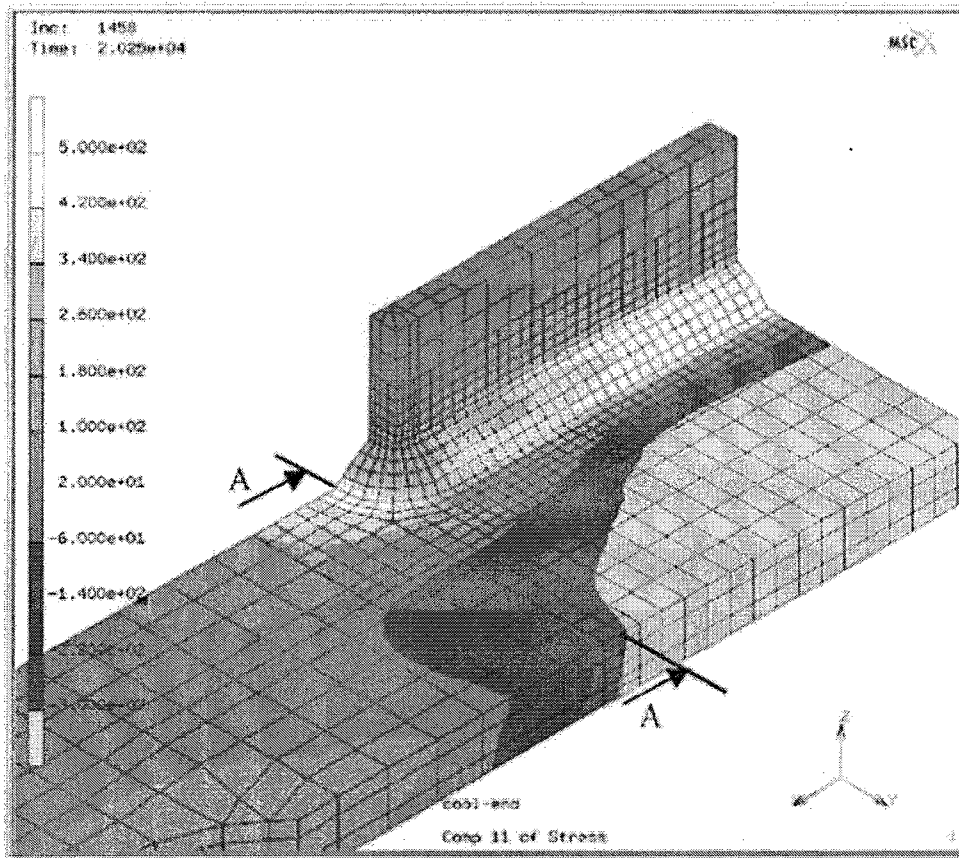


Figure 2.8: Analysis of the weld-induced residual stresses in the longitudinal direction (Rörup, 2005)

2.6 Neutron Diffraction

Neutron diffraction is a non-destructive test method. This method uses either a steady state reactor or a pulsed neutron source. A steady state reactor is designed for research and produces a high neutron flux with a minimal amount of heat, in contrast to a reactor used for nuclear power. The reactor generates a Maxwellian distribution of neutron energies that are dependent on temperature. A monochromator is used to select a single usable wavelength from the neutron beam, which is used to provide the scattering data from the material. A steady state reactor produces a constant wavelength for testing procedures. A pulsed neutron source generates neutrons using a process called spallation. A burst of high-energy particles (protons or electrons) strike a metal sheet which produces a broad range of neutron energies with a broad range of velocities. Therefore, these neutrons will take varying amounts of time to reach the detector or time-of-flight instrument, producing the scattering information of the material.

Neutron diffraction utilizes the crystal lattice of the specimen material as an atomic strain gauge. The average elastic lattice strain in the gauge volume is calculated as the difference in the lattice plane spacing compared to the lattice plane spacing of the stress-free sample. A beam of neutrons, with wavelength λ , from a continuous source diffractometer is passed through the sample and diffracts in accordance with Bragg's law, as in Equation 2.1.

$$\lambda = 2d_{hkl} \sin \theta_{hkl}^B \quad (2.1)$$

where, d_{hkl} is the lattice spacing of the planes hkl in the crystalline solid, as shown in Figure 2.9.

The $2\theta_{hkl}^B$ is the angle at which the neutrons are scattered coherently and elastically by the properly oriented lattice planes hkl and is called Bragg's angle. In this figure, the incident beam is labelled as k_i and the refracted beam as k_f . G_{hkl} is the reciprocal lattice vector, perpendicular to the lattice planes.

Crystal space lattices are categorized according to their symmetry, translation, reflection, and rotational characteristics. There are 14 crystal space lattices called *Bravais lattices*, the most common for engineering materials are the *fcc*, *bcc*, and *hexagonal*.

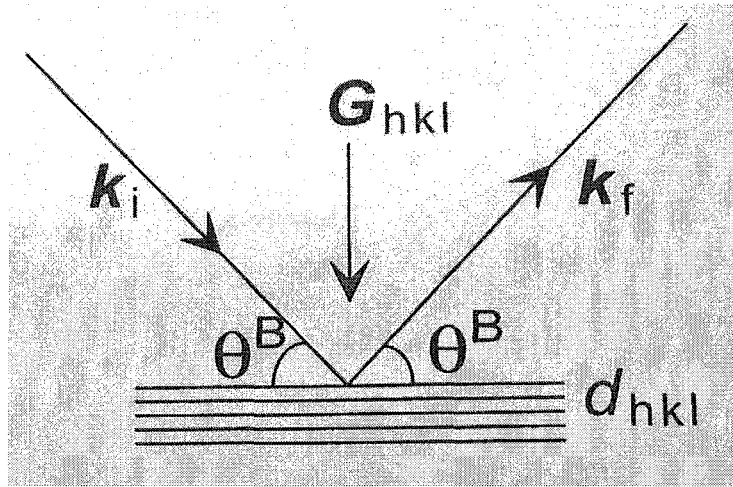


Figure 2.9: Lattice spacing with incident (k_i) and refracted (k_f) beam (Hutchings, et al., 2005)

All lattice points are on a plane in the crystal, known as *Miller indices*, and denoted hkl . The hkl plane intersects the axes of the unit cell at a/h , b/k and c/l , where hkl are the lowest integers with the proper ratio of intercepts, as shown in Figure 2.10. As stated before, the perpendicular distance between planes is d_{hkl} .

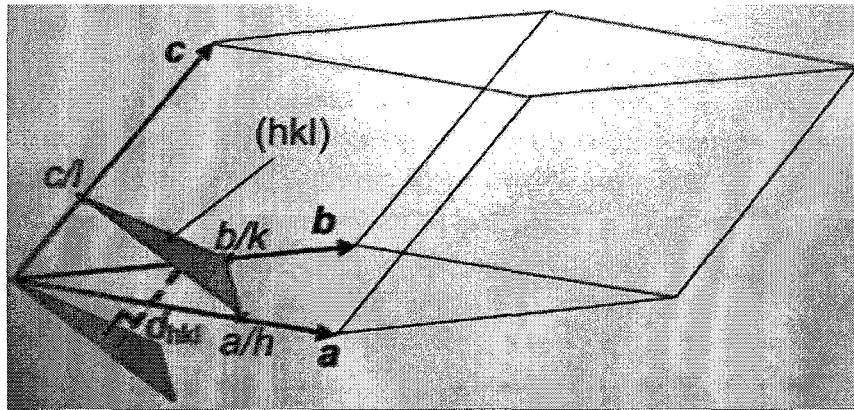


Figure 2.10: Lattice planes (Hutchings, et al., 2005)

The de Broglie wavelength of the neutron, λ , is related to the momentum, p , of the particle as shown in Equation 2.2.

$$p = m_n v = \frac{hk}{2\pi} = hk \tag{2.2}$$

where, m_n is the mass of the neutron, v is the velocity, h is Planck's constant, k is the wave vector of the neutron with a magnitude of $2\pi/\lambda$. The energy of the neutron is shown in Equation 2.3.

$$E = \frac{1}{2}m_n v^2 = h\nu \quad (2.3)$$

where ν is the frequency of radiation. For wavelengths useful for diffraction, thermalized neutron energies are significantly less than the equivalent energies of X-rays or electrons.

The lattice spacing (d_{hkl}) expands with tensile stresses and contract with compressive stresses. The difference in lattice spacing (Δd_{hkl}) is measured by the shift in Bragg diffraction angle, $2\theta_{hkl}^B$. Strain in the direction of the scattering vector is given by Equation 2.4.

$$\varepsilon_{hkl} = \frac{\Delta d}{d} = -\Delta\theta_{hkl} \cot \theta_{hkl} \quad (2.4)$$

As a neutron approaches the nucleus of an atom, four outcomes are possible: (i) coherent scattering, (ii) incoherent scattering, (iii) absorption by the nucleus, and (iv) the most likely event is no scattering. Coherent scattering relates the space and time between atoms, whereas incoherent scattering is the individual atom relations with space and time. When the neutron is absorbed, the compound formed with the nucleus creates an emission of γ -rays, which may radioactively decay. The coherently scattered neutrons diffract at well-defined angles allowing for ease of measurement, whereas, incoherent scattering is isotropic and creates a background beneath the diffraction peaks, much smaller than the diffraction peaks from the coherently scattered neutrons.

Neutron diffraction can penetrate tens of centimetres into common engineering materials and is a non-destructive testing method that can monitor the stress changes due to an environmental factor and external loading. Neutron diffraction measures the strain averaged over a sample volume defined by apertures, called Nominal Gauge Volume (NGV). The Instrumental Gauge Volume (IGV) is the volume over which the average strain is measured in a sample and is therefore, larger than the NGV. The Sampled Gauge Volume (SGV) is the volume over which the strain measurement is averaged, taken from the diffraction peak in

the IGV. If the sampled gauge volume is greater than the characteristic volume, then the corresponding strain is not measured since it averages to zero.

The neutron diffraction method collects the strain measurements of the specimen which are then converted using the appropriate formulas and constants to stress values. The validity of the collected strain values can be determined by checking the full width half maximum (FWHM) values and the intensity of the neutron beam values. The above equations show the theoretical background when determining the stress values from the measured strain values. The following equations show the practical formulas used for manipulating the strain data collected during the neutron diffraction method.

The lattice spacing and error in lattice spacing is calculated using the collected ϕ values as shown in Equations 2.5 and 2.6, respectively.

$$d\text{-spacing} = \left| \frac{\lambda}{2 \times \sin\left[\text{radians}\left(\frac{\phi - \phi_0}{2}\right)\right]} \right| \quad (2.5)$$

$$\mu d\text{-spacing} = \left| \frac{\lambda}{2 \times \sin\left[\text{radians}\left(\frac{\phi - \phi_0 + \mu\phi}{2}\right)\right]} \right| - (d\text{-spacing}) \quad (2.6)$$

The microstrain values and error in microstrain are then calculated using the d-spacing and μd -spacing values, shown in Equations 2.7 and 2.8, respectively.

$$e = \left(\frac{d\text{-spacing}}{d_0} - 1 \right) \times 1000000 \quad (2.7)$$

$$\mu e = \left(\frac{d\text{-spacing}}{\mu d\text{-spacing}} \right) \times 1000000 \quad (2.8)$$

The stress values can now be calculated for each component using all three strain values. The normal, transverse, and longitudinal stress values are shown in Equations 2.9 – 2.11, respectively.

$$\sigma_{Normal} = \frac{E}{1+\nu} \left(\varepsilon_{Normal} + \frac{\nu}{1-2\nu} (\varepsilon_{Normal} + \varepsilon_{Transverse} + \varepsilon_{Longitudinal}) \right) \quad (2.9)$$

$$\sigma_{Transverse} = \frac{E}{1+\nu} \left(\varepsilon_{Transverse} + \frac{\nu}{1-2\nu} (\varepsilon_{Normal} + \varepsilon_{Transverse} + \varepsilon_{Longitudinal}) \right) \quad (2.10)$$

$$\sigma_{Longitudinal} = \frac{E}{1+\nu} \left(\varepsilon_{Longitudinal} + \frac{\nu}{1-2\nu} (\varepsilon_{Normal} + \varepsilon_{Transverse} + \varepsilon_{Longitudinal}) \right) \quad (2.11)$$

The error in the above stress values can be further calculated for each component shown in Equations 2.12 – 2.14.

$$\mu\sigma_{Normal} = \frac{E}{1+\nu} \sqrt{\left(\frac{\sigma_{Normal}^2}{1+\nu}\right) + \left(\frac{\nu}{1-2\nu}\right)^2 (\sigma_{Normal}^2 + \sigma_{Transverse}^2 + \sigma_{Longitudinal}^2)} \quad (2.12)$$

$$\mu\sigma_{Transverse} = \frac{E}{1+\nu} \sqrt{\left(\frac{\sigma_{Transverse}^2}{1+\nu}\right) + \left(\frac{\nu}{1-2\nu}\right)^2 (\sigma_{Normal}^2 + \sigma_{Transverse}^2 + \sigma_{Longitudinal}^2)} \quad (2.13)$$

$$\mu\sigma_{Longitudinal} = \frac{E}{1+\nu} \sqrt{\left(\frac{\sigma_{Longitudinal}^2}{1+\nu}\right) + \left(\frac{\nu}{1-2\nu}\right)^2 (\sigma_{Normal}^2 + \sigma_{Transverse}^2 + \sigma_{Longitudinal}^2)} \quad (2.14)$$

James et al. (2006) used neutron diffraction technique for measurement of residual stress in high strength steel (tensile strength > 600 MPa) butt welds and to determine how residual stress depends on various factors such as, weld heat input, plate thickness, and filler material. The welding method used was metal inert gas (MIG) with a shielding gas composed of 80% argon and 20% carbon dioxide. The transverse stress measurements were made using neutron diffraction at mid-depth and 1 mm below the surface. The normal and longitudinal stress values were also collected. However, the study primarily focused on fatigue cracking, which initiates at the toe of the weld and develops parallel to the weld as a result of transverse stresses. The normal stresses were in compression in the upper portion of the plate and in tension in the lower portion of the plate. However, these values were small and all nearing zero therefore, producing a plane stress problem. The study also evaluated the use of undermatched, matched, and overmatched filler material. The specimen with undermatched filler material exhibited lower tensile maximum stresses than the matched and overmatched specimens. The compressive maximum stresses in the undermatched specimen are associated with the heat-affected zone, while in the overmatched specimen; the compressive maximum stresses were outside of the heat-affected zone. Specimens with two plate thicknesses were tested: 8 and 12 mm, and the thinner plate showed higher residual stress values than the thicker plate due to the fast rate of cooling, which were worsened by the

lesser weld heat input. The details of the specimens are shown in Figure 2.11. The stress values obtained from the 12 mm thick specimen with overmatched weld metal with a low heat input (see Figure 2.11(c)) are shown in Figure 2.12.

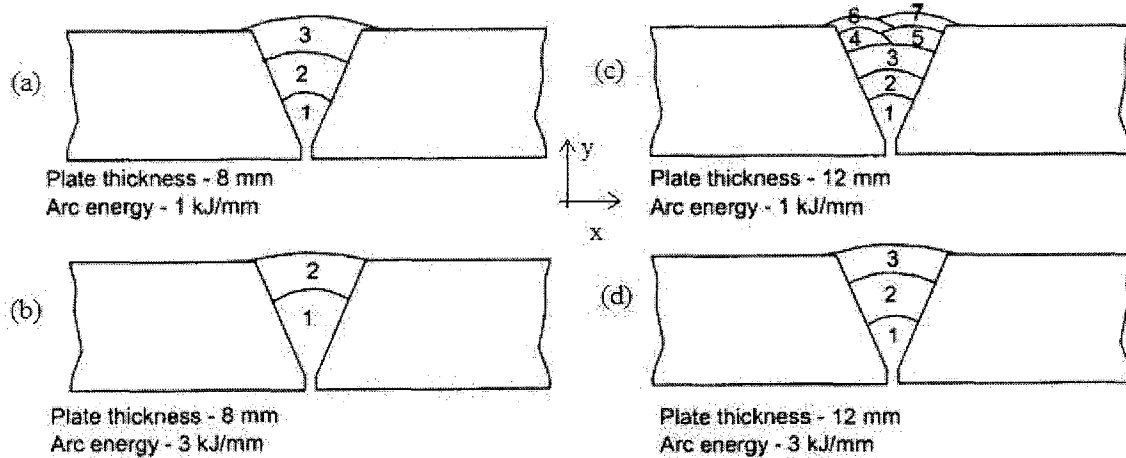


Figure 2.11: Cross-sectional (Y-Z) details of the multipass weld runs used to make the butt joints in the 8mm and 12mm thick plates of RQT701 steel - (a) 8 mm plate thickness with low heat input (1 kJ/mm), (b) 8 mm plate thickness with high heat input (3 kJ/mm), (c) 12 mm plate thickness with low heat input, and (d) 12 mm plate thickness with high heat input (James, et al., 2006)

Paradowska et al. (2006) examined the reference samples used in the neutron and synchrotron X-ray diffraction testing. The pseudo-strain values were the object of the testing and relate to the difference between the lattice spacing at a point and the average spacing across the sample. The specimens were low carbon steel welded using the flux-cored arc welding (FCAW) process. The samples were then created using electro-discharge machining (EDM) to generate a cube and a comb for testing. The measurements were taken in the transverse and normal directions of the weld using both methods as shown in Figure 2.13 and Figure 2.14, respectively. The final values showed that both neutron and synchrotron X-ray diffraction methods, the reference sample may be taken from the parent material. The microstructure and texture in the weld and the heat-affected zone do not warrant the expensive procedure of manufacturing a comb for the specific reference values of each area.

Wimpory et al. (2003) measured residual stress in T-plate ferritic steel weldments of 25 mm, 50 mm, and 100 mm thick base plates for residual stress using neutron diffraction and deep hole drilling methods. The 25 mm thick base plate was welded using a T-fillet weld and the

50 mm and 100 mm thick base plates were welded using partial penetration welds. The 25 mm and 50 mm plates were restrained to prevent distortion, however the 100 mm thick plate (Figure 2.15) was rigid enough and thus, no clamps were used. The finished welded specimens were sliced into 12.5 mm thick samples for measuring residual stresses using neutron diffraction method. A 100 mm thick section of the 100 mm thick T-plate weld was used for the deep-hole drilling method. The neutron diffraction tests were conducted at three different nuclear reactors; two monochromatic sources and one polychromatic source.

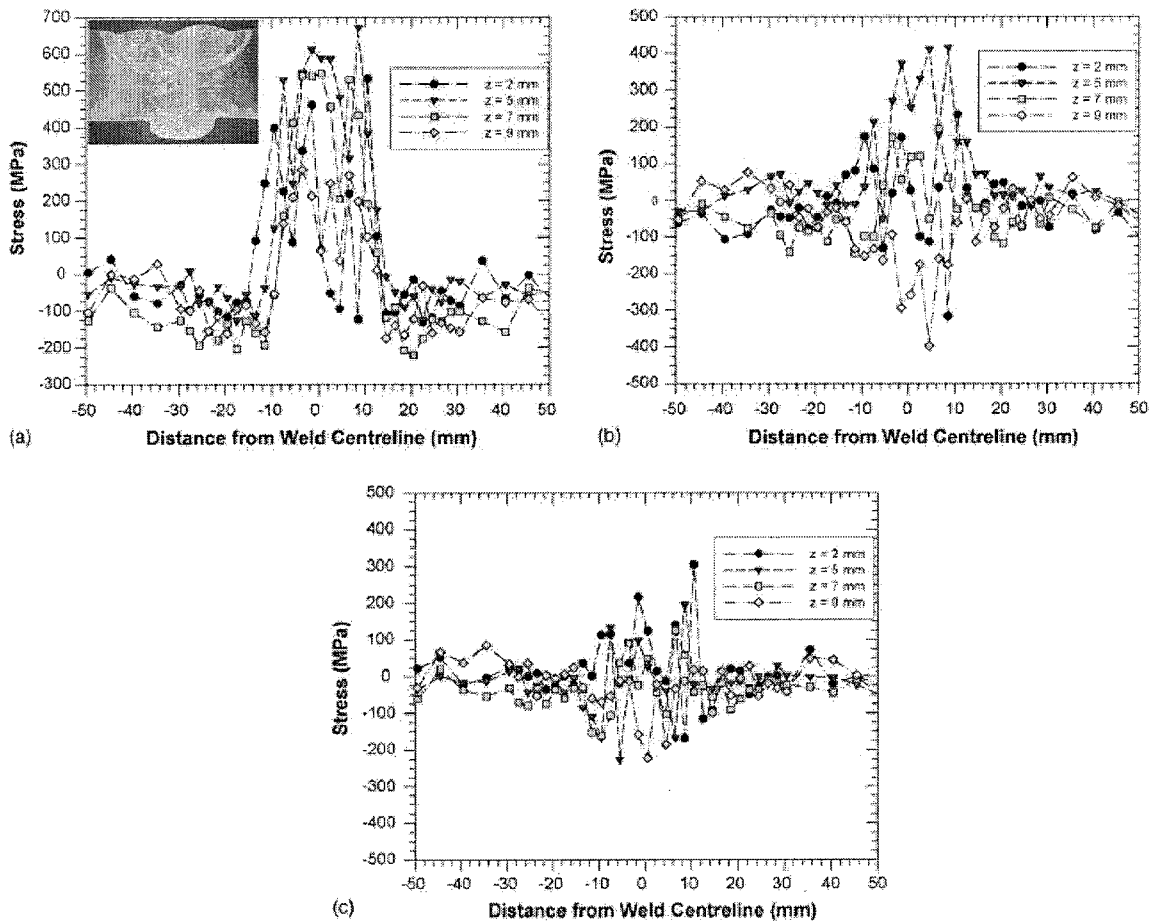


Figure 2.12: Specimen - 12 mm thick, overmatched weld metal at low heat input 1 kJ/mm (a) Longitudinal (x) stress profile at four depths (b) Transverse (y) stress profile at four depths (c) Through-thickness (z) stress profile at four depths (James, et al., 2006)

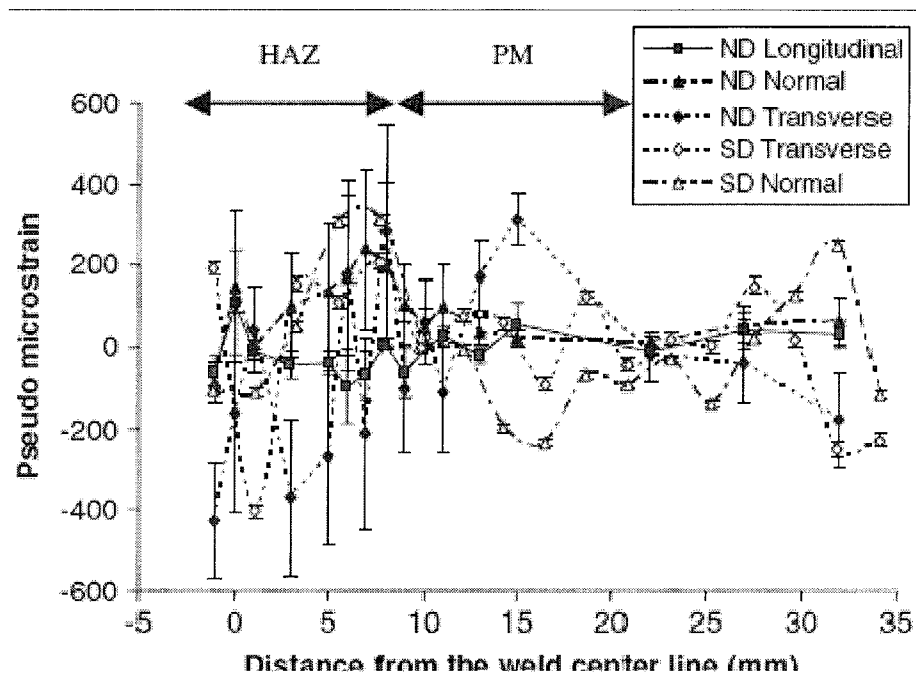


Figure 2.13: Pseudo-strain measured by ND and SD across the weld, (PM = parent material, HAZ = heat affected zone, WM, weld material) (Paradowska, et al., 2006)

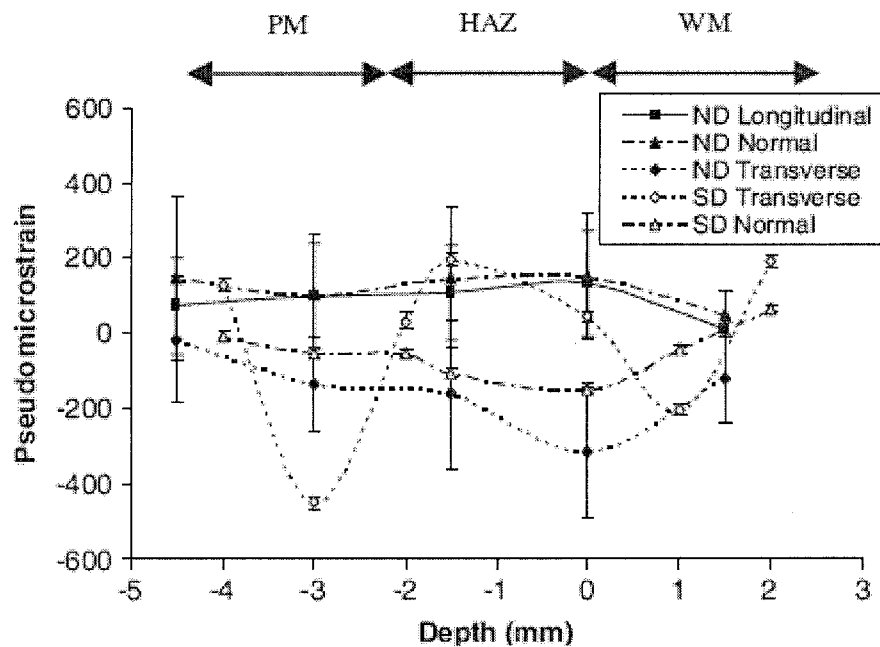


Figure 2.14: Pseudo-strain measured by ND and SD through the thickness (Paradowska, et al., 2006)

The reference samples were taken from the base plate material in an area of no stress. A reference sample should also have been taken in the weld material for comparison. The steps in the deep-hole drilling method were as follows: a smooth reference hole was drilled and measured at various depths and angles then a cylinder surrounding the reference hole was extracted and the reference hole was again measured at the same locations. This method provided the longitudinal and transverse residual stresses. The normal stresses could be obtained if the axial distortions were also measured, but were not recorded in this study. The deep-hole measurements were taken at the point of intersection between the plate and the weld and continued towards the edge of the plate, as shown in Figure 2.15. Measurements were not taken into the weld and the stiffener. The deep-hole measurements and the neutron diffraction results were compared and showed a good agreement as shown in Figures 2.16 and 2.17.

Neutron diffraction measurements were also taken on a post-weld heat-treated sample of a 25 mm T-plate weld. The results showed that overall the residual stress in the sample were close to zero, however a post-weld heat treatment is not feasible in the construction of a ship. The results of all of these experiments were also compared with previous experiments that were conducted and again showed a good agreement. The results were also compared with the British Energy R6 and BS 7910 which show representations of residual stress fields for varying weld configurations. This comparison showed that these standards are very conservative and do not provide a very accurate picture of the stress distribution.

Lorentzen and Ibsø (1995) evaluated the residual stresses in offshore welds using neutron diffraction method for better understanding of the fatigue life of the structure when imposed to cyclic and stochastic loading. The specimens were constructed of St.52-3 (Fe510C) steel of 8 mm and 16 mm thicknesses, and were butt welded on either side of the plate with 5 and 10 mm plates, respectively. No post-weld heat treatments were used. The strain measurements were taken in the longitudinal direction only and the normal and transverse directions were ignored. The two directions were disregarded because of tests that were previously completed indicates that the principal directions change as a function of depth into the material. Therefore, to properly measure internal strains, the principal axes must be re-evaluated at all measurement depths. Only the surface stresses were found for this study

since fatigue cracks generally occur due to the high tensile stresses at the surface of the material. The values obtained showed a maximum residual stress value of 50% the material yield stress.

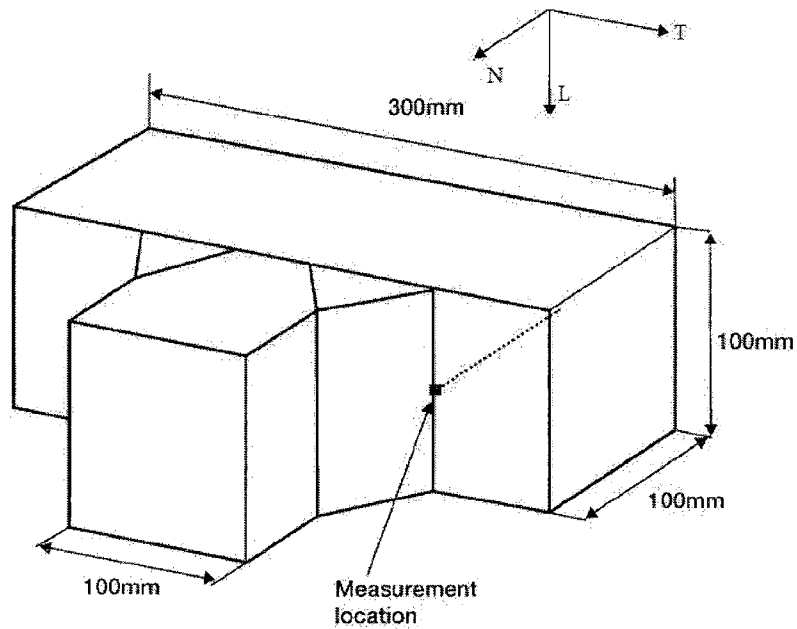


Figure 2.15: Location of deep-hole drilling measurements on the 100 mm thick plate specimen (Wimpory, et al., 2003)

Pearce and Linton (2006) used neutron diffraction method to determine the residual stresses within a curved plate and a butt weld specimen. Both specimens were constructed from BIS 812 Ema Steel. The measurements were conducted using the 211 peak and neutrons with a wavelength of 1.4 Å. The stresses were measured in the longitudinal, transverse, and normal directions. The results shown in Figure 2.18 have similar profiles as previously measured specimens using different methods of measurement.

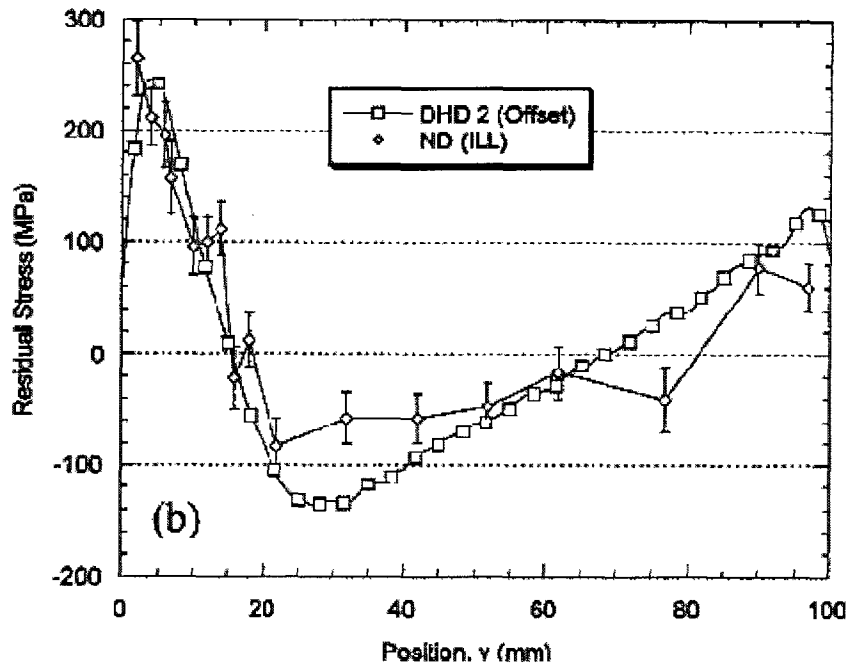


Figure 2.16: Transverse stresses in the 100 mm T-plate - ND measurement on a 12.5 mm slice and DHD measurement (Wimpory, et al., 2003)

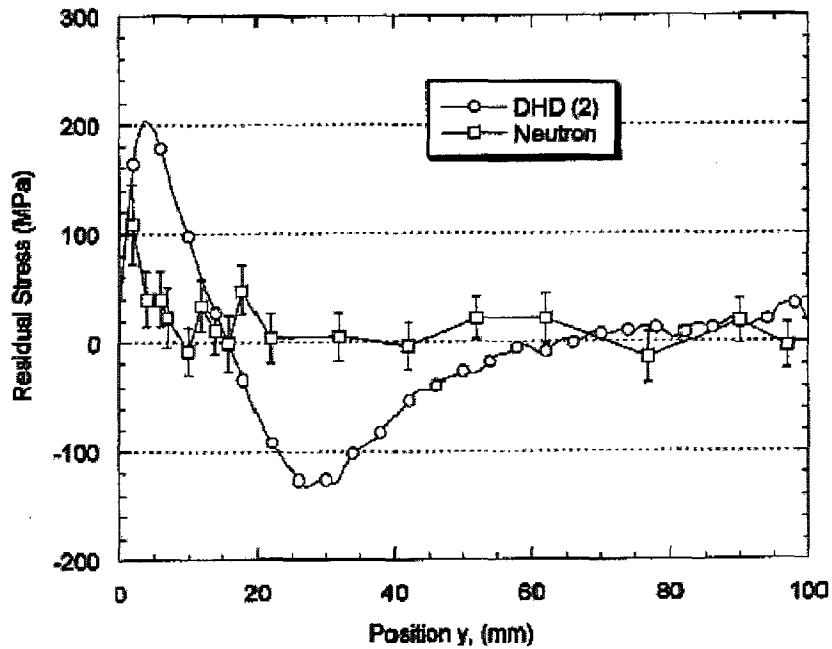


Figure 2.17: Longitudinal stresses in the 100 mm T-plate obtained by ND on a 12.5 mm slice and by DHD (Wimpory, et al., 2003)

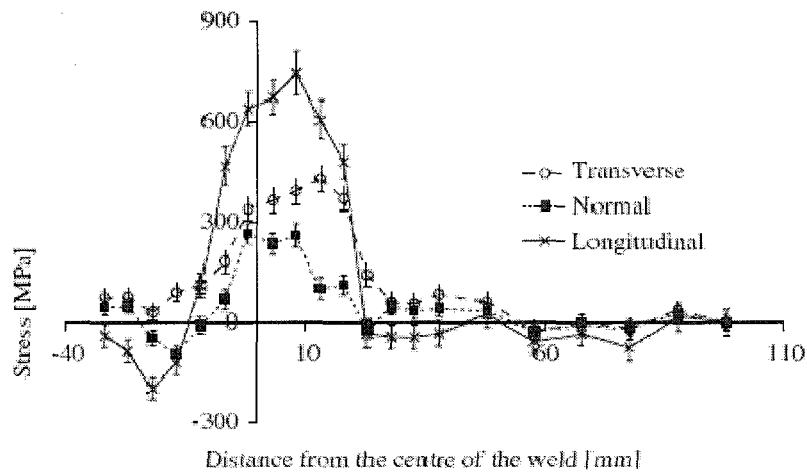


Figure 2.18: Three-dimensional stresses 10mm from surface of side B—flat butt weld (Pearce, et al., 2006)

Webster and Wimpory (2001) suggested procedures for obtaining consistent results using the neutron diffraction method of measurement. Their study shows that by placing the beam apertures as near the specimen as possible minimizes the irregularities in identifying the centroid of the specimen. Planes that do not exhibit bulk behaviour and are affected by plastic strain must be ignored. Single crystals within these planes are anisotropic and when subjected to different reflections will result in different strains, forming an erroneous field of stress. A proper value for the stress-free lattice spacing must also be obtained. The stress-free values should be taken from the parent material, as well as from the welding material.

Price et al. (2006) examined the residual stresses caused using MIG (metal inert gas) welding of a single bead-on-plate of low-carbon steel and the influence of restraint. The study was conducted using a 200 x 100 x 12 mm plate, where the first specimen was unrestrained and the second specimen was fully restrained by tack welding to a very thick steel plate. A 14 mm weld was made through the centre of the plate as shown in Figure 2.19.

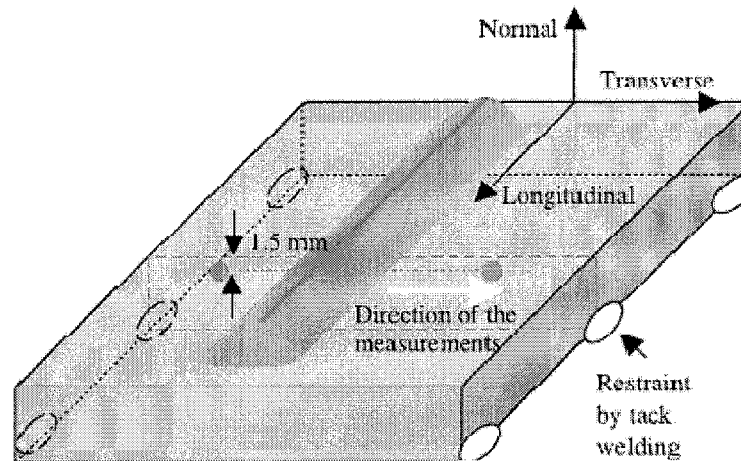


Figure 2.19: The direction of the measurements (transverse x, normal y, longitudinal would be z) using neutron diffraction on the single bead-on-plate (Price, et al., 2006)

The neutron diffraction measurements were undertaken using a wavelength of 1.4 \AA and detector angle of $2\theta_B = 73.5^\circ$. The transverse and normal stresses were found to be low, especially compared to the fully restrained specimen, due to the deformation during welding of the unrestrained specimen. In the centre of the weld the normal and transverse stresses were compressive for the unrestrained specimen and tensile for the fully restrained specimen. The peak stress was in the longitudinal direction occurred near the centre of the weld, and was observed to be higher than the specified yield stress of 285 MPa in the parent metal and 445 MPa in the weld metal; this is due to the increased hardness of the steel in the weld region. These peak values were also found to be higher in the fully restrained specimen compared to the unrestrained specimen, as shown in Figure 2.20. The experimental results of the unrestrained specimen were compared with three-dimensional finite element modelling; using a commercial program called Sysweld+. Qualitatively, all of the data for transverse, normal, and longitudinal values were in agreement with the observed values during the experiments. However, the longitudinal stress values were in disagreement which was a result of the unrefined mesh and the true calibration of the welding heat source in the model.

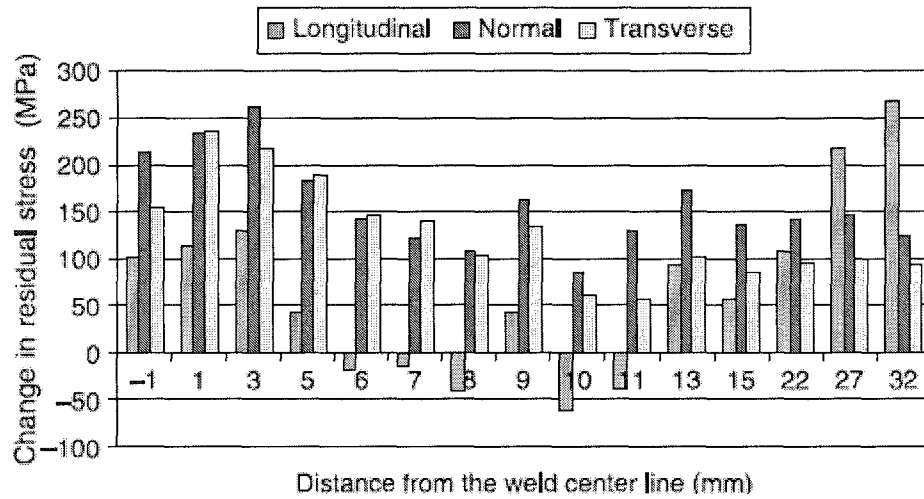


Figure 2.20: Change in stress in fully restrained specimen in comparison to unrestrained specimen (Price, et al., 2006)

Paradowska et al. (2005) studied the residual stress distribution in single and multi bead-on low carbon steel welds and correlated the data to construction methods and integrity specifications. The effect of restraint, the start and end of the weld and multi-pass welds were closely examined using the neutron diffraction technique. The hardness and microstructure was determined across the plate, weld, and heat-affected zone. The hardness of the weld and the heat affected zone were a result of a critical cooling environment and the lack of a post-weld heat treatment. The results showed that for the unrestrained specimen the normal and transverse stresses in the centre of the weld were compressive, whereas in the restrained specimen these stresses were in tension. Overall, the transverse and normal stresses were low in the unrestrained specimen as it was permitted to deform during the welding process. The longitudinal peak stress in the weld was higher than the yield stress of the plate metal, which corresponds to the increased hardness values in the weld and heat affected zone. The residual stresses in the transverse and normal directions peaked at half the maximum longitudinal stress values, which occurred in the heat-affected zone below the middle of the weld bead. The start and end of the weld had high increases in stress levels and surpassed the yield strength of the plate material. For the plates with two, three, and four weld passes, the welds overlapped 50%. When the second weld pass was made, the weld underneath the overlap the residual stress values increased threefold but the uncovered weld

portion increased by only 70%. For the third weld pass, the stress remained the same beneath the weld and decreased under the second pass to almost zero. The final weld pass caused the residual stress transfer from all other weld passes into the final weld with a general widening of the peak stress field. The tensile residual stresses in the toe of the weld were reduced, with the fourth weld pass, to more favourable compressive values and lower tensile values. The collected data can be utilized in the design of welds. The longitudinal stresses cause transverse hydrogen cracking, in the toe of the weld the transverse stresses cause the introduction of fatigue cracks, and the sequence of multi-weld passes greatly affects the distribution of the residual stress field.

Holden et al. (2006) investigated several factors relating to measurement of residual stress in welds. These factors include the varying microstructure through the weld and the change in plastic deformation in the weld zone. They emphasized the importance of obtaining the reference specimens from a companion weld, in order to understand and determine more accurate stress distributions. Three different specimens using neutron diffraction were studied: a butt weld between 8.6 mm thick, highly textured Zr-4 plates, a double-v butt-weld between 10 mm weakly textured high-strength steel plates, as shown in Figure 2.21, and a double-v butt-weld between 10 mm hot-rolled 304-type stainless steel plates. The results of their study confirmed that texture near the weld does not affect the stress field. Also, Type II strains from annealing and cooling can affect the macroscopic strains; therefore, intergranular strains can affect the measurement values.

Ganguly et al. (2006) examined the residual stresses in a 12-mm-thick variable-polarity plasma-arc welded aluminum 2024-T352 alloy plate using neutron diffraction. The residual stresses were measured using a combination of neutron and synchrotron X-ray diffraction after the plate was machined down to 7 mm thickness on either side of the weld (typical machining for the aerospace industry). The comparison of the two methods is shown in Figure 2.22. Synchrotron X-ray diffraction measurements were quick, made high penetration depths and allowed for very small gauge-volumes. However, synchrotron X-rays have very low diffraction angles, so it was impractical to measure strain in the normal direction. Therefore, a combination of synchrotron X-ray measurement for the longitudinal and transverse directions and the use of neutron diffraction for the normal direction provided

excellent results. The transverse direction was measured using both methods to compare results obtained from the different machines. A stress-free reference comb, measured using both methods, showed a deviation of d_0 (stress-free lattice spacing) across the weld. The 12 mm thick specimens were also compared with the contour method and the results were agreeable. It was found that the machining stresses caused by skimming the specimen from 12 mm to 7 mm caused little change in the stress distribution. The residual stress results showed high tensile stress in the longitudinal direction near the weld and the stresses in the normal and transverse directions were considerably lesser.

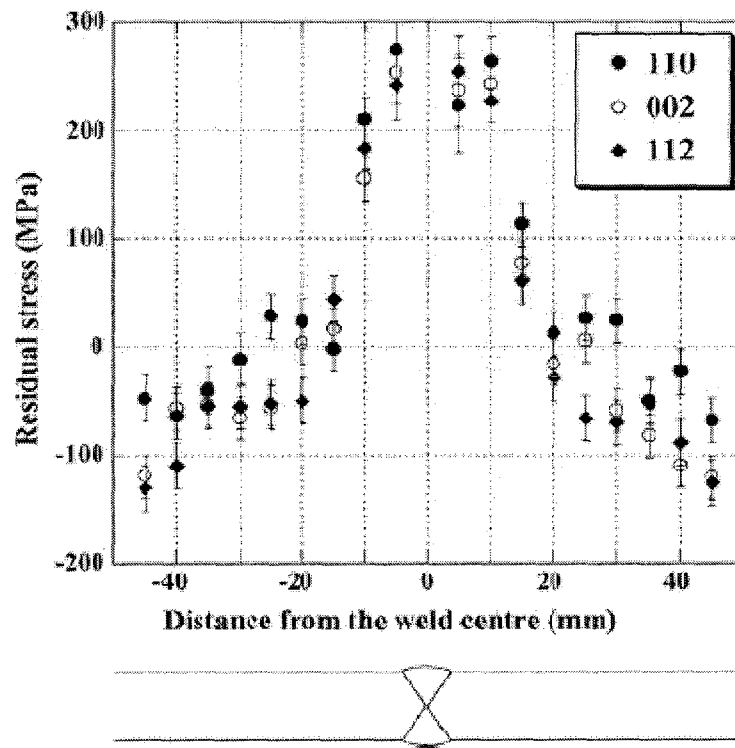


Figure 2.21: Longitudinal stress derived from measurements of {110}, {002} and {112} reflections in the high strength steel SNC631 as a function of position through the weld (Holden, et al., 2006)

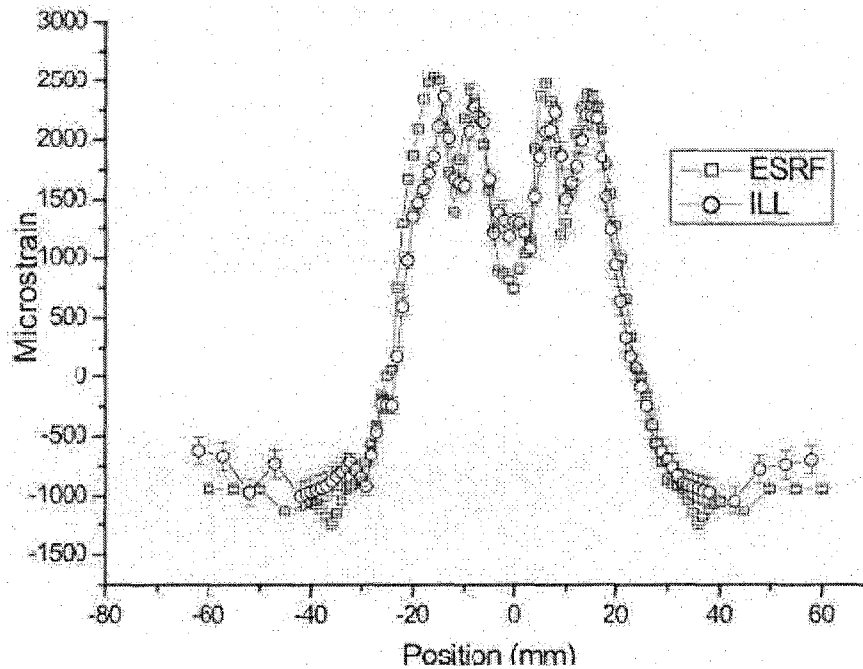


Figure 2.22: Centerline longitudinal strain measured in the two as-welded 12-mm-thick plates using neutrons and synchrotron X-rays (Ganguly, et al., 2006)

2.7 Chalk River Laboratories, Atomic Energy of Canada Limited Facility

Chalk River Laboratories (CRL) is equipped with a CANDU (CANada Deuterium Uranium) reactor, which uses pressurized heavy water (deuterium oxide) and uranium as fuel in the reactor. The source originates in an area of the moderator/reflector specially designed to optimize the thermal neutron flux. The beam tubes transport neutrons from the source to the region beyond the outer shielding of the reactor where neutron scattering instruments are situated. The beam tube usually contains an absorbing shutter to switch off most of the beam, or can be flooded with water to reduce the beam intensity to very low levels. The latter allows work to be carried out safely in the instrument's beam exit region, where monochromating crystals or choppers may be located. The energy of the neutrons in the core of a reactor (2 to 3 MeV) is much too high to be useful for diffraction experiments and therefore, thermalized by a moderator.

Guide tubes are usually of rectangular cross-sections and, as the walls must be optically flat, made of float glass usually coated with a metal such as nickel. The use of a slightly bent

guide, of several kilometres radius, allows for the removal of unwanted γ and fast neutron background, being transmitted through the walls into a biological shielding absorber surrounding the guide. The use of guides enables neutron beams to be transported to “guide halls,” which are located outside the main reactor shell. The various instruments on the same guide may take different vertical sections of the guided beam or the part of the beam transmitted through the monochromator of an upstream instrument. The design of the reactor is shown in Figure 2.23 and is being used for the current study at the University of Windsor.

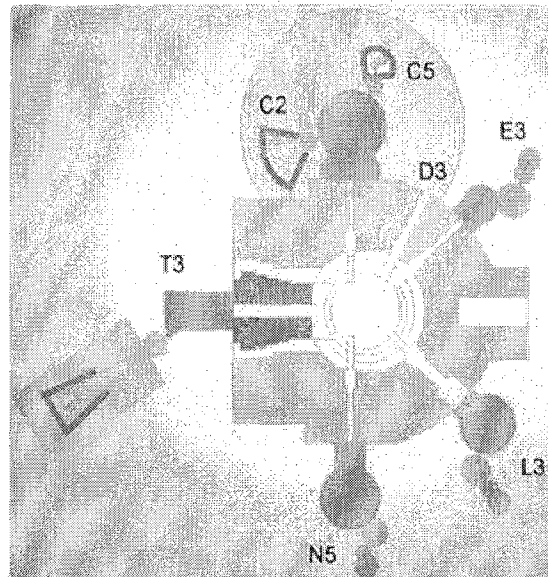


Figure 2.23: Layout of the Chalk River Laboratories (Canada, 2008)

The current study will use the L3 Spectrometer, an ANDI Diffractometer that is equipped with a 32-wire position sensitive detector. This equipment is shown in Figure 2.24.

The National Research Universal Reactor at the CRL produces 120MW, with a 3×10^{18} neutron/m² thermal neutron flux. Key features of the centre include:

Stress-scanner: It has a typical minimum spatial resolution of 1 mm³, locating accuracy better than 0.1 mm, strain precision 0.5E-4, 32-element multiwire ³He detector for high throughput, and a selection of computer-controlled positioning systems, handling loads up to 500 kg.

Powder Diffractometer: An 800-channel detector spanning 80 degrees of scattering angle simultaneously for high throughput with continuously variable wavelength and adjustable collimation before monochromator 0.2, 0.4 or 0.6 degrees.

Weld Station: This is used for in-situ studies of GTAW (gas tungsten arc welding) with a stationary welding torch and moving specimen.

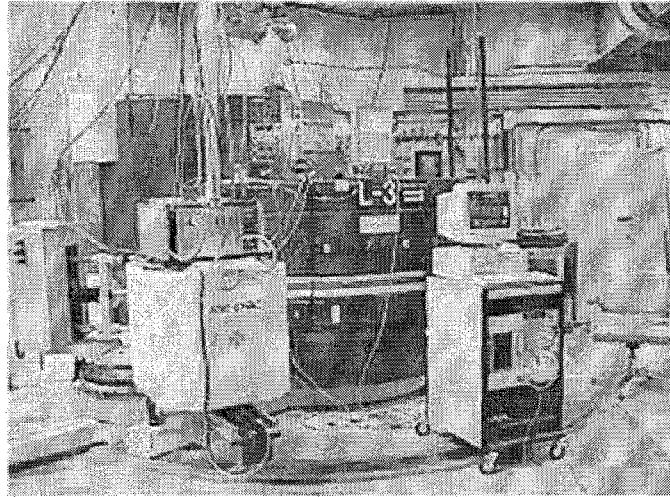


Figure 2.24: L3 Spectrometer at Chalk River Laboratories (Canada, 2008)

Typically, the danger of contamination at a neutron laboratory is nominal, with radiation being the chief concern; monitors are usually found on the equipment throughout the laboratory. Access to the measurement equipment is restricted by the use of interlocks when the neutron beam is engaged. All possible radiation is viewed as potentially hazardous, and exposure should be limited. The ALARA (as low as reasonably achievable) principle of exposure to radiation should always be respected.

A health physicist assesses the radiation profile of a specimen after testing and determines whether to grant immediate access or requests the specimen to be placed in a radioactive material storeroom until the radioactive decay can occur. Usually the radiation level of the material to be permitted to leave the facility is $0.1 \mu\text{Sv}$ at its surface. When a subject requires immediate removal from the facility, there are shielding, packaging, and certification requirements that are met to comply with national and international standards.

3 Material Properties and Welding Specifications

3.1 Material Properties

The material used in this study for the plates and stiffeners was 350 WT steel (CSA, 2004). A chemical composition of the parent metal, the stiffener metal, and the weld wire metal are shown in Table 3-A. The mechanical properties of the parent metal, the stiffener metal, and the weld wire metal are shown in Table 3-B. The weld wire information was provided by the supplier and the data for the plate and the stiffener were completed in the structures lab at the University of Windsor, ON, Canada. Quantity of material required for all testing was ordered at the same time to ensure the same materials for all tests. All of the specimens were cut from two large plates using water jet technology in order to minimize the additional residual stresses induced by the cutting process. The stiffeners were L-shaped of dimension 127 mm x 76.2 mm x 9.53 mm. They were cut from one large stiffener using a band saw; this is also a cold-cut method.

The material metallurgical testing was completed by Schmolz + Bickenbach in Windsor, ON, Canada. The company uses optical emission spectrochemical analysis to produce the results shown in Table 3-A. Material samples were sent of varying sizes for the testing, shown in Figure 3.1, where each square is 5 mm x 5 mm.

3.2 Mechanical Properties of Material

Quasi-static tension (pull) tests were conducted according to ASTM Standard (ASTM, 2008a) in the Civil Engineering Laboratory at the University of Windsor. Two samples cut from the plate material were tested and showed to have higher yield strength than recommended for a 350 WT steel (CSA, 2004). The average modulus of elasticity and first yield stress for the plate material obtained from the pull tests are 205 GPa and 405 MPa, respectively (Figure 3.2). The modulus of elasticity of the angle section was found to be 204 GPa and the first yield stress was found to be 350 MPa. The elastic limit was determined from the first non-linear point (first yield point) of the nominal stress-strain plot. Yield stress

was calculated at upper yield limit, or 0.2% yield stress at 410 MPa for the plate material and 345 MPa for the angle section. Full nominal stress-strain curves for two plate samples and two angle samples are shown in Figure 3.2.

3.3 Welding Specifications

Metal core arc welding (MCAW) process was used for welding the stiffeners. A licensed welder at the Windsor Welding Institute, Windsor, ON, completed all the welding process. The properties of the wire metal that was used were detailed in the previous section. The diameter of the wire metal was 0.89 mm (0.035 in) and the wire speed was 231 mm/sec (9.1 in/sec). The specimens were fully restrained during the welding and the cooling process. Large C-clamps were used to restrain the specimen to the welding table. Depending on the specimen, up to six clamps were used on the plate and two clamps used to hold each stiffener in place during the welding and cooling process. Specimen 1 was accidentally released from restraints after ten minutes of completion of the welding and this caused a 5° bend upwards in the plate on either side of the weld. The heat input used was calculated to be moderate and was controlled using a constant current and welding speed shown in Table 3-C.

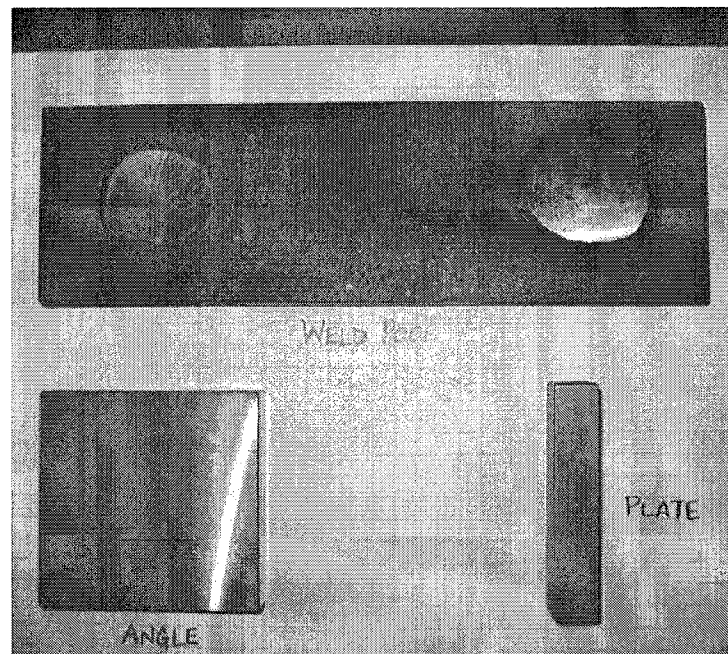


Figure 3.1: Material samples for metallurgical testing

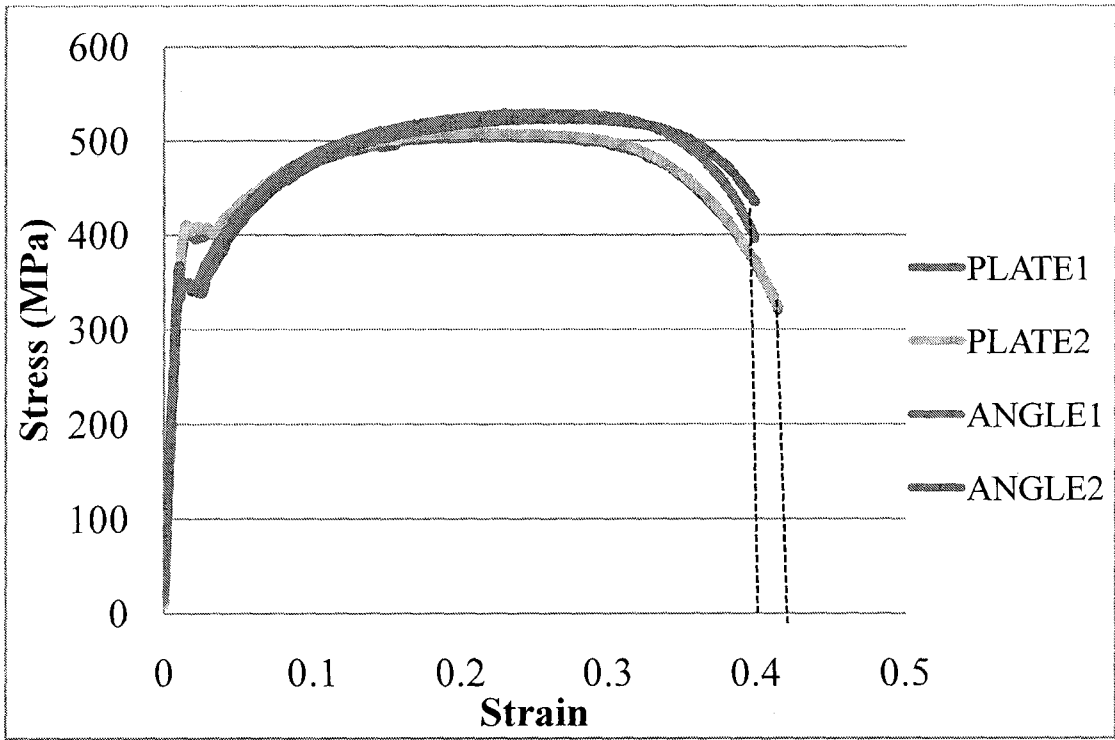


Figure 3.2: Stress-Strain Curve

Table 3-A: Chemical Composition of Material

	C (%)	Cr (%)	Cu (%)	Mn (%)	Mo (%)	Ni (%)	P (%)	S (%)	Si (%)	V (%)
Plate	0.09	0.08	0.12	1.28	0.02	0.07	0.022	0.004	0.07	<0.01
Stiffener	0.17	0.08	0.33	0.94	0.04	0.15	0.016	0.022	0.18	<0.01
Weld Pool	0.09	0.07	0.15	1.25	0.02	0.05	0.008	0.014	0.55	<0.01

Table 3-B: Mechanical Properties of Material

Metal	Grade	Specifications	Testing Conditions	Average Ultimate Strength (MPa)	Average Yield Strength (MPa)	Elongation at rupture (%)
Plate	350WT	C.S.A. G40.21-50WT - Cat. 3	Chemical: ASTM-E415, Impact & Tensile Test: ASTM-A370	527.5	405	41
Stiffener	300W	C.S.A. G40.21-04 44W/50W ASTMA709-05b ASME SA36		507.3	350	39
Weld Wire**	E70C-6M H4, $\phi =$ 0.0045 in	AWS A5.18-2005 ASME SFA5.18	As welded, -29 °C, 250 Amps, 28 V, Charpy-V-Notch	607	530	28 (2")

Table 3-C: Welding Specifications

Specimen	Stiffener	Average Voltage (V)	Average Current (A)	Wire Speed (in/min)	Time for 1 Pass (sec)	Travel Speed (mm/min)	Heat Input (kJ/mm)	# of Stops	Cooling Time (min)
2	1 – 600 mm	25.6	185	231	338	106.5	2.67	1 for 1 minute	55
3	1 – 600 mm	25.4	185	231	270	133.3	2.12	None	120
	2 – 600 mm	26	188	231	320	112.5	2.61	1 for 1 minute	120

4 Test Method and Test Results

4.1 Test Matrix

Three specimens, as shown in Table 4-A, were built and tested. The first specimen was a square plate with no stiffeners (Figure 4.1). This specimen was used to determine the level of stresses that was created during hot roll process. The second specimen was a rectangular plate with one stiffener welded off-centre (Figure 4.2). The third specimen was a rectangular plate with two stiffeners welded 250 mm on centre (Figure 4.3).

Table 4-A: Test Matrix

Specimen	Base Plate (L x W x D)	Stiffener Details	Welding Method
1	400 mm x 400 mm x 9.5 mm	No stiffener	No welding
2	600 mm x 400 mm x 9.5 mm	One 600 mm long stiffener at 150 mm from edge	MCAW
3	600 mm x 400 mm x 9.5 mm	Two 600 mm stiffeners spaced 250 mm apart (75 mm from both edges)	MCAW

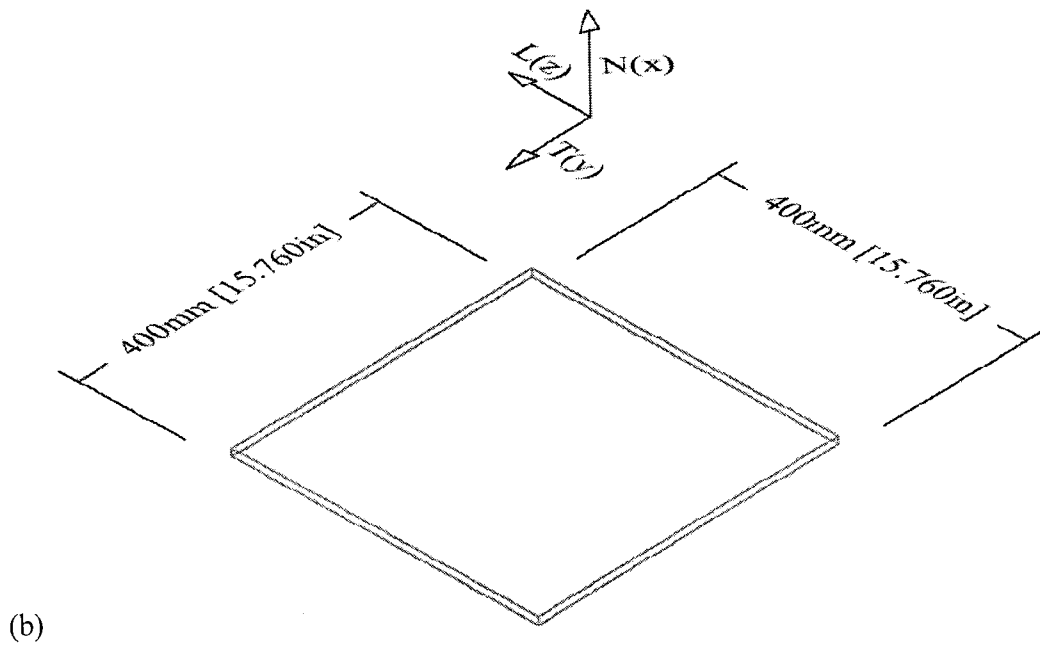
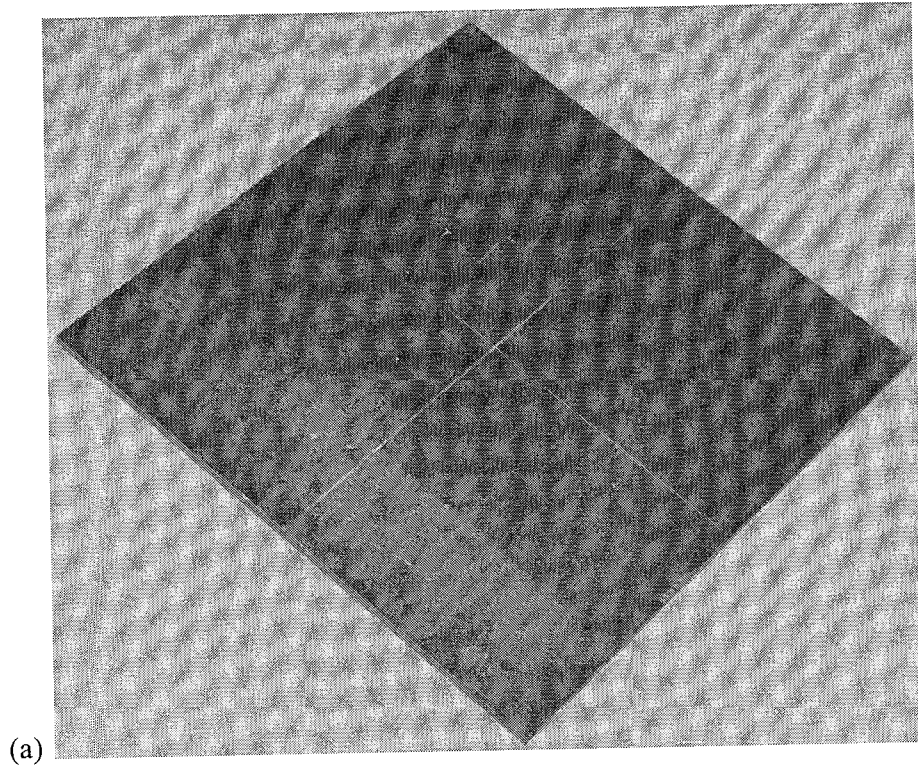


Figure 4.1: Specimen 1 (a) Photo (b) Sketch

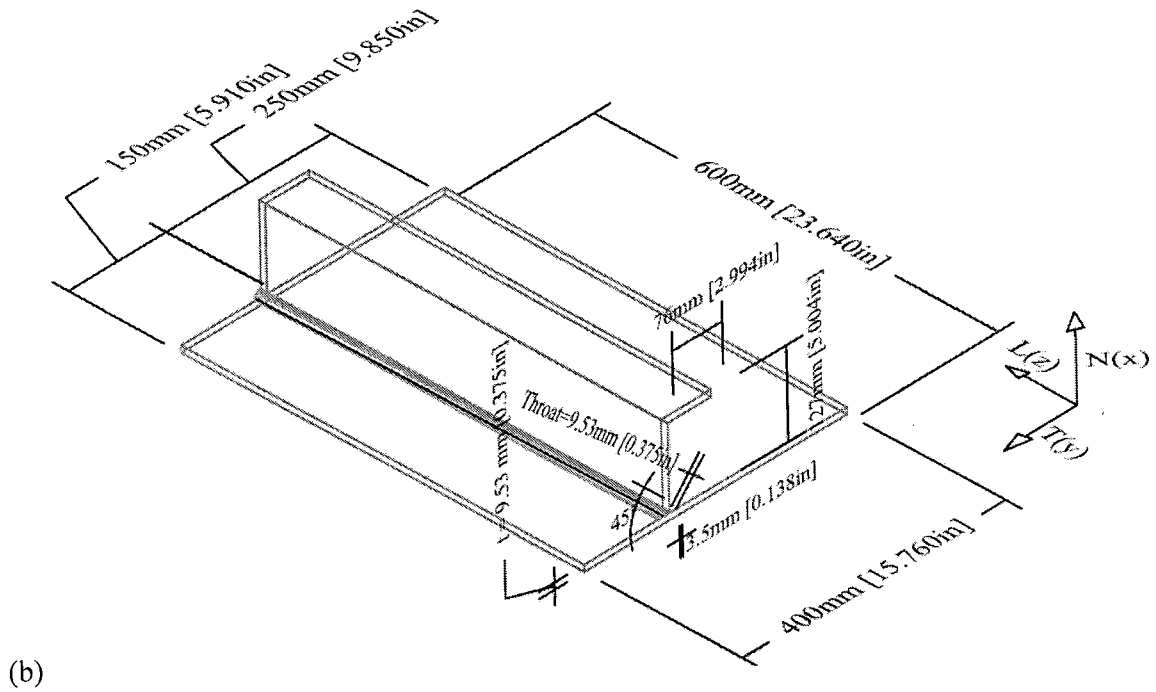
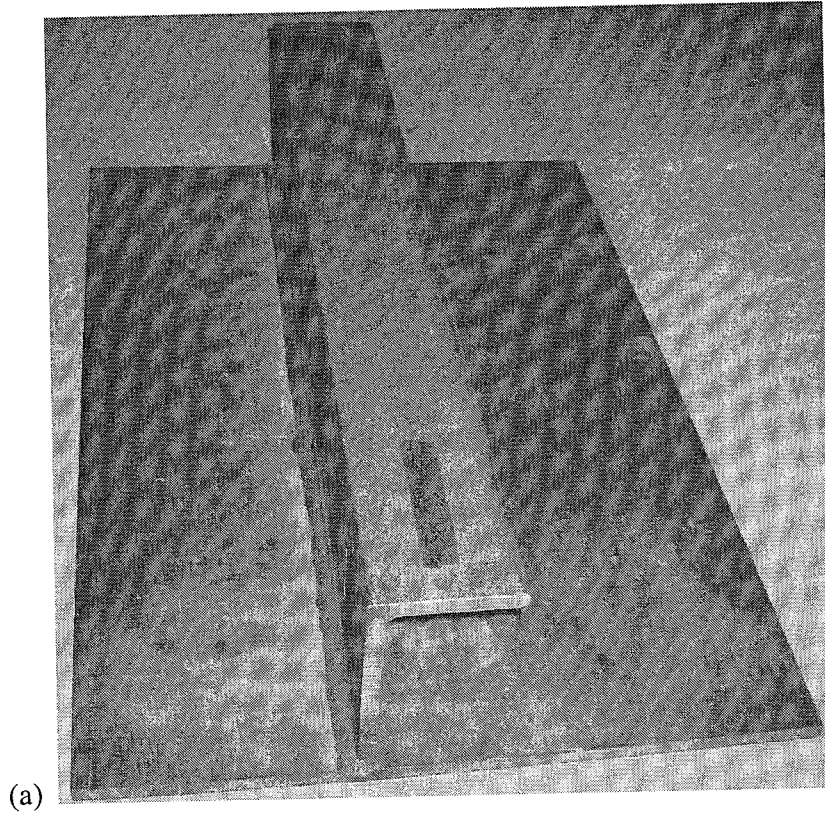


Figure 4.2: Specimen 2 (a) Photo (b) Sketch

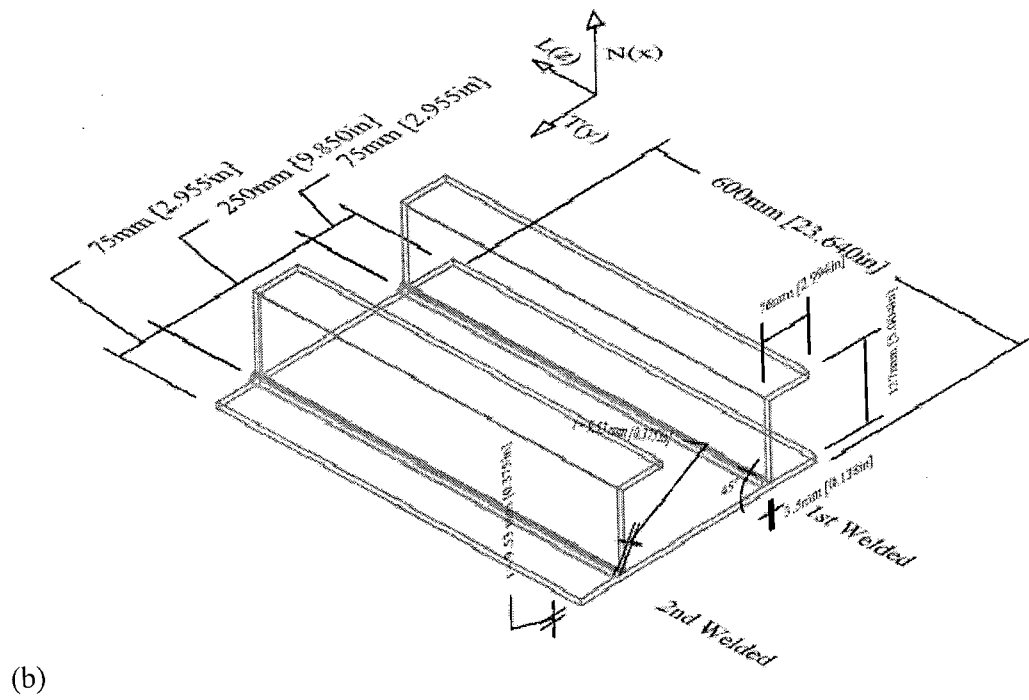
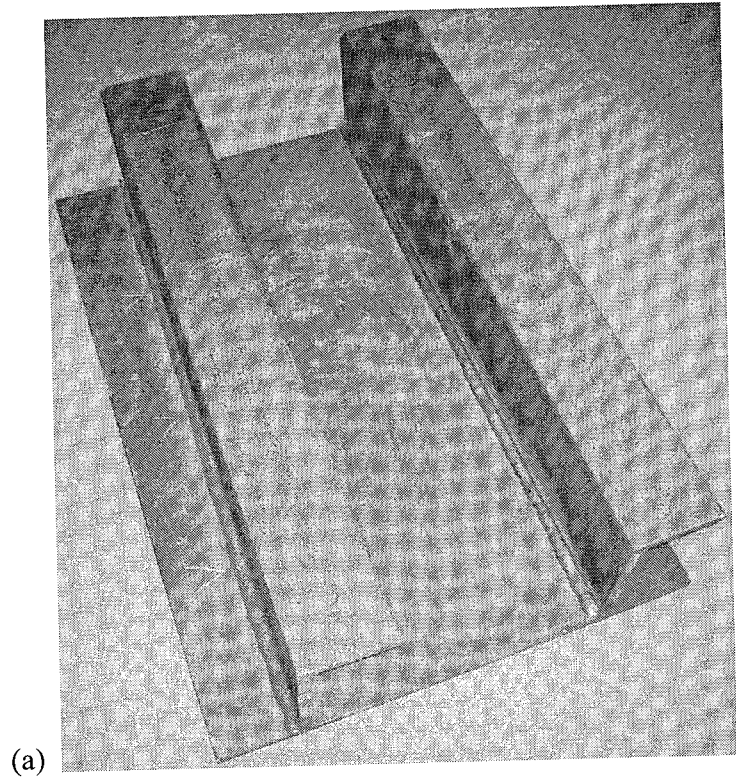


Figure 4.3: Specimen 3 (a) Photo (b) Sketch

4.2 Test Set-up

Neutron diffraction (ND) method was used to measure all the three normal stress components and measurements were carried out on L3 Spectrometer at the Chalk River Laboratories (CRL), Canada. The test set-up was required to be changed and adjusted for each specimen and for measurements of each stress component since the specimen dimensions were very large. As a result, the time required for stress measurements for the three specimens was almost three times of what was originally estimated. The test set-up required specialized skills and careful attention. Detailed discussion on ND method is provided in Chapter 2.

The centre of rotation of the mounting platform was located by moving the horizontal plane (X and Y components) as well as rotating the ψ angle (angle between the neutron beam and the detector). The centre of rotation is found in order to align the incident and scattered slits for alignment of the specimen. It is not possible to identify the exact location of the measurements if proper alignment is not ensured.

There are two telescopes that were used to align the centre of rotation. The first telescope called the “tilted telescope” is used to sight the y-centre (Figure 4.4) and the second telescope called the “level telescope” is used to sight the x-centre (Figure 4.5). In order to align each of these telescopes properly a wire is mounted, driven, and rotated until the telescopes are aligned. Once the centre is found the values are preset to zero and a plumb bob is adjusted to coincide with the centre as well. This plumb bob was used as a back-up for centering in case the telescopes were accidentally knocked out of place during measurements. The rotation of ψ (angle between the neutron beam and the detector) is adjusted to centre as well as the incident and detector slit positions. (International Organization for Standardization, 2001)

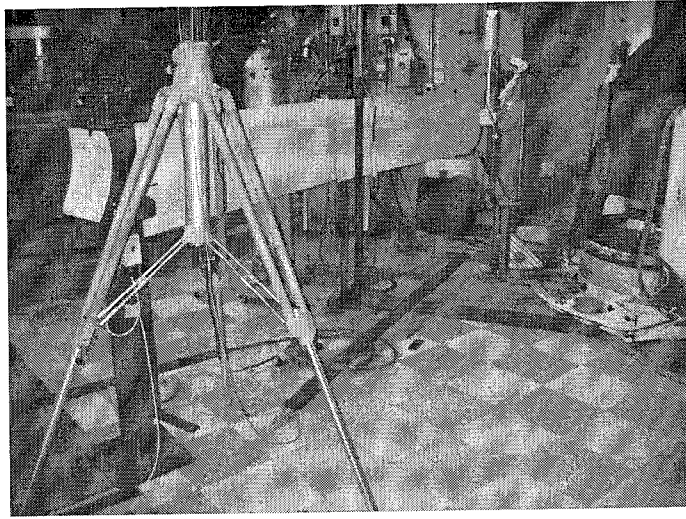


Figure 4.4: Tilted telescope aligned to y-centre

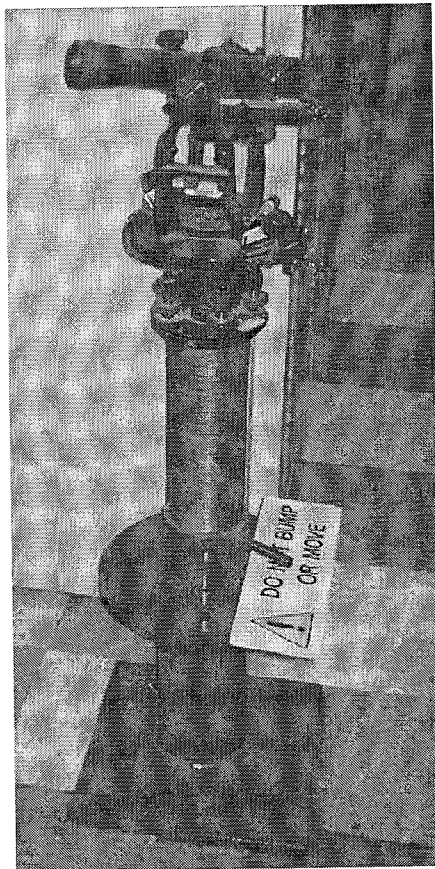


Figure 4.5: Level telescope aligned to x-centre

A computer software program called “powder” was used to determine the initial wavelength (λ). For steel with its main component BCC phase has numerous Miller indices; the program calculates the optimal wavelength for the material to be measured. The monochromating crystal that was used in this study is Germanium (Ge) and its optimal reflection angle was calculated once the wavelength was chosen.

Two different set-ups and several scattering slit sizes were used. The specifications of each set-up are shown in Table 4-B. The second set-up was necessary when the plate specimen was positioned for the 45° longitudinal strain measurement since in this orientation the neutron counts were very low. By changing the wavelength (λ) and subsequently, the reflection of the monochromating crystal ($2\theta_M$) and ψ angle it was possible to continue the scans at a relatively faster rate. The scattering slit size also varied throughout the specimens from as small as 1 mm x 1 mm x 2 mm to as large as 1.5 mm x 1.5 mm x 20 mm. The count times for each measurement were optimized to collect the required amount of data in a shorter amount of time, given that there were so many measurement points where the stresses were required to be collected across all of the specimens.

Table 4-B: Set-up Specifications

Set-up	Wavelength	Reflection of Ge crystal	$2\theta_M$	Ψ
1	1.6650 Å	115	98.93°	-44.9°
2	1.5398 Å	11 $\bar{5}$	90°	-41.4°

4.3 Stress-free Reference Samples and Nickel Calibration

The stress-free reference samples for the plate were produced on-site at the CRL. Three small “matchstick” prisms were cut, with the longest dimension in the longitudinal direction of the plate specimens, as shown in Figure 4.6. The first reference sample had dimensions of 2 mm x 2.5 mm x 20 mm (Normal x Transverse x Longitudinal). The second reference sample was shorter than the first one. However, the second specimen was also parallel to the longitudinal axis of the plate with dimensions of 2 mm x 2.5 mm x 15 mm (Normal x

Transverse x Longitudinal). The third reference sample was cut perpendicular to the longitudinal axis with dimension of 2 mm x 10 mm x 2.5 mm (Normal x Transverse x Longitudinal).

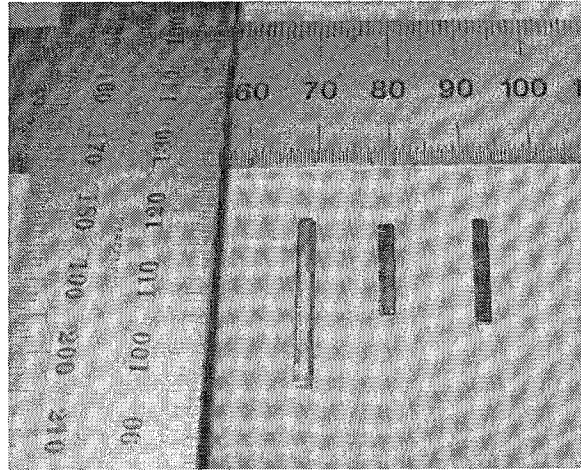


Figure 4.6: Stress-free reference samples

The nickel calibration is a small cadmium container filled with nickel powder, as shown in Figure 4.7. The nickel calibration values were used in all of the final stress value calculations. The angle between the incident beam and the refracted beam is φ and the φ_0 is the angle corresponding to the reference sample. The values of λ and φ_0 , as well as their error values, were found using a standard deviation and chi-squared fit. The nickel calibration was completed at the beginning and end of each set-up to ensure consistency in the numbers throughout the entire set of measurements. The values for λ and φ_0 were specific to one test set-up and for a specific value of $2\theta_M$.

4.4 Residual Stress Mapping

The neutron diffraction method was carried out to determine the three-dimensional stress distributions for all the three specimens. Examples of some of the raw data collected are shown in Appendix A.

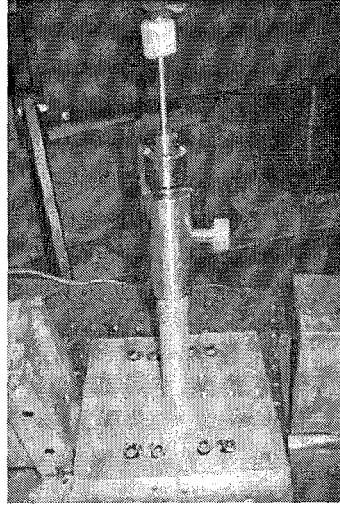


Figure 4.7: Nickel-reference sample in cadmium container

4.4.1 Neutron Diffraction Method

The neutron diffraction method is outlined in the Literature Review (Chapter 2) and the method is used here to calculate the residual stress values. The d-spacing and the error in d-spacing (μ d-spacing) values are calculated by comparing the φ value to the φ_0 values, shown in Equations 4.1 and 4.2, respectively. The strain components were calculated by comparing the d-spacing to the stress-free reference d-spacing using Equation 4.3 and the error in the strain ($\mu\varepsilon$) values compares the d-spacing with the d-spacing error shown in Equation 4.4.

$$d\text{-spacing} = \left| \frac{\lambda}{2 \sin\left(\frac{\varphi - \varphi_0}{2}\right)} \right| \quad (4.1)$$

$$\mu d\text{-spacing} = \left| \frac{\lambda}{2 \sin\left(\frac{\varphi - \varphi_0 + \mu\varphi}{2}\right)} \right| - (d\text{-spacing}) \quad (4.2)$$

$$\varepsilon = \left(\frac{d\text{-spacing}}{d_0} - 1 \right) \times 1000000 \quad (4.3)$$

$$\mu\varepsilon = \left(\frac{\mu d\text{-spacing}}{d\text{-spacing}} \right) \times 1000000 \quad (4.4)$$

4.4.1.1 Specimen 1

Specimen 1 as shown in Figure 4.8 was a plane plate with dimensions of 400 mm long (L) x 400 mm wide (T) x 9.5 mm thick (N). No stiffener was welded on this specimen. The objective was to determine if there were any stresses in the parent plate due to the hot rolling process and the cutting process. The specimen was measured for residual strain along the longitudinal (Z) and transverse (Y) directions at seven depths through the normal (X) direction. Figure 4.8 shows the origin (point 1) and the lines (1-2 and 1-3) on which the measurements were taken. All the three strain components were measured to calculate all three stress components.

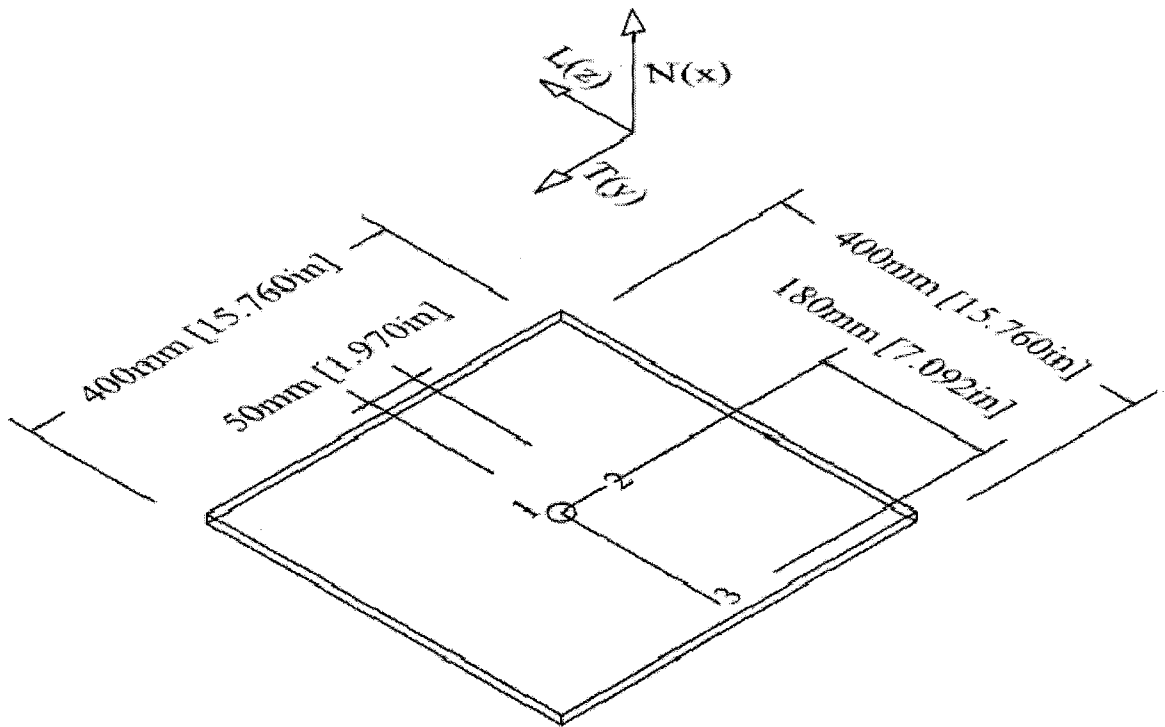


Figure 4.8: Detail for measurement points for Specimen 1

4.4.1.1.1 Normal Stress for Specimen 1

The normal stresses are calculated using Equation 4.5.

$$\sigma_{Normal} = \frac{E}{1+\nu} \left(\varepsilon_{Normal} + \frac{\nu}{1-2\nu} (\varepsilon_{Normal} + \varepsilon_{Transverse} + \varepsilon_{Longitudinal}) \right) \quad (4.5)$$

where,

E = modulus of elasticity

ν = Poisson's ratio = 0.3

ϵ = the strain value for a particular component

The normal stress is the stress component in the direction through the plate thickness (in the direction of N or X in Figure 4.8) and they were measured at 10 mm intervals along the transverse direction (T or Y) for 50 mm length from the centre of the plate (that is, along line 1-2) and at 20 mm, 40 mm, and 60 mm intervals along the longitudinal direction (L or Z) for 180 mm length from the centre of the plate (that is, along line 1-3). The measurements were taken at seven depths through the thickness of the plate (N or X) at each measurement point. Therefore, a total of 77 (=7 x 11) measurements were acquired for 11 (5 in transverse or Y direction + 5 in longitudinal or Z direction + origin) measurement points.

The normal stresses on lines 1-2 and 1-3 are shown in Figures 4.9 and 4.10, respectively. In these figures each line shows the stress levels through the depth of plate at a specific distance from the origin (point 1 in Figure 4.8). Each line shows how the normal stress component (stress component in the direction of X or N in Figure 4.8) at a particular measurement point changes through the depth (thickness) of the plate specimen. For example, the line shown with no marker in Figure 4.9 represents the normal stress value at a point which is 10 mm away from the centre (Point 1) of the plate specimen and along line 1-2 (Figure 4.8). Figures 4.11 and Figure 4.12 show three-dimensional views of the normal stresses in the transverse and longitudinal directions, respectively. It can be seen that the first measurement point was at 0.6 mm below the top surface of the plate and the last measurement point was at 8.4 mm below the top surface or 1.1 mm above the bottom surface of the plate.

The normal stresses show a consistent nature across the plate in both the transverse and longitudinal directions. The stress values range from -42 MPa to +78 MPa, though in most cases it was between -20 MPa and +30 MPa and are mostly within the error bars of each other.

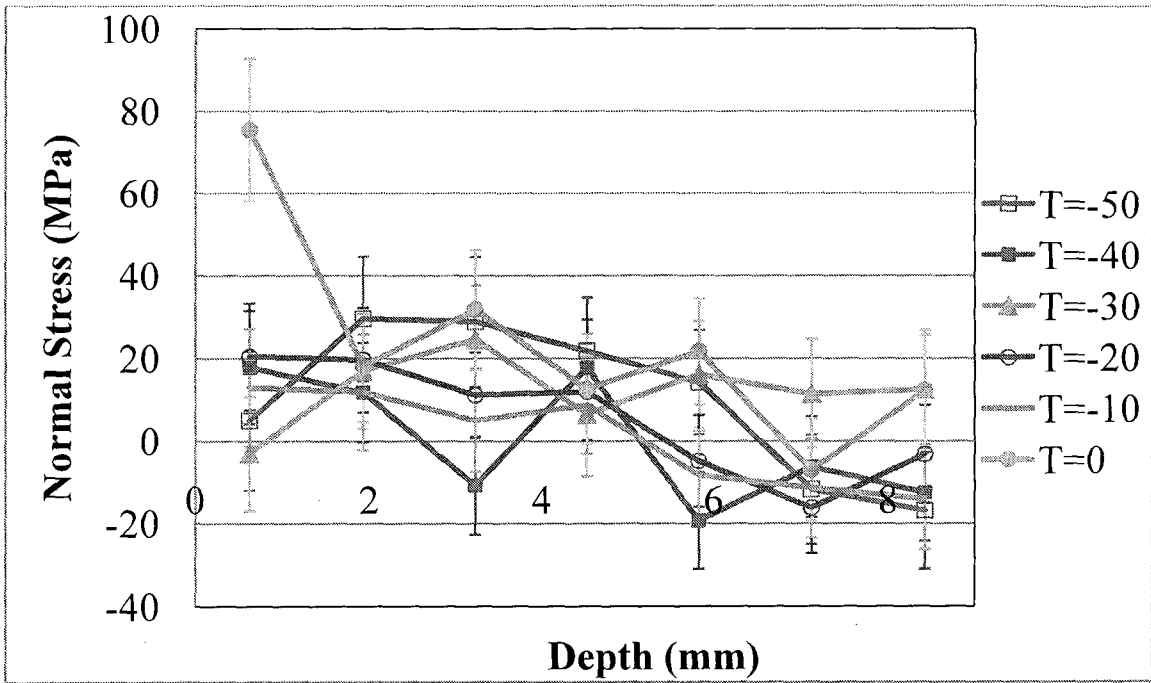


Figure 4.9: Normal stress at various depths in transverse (T or Y) direction (line 1-2)

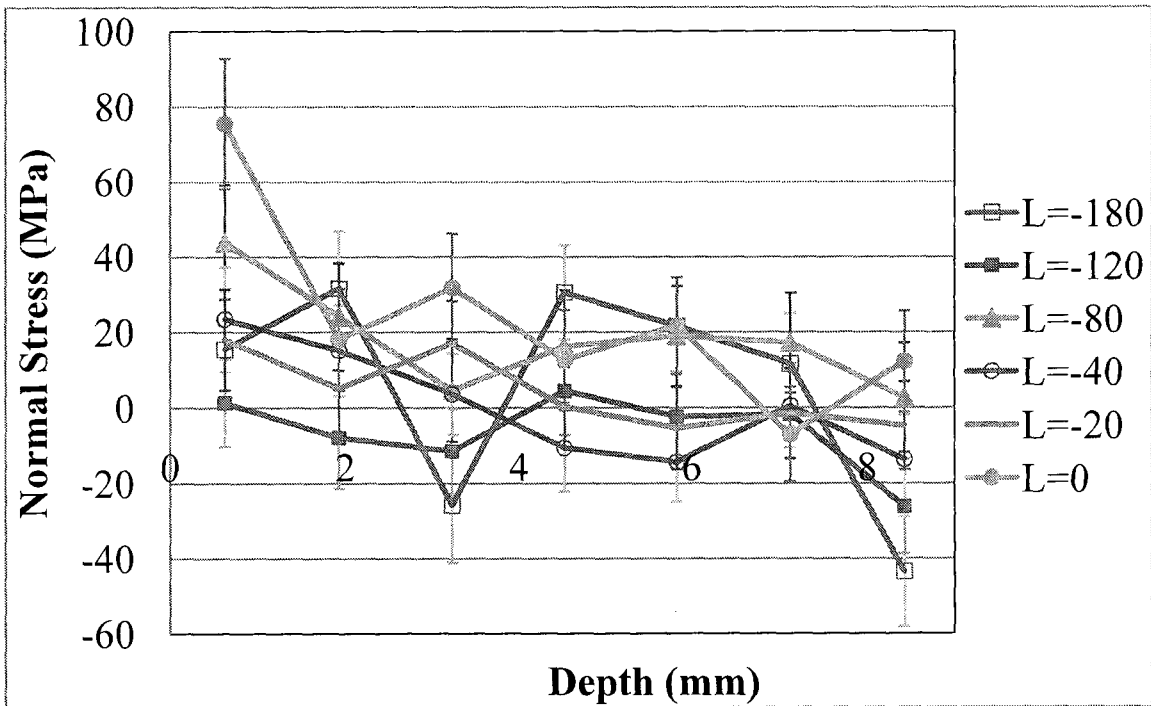


Figure 4.10: Normal stress at various depths in longitudinal (L or Z) direction (line 1-3)

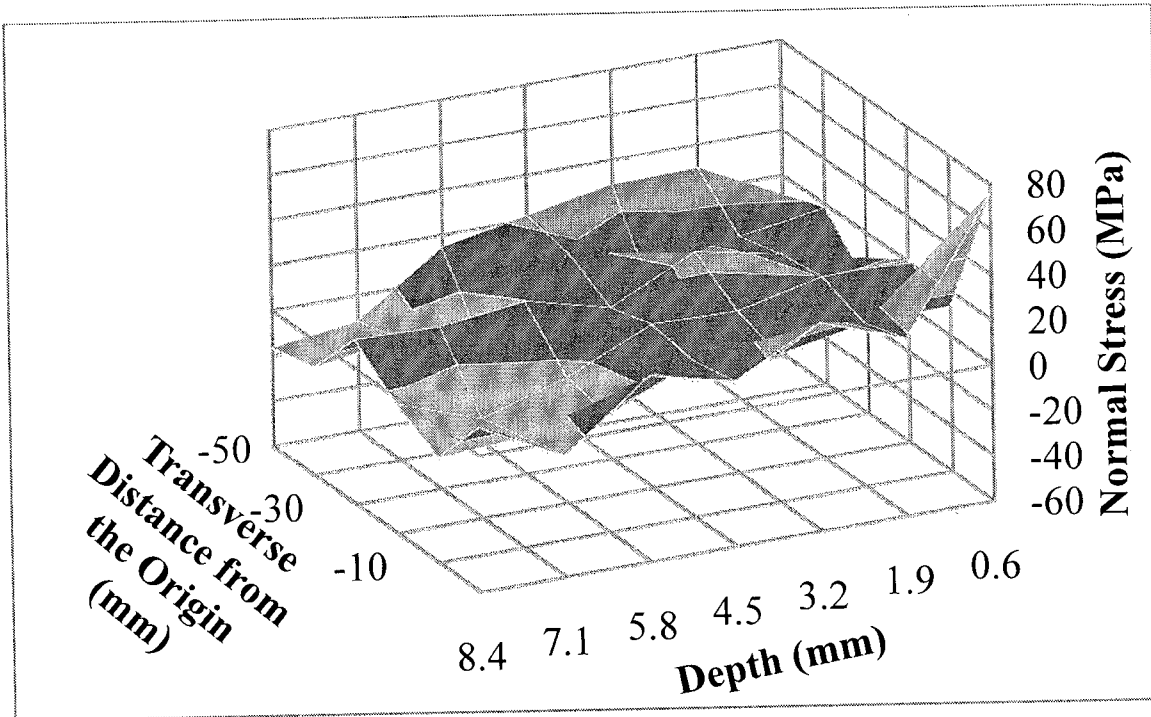


Figure 4.11: 3-D view of normal stress distribution in transverse (T or Y) direction

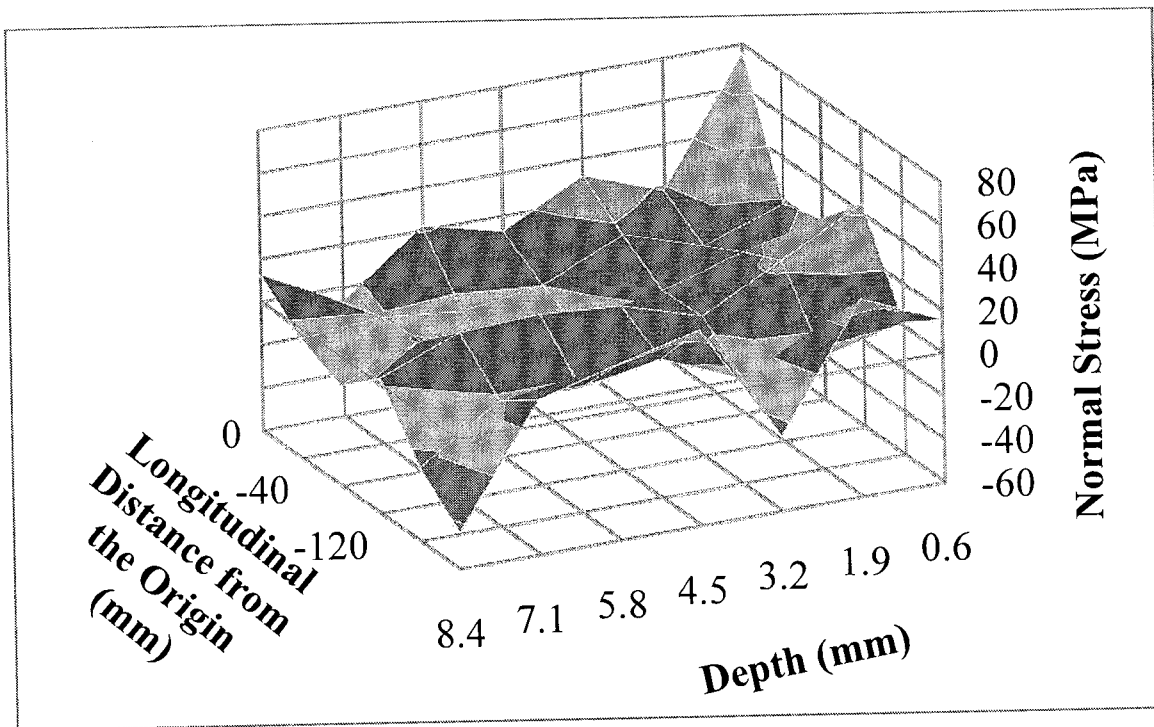


Figure 4.12: 3-D view of normal stress distribution in longitudinal (L or Z) direction

4.4.1.1.2 Transverse Stress from Specimen 1

The transverse stresses are calculated using all three strain components using Equation 4.6.

$$\sigma_{Transverse} = \frac{E}{1+\nu} \left(\varepsilon_{Transverse} + \frac{\nu}{1-2\nu} (\varepsilon_{Normal} + \varepsilon_{Transverse} + \varepsilon_{Longitudinal}) \right) \quad (4.6)$$

The transverse stress is the stress in the direction of what would be perpendicular to the stiffener if there was a stiffener on this plate (direction T or Y in Figure 4.8). The stress measurements for transverse component were acquired at the same measurement points as were acquired for the normal component, that is at 10 mm intervals along the transverse direction (line 1-2) and up to a distance of 50 mm from the centre (point 1) of the plate and at 20 mm, 40 mm and 60 mm intervals along the longitudinal direction (line 1-3) and up to a distance of 180 mm from the centre (point 1) of the plate. The measurements were taken at seven depths through the thickness of the plate at each point thus, a total of 77 (= 7 x 11) measurements were obtained.

One dimensional distributions for the transverse stress component on lines 1-2 and 1-3 are shown in Figures 4.13 and 4.14, respectively. Each line shows the stress levels through the depth of plate at a specific measurement point. Figures 4.15 and 4.16 show three-dimensional distributions of the transverse stress component in the transverse (T or Y) and longitudinal (L or Z) directions, respectively.

The transverse stress distributions show a clear and consistent pattern through the thickness (along N or X) of the plate. It can be seen that the transverse stress value changes its sign from positive to negative, then from negative to positive and finally, to negative again as the depth of the plate increases. The maximum negative value of transverse stress is at about 3 mm below the top surface and the maximum positive stress value is at about 6 mm from top surface. The change in transverse stress values through the thickness of the plate indicates that the parent plate had a locked-in bending stress in the transverse direction and it may have happened due to the rolling process of plate production.

A cold cut method called “water-jet cut” was used in this study and it is assumed that this did not introduce any additional stresses. The range of stresses in the transverse component also

have a broader range than the normal stresses from roughly -110 MPa to +80 MPa. The error bars are not shown on these Figures since the results are reasonably consistent. There are a few points that do seem to vary from most of the others, however, they are still within the error limit.

The three-dimensional distributions (Figures 4.15 and 4.16) show a better representation of the bending stress in the transverse and longitudinal directions through the depth. These Figures also show the changes in maximum negative and positive stresses along both the transverse (T or Y) and longitudinal (L or Z) directions. It is observed that the transverse stress value at a specific measurement depth (at a specific depth in the N or X direction) does not change much with the change in distance from the origin in the transverse (Y) or longitudinal (Z) direction.

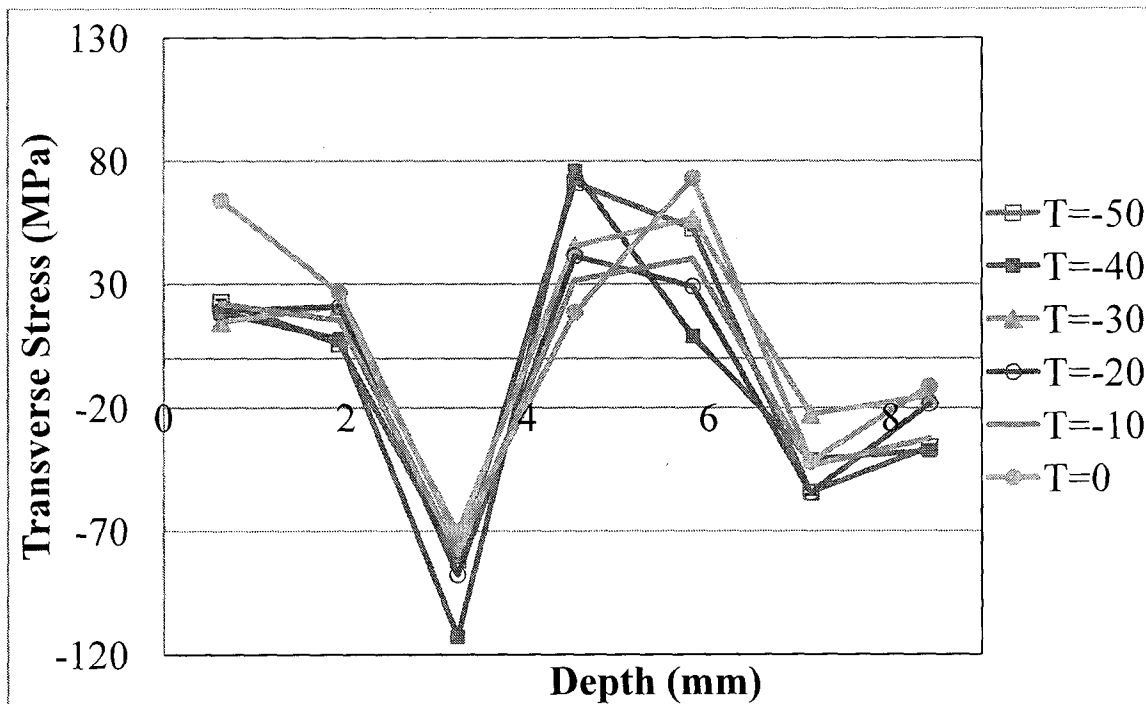


Figure 4.13: Transverse stress at various depths in transverse (T or Y) direction (line 1-2)

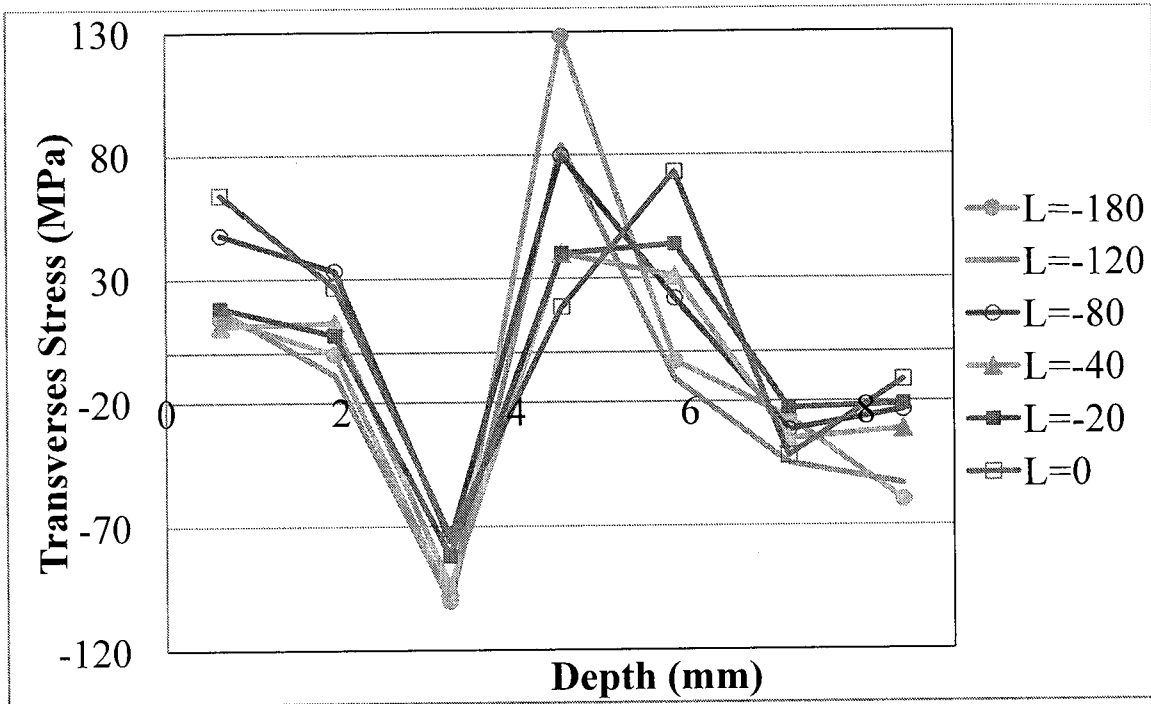


Figure 4.14: Transverse stress at various depths in longitudinal (L or Z) direction (line 1-3)

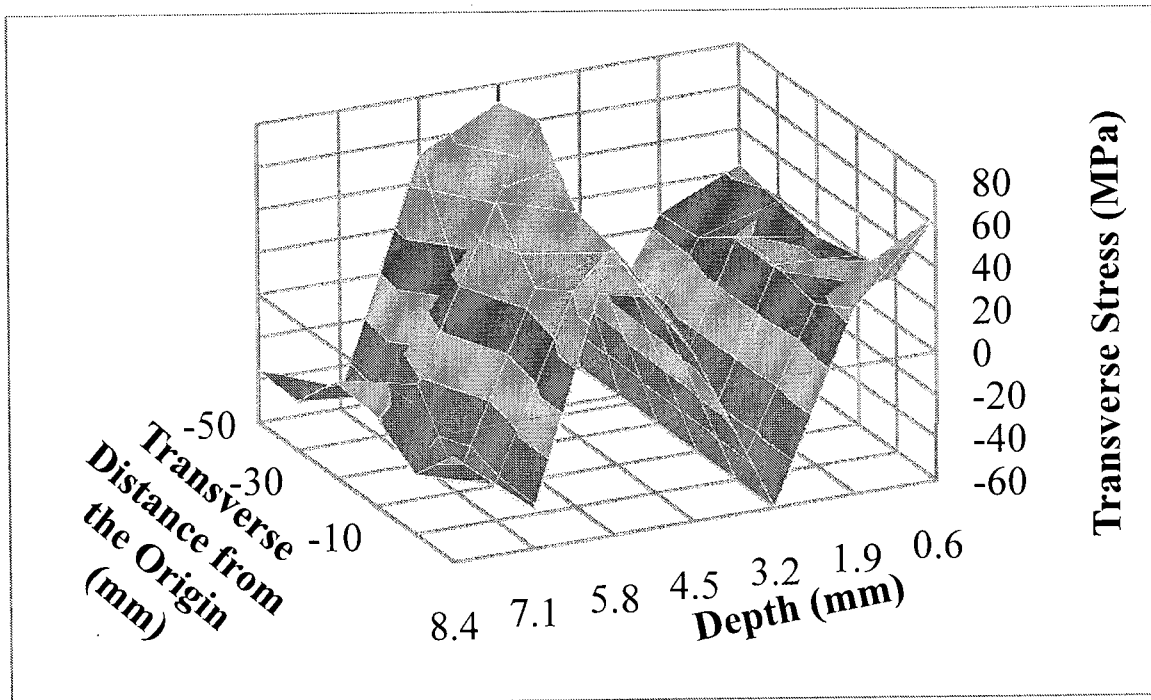


Figure 4.15: 3-D view of transverse stress distribution in transverse (T or Y) direction (line 1-2)

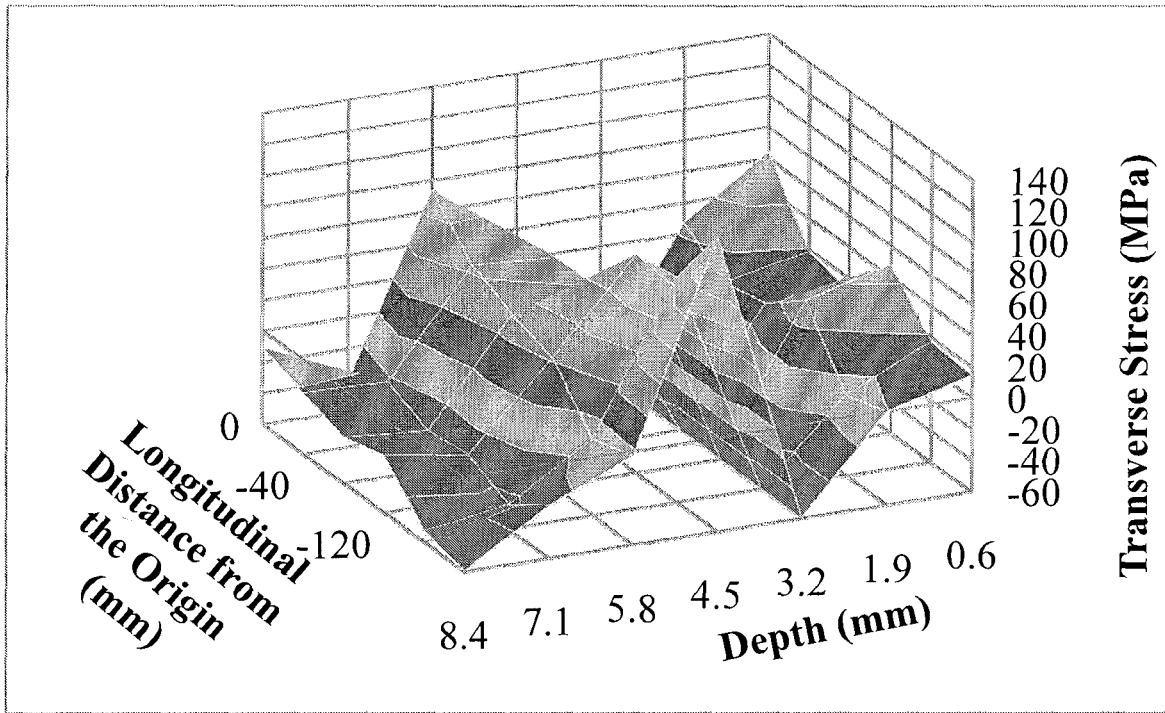


Figure 4.16: 3-D view of transverse stress distribution in longitudinal (L or Z) direction (line 1-3)

4.4.1.1.3 Longitudinal Stress from Specimen 1

The longitudinal stresses are calculated using Equation 4.7.

$$\sigma_{Longitudinal} = \frac{E}{1+\nu} \left(\epsilon_{Longitudinal} + \frac{\nu}{1-2\nu} (\epsilon_{Normal} + \epsilon_{Transverse} + \epsilon_{Longitudinal}) \right) \quad (4.7)$$

The longitudinal stress is the stress in the direction of what would be parallel to the stiffener (direction along L or Z in Figure 4.8) if there was a stiffener on this plate. The stress measurements were taken at the same measurement points along lines 1-2 and 1-3 in Figure 4.8 as was done for the other two stress components that is at 10 mm intervals along the transverse direction (line 1-2) and until 50 mm from the centre (point 1) of the plate and at 20 mm, 40 mm, and 60 mm intervals along the longitudinal direction (line 1-3) and until 180 mm from the centre (point 1) of the plate (see Figure 4.8). The measurements were taken at seven depths through the thickness (in N or X direction) of the plate at each point, for a total of 77 points (11 locations x 7 depths).

Figures 4.17 and 4.18 illustrate one-dimensional distributions of longitudinal stresses for Specimen 1. Three-dimensional longitudinal stresses are shown in Figures 4.19 and 4.20.

The longitudinal stresses show a consistent and similar pattern as was found for transverse stress distribution. (Please compare Figure 4.17 with Figure 4.13 and compare Figure 4.18 with Figure 4.14). Therefore, it is obvious that a bending stress in the longitudinal direction as well was created during the rolling process of the plate. The maximum negative (compression) longitudinal stress was found at 3 mm below the top surface of the plate and the maximum positive (tension) longitudinal stress was found at 6 mm below the top surface of the plate. The range of longitudinal stress values were found to be between -40 MPa to +90 MPa. The error bars are not shown on these plots because a consistent pattern in stress distribution is found. The variance of the points is still close to within the error limits.

The three-dimensional distributions (Figures 4.19 and 4.20) also show the bending stress through the depth as well as the shallower maximum and minimums along the plate in both the transverse (T or Y) and longitudinal (L or Z) direction, similar to the transverse stress distribution.

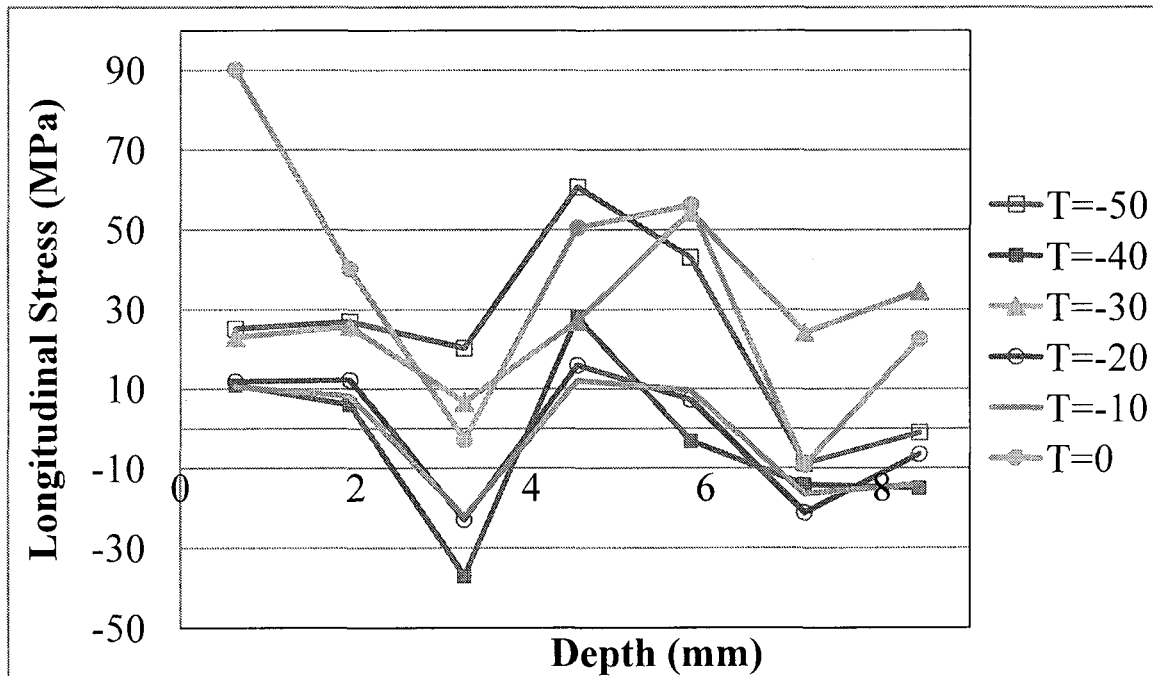


Figure 4.17: Longitudinal stress at various depths in transverse (T or Y) direction (line 1-2)

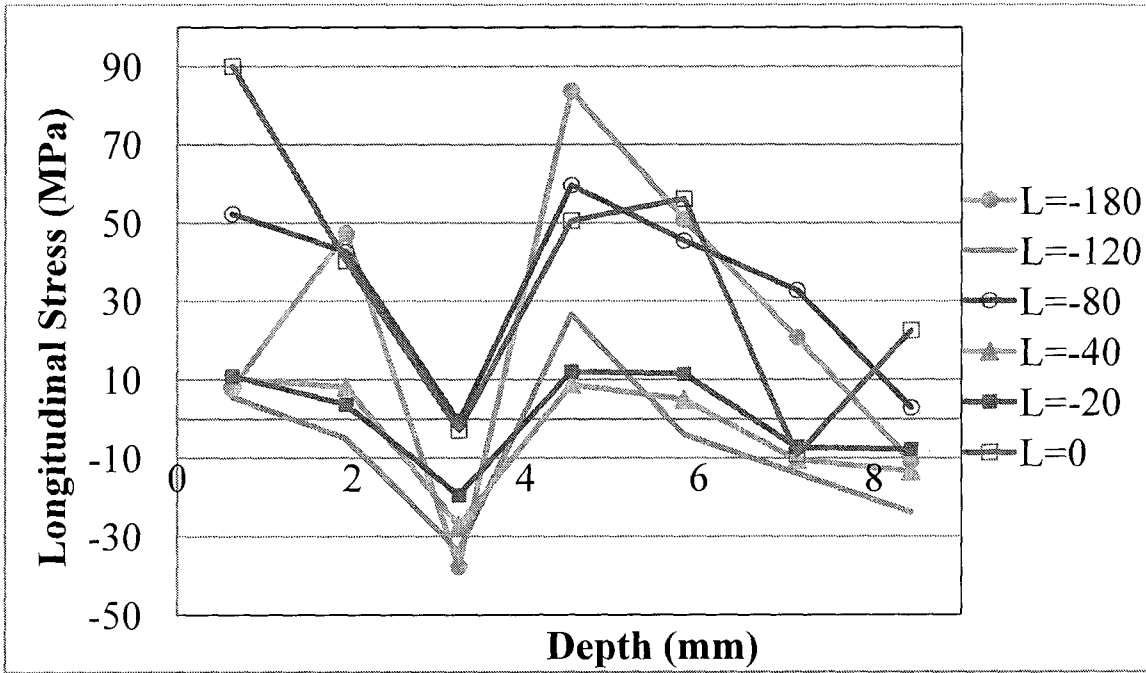


Figure 4.18: Longitudinal stress through depth in longitudinal (L or Z) direction (line 1-3)

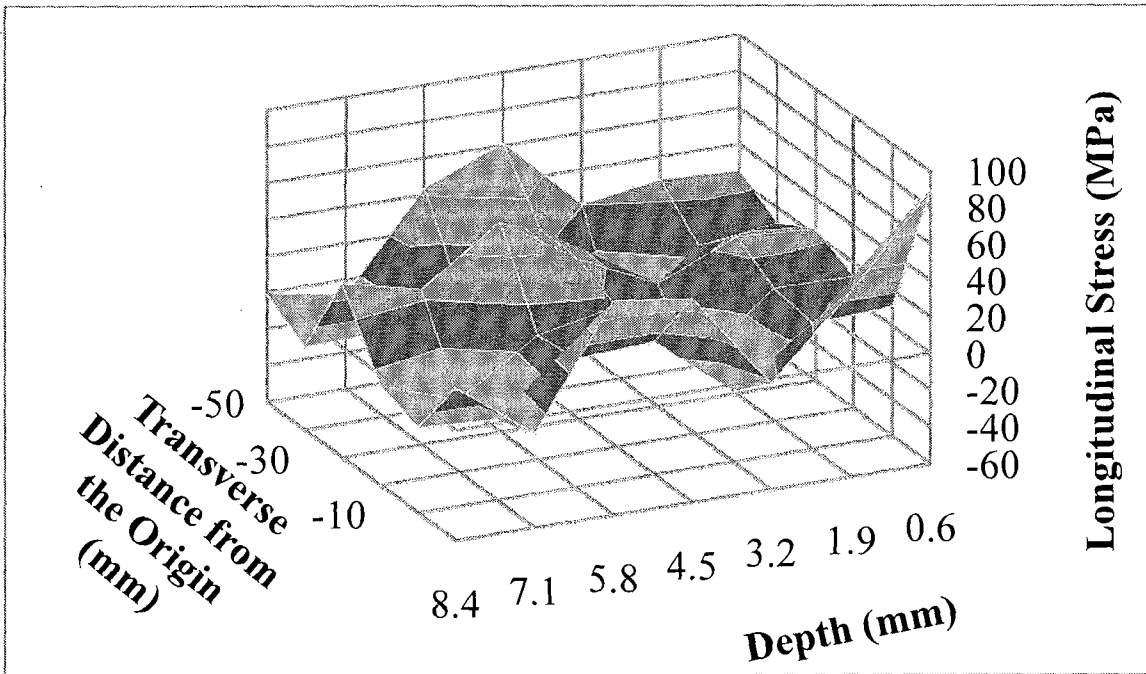


Figure 4.19: 3-D view of transverse stress distribution in transverse (T or Y) direction (line 1-2)

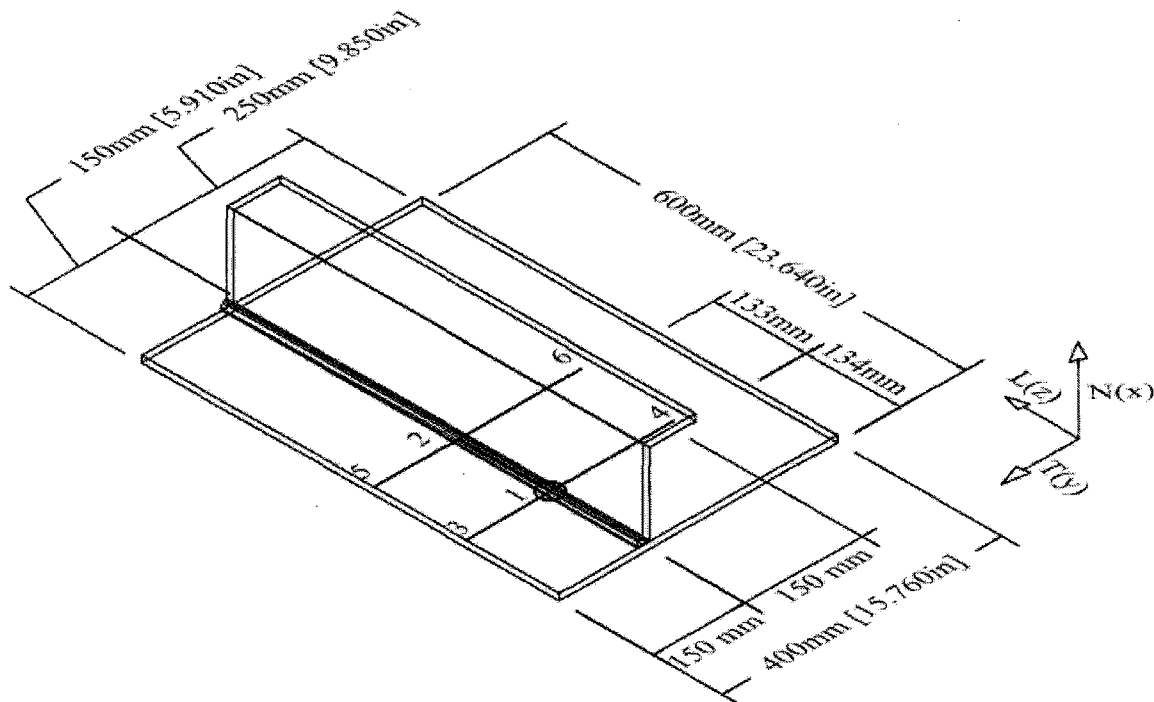


Figure 4.21: Detail for measurement points for Specimen 2

4.4.1.2.1 Normal Stress for Specimen 2

The normal stresses (σ_x or σ_{normal}) are calculated using all three strain components as shown in Equation 4.5. The normal stress was measured along the transverse direction until 150 mm on either side of the stiffener (line 3-4 and line 5-6) and 133 mm along the weld centreline (line 1-2) in the longitudinal direction (Figure 4.21).

As mentioned in Section 3.3 (Table 3-C), the welding for this specimen could not be completed in a single non-stop run. The welding was stopped once and restarted after one minute at point 2 in Figure 4.21. The stop and start caused the weld overlap at that point. The distance of 133 mm ($z = 133$ mm) was chosen based on the location of a stop and start (point 2 in Figure 4.21) in the welding process. The location of the origin (point 1 in Figure 4.21) was chosen at the mid-length between point 2 and the edge of the plate such that edge effects and weld inconsistencies (stop and start in welding) are minimized. The spacing of the measurements was as small as 1 mm near the centre of the weld and gradually increased up to 40 mm further away from the weld in the transverse direction, as shown in Figure 4.22. For line 3-4, the measurements were taken at seven depths of the plate (through N or X axis)

along the transverse (Y) direction at 31 locations, for a total of 217 ($=31 \times 7$) measurement points. Measurements on line 5-6 (at $z = 133$ mm in Figure 4.21) were also acquired at 31 locations as was acquired for line 3-4 but at three depths for a total of 93 ($=31 \times 3$) measurement points. The measurements along the weld centreline (line 1-2) were only taken at one depth (at $N = X = 8.9$ mm) that is near the welded surface of the plate since it was found that the normal stress component does not change much through the thickness of the plate and the depth closest to the welded stiffener is of most interest. However, these stress values showed changes at points where weld was not uniform or welding was interrupted such as at point 2, where welding was stopped and started. These measurements were taken at seven points plus at other two points at $z = 0$ mm (point 1) and $z = 133$ mm (point 2). The total number of measurements taken on this specimen is 317 points ($= 217 + 93 + 7$).

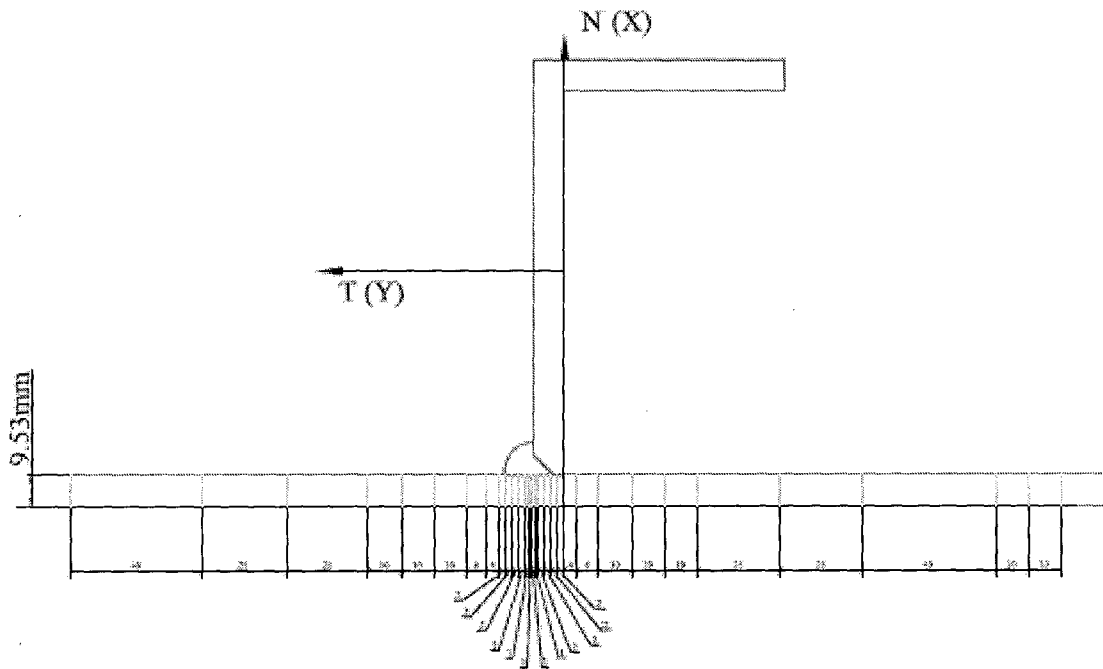


Figure 4.22: Measurement spacing in the transverse direction (mm)

One dimensional distributions for normal stresses (σ_x or σ_{normal}) for lines 3-4 (at $z = 0$ mm) and for line 5-6 (at $z = 133$ mm) are shown Figures 4.23 and 4.24, respectively. Each line shows the variation in normal stress through the cross-section or depth (depth, N) of the plate at a specific distance from the origin (point 1 in Figure 4.21). It should be noted that a

different graphical representation is shown for this stress component, as compared to the Figures for Specimen 1. For example in Figure 4.23, the line with the open squares shows the stress levels at 1.1 mm from the bottom face (the face of the plate with no stiffener) of the plate and the line with crosses shows the stress values closest to the surface of the pate with stiffener. Figure 4.24 shows the same distribution for normal stress but for line 5-6 (at $z = 133$ mm). Only three measurements along the depth were obtained to reduce the beam time. The three-dimensional stress plots are not shown for this stress component since they do not provide any valuable information.

Like Specimen 1, the distributions for normal stress do not show any specific pattern and this is primarily due to the nature of pre-existing locked-in normal stresses in the parent plate that may have developed from the rolling process. The stress values range from about -75 MPa to +150 MPa, with the maximum value near the weld centreline. These values are nearly double the values found in the parent plate, that is, Specimen 1 (Specimens 1 had the stress values in the range of -40 MPa to +80 MPa).

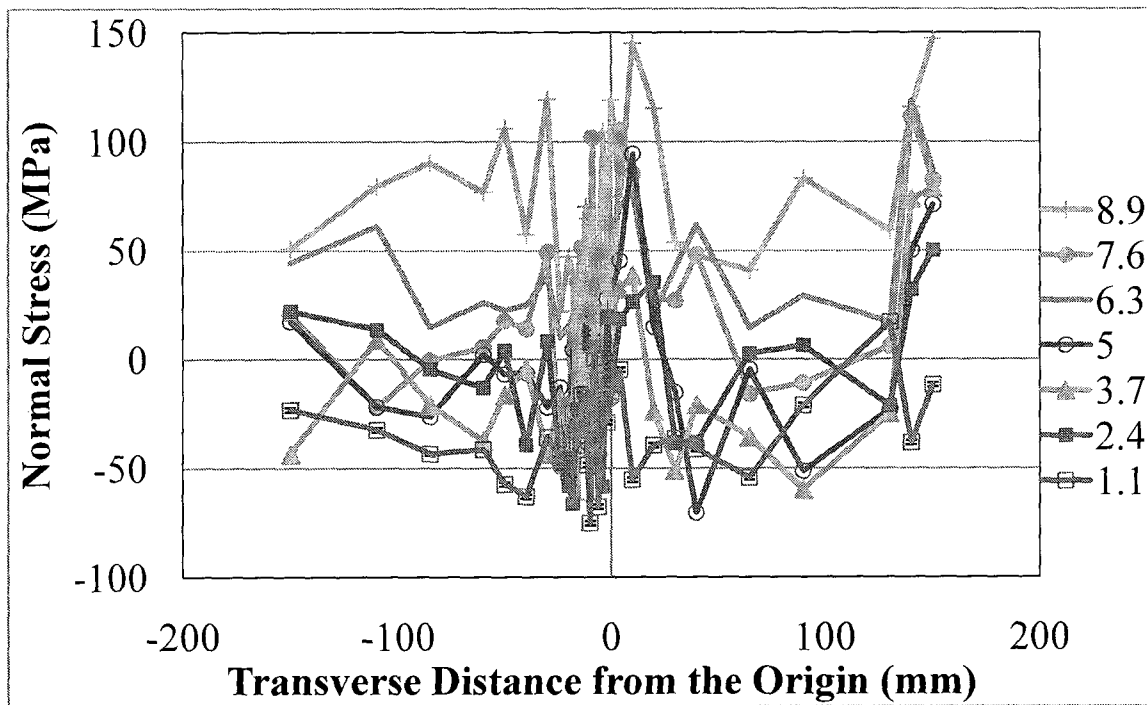


Figure 4.23: Normal stress at various depths in transverse (T or Y) direction (at $z = 0$ mm, line 3-4)

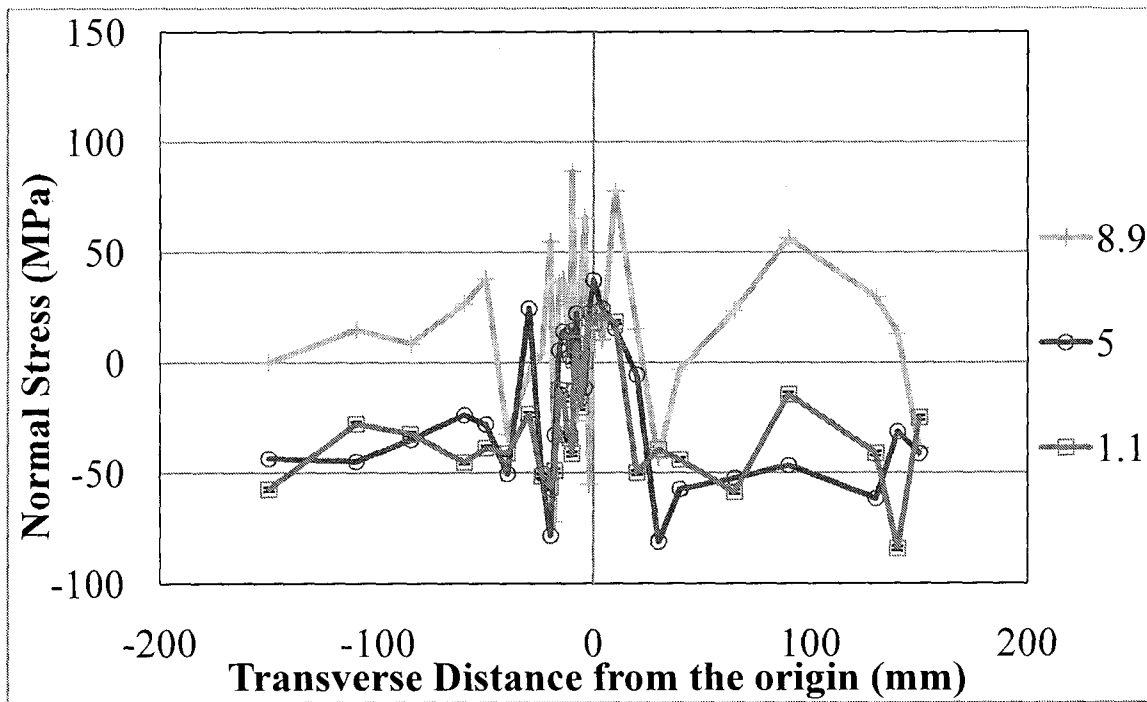


Figure 4.24: Normal stress at various depths in transverse (T or Y) direction (at $z = 133$ mm, line 5-6)

4.4.1.2.2 Transverse Stress for Specimen 2

The transverse stresses (σ_y or $\sigma_{\text{transverse}}$) are calculated using Equation 4.6 and measured at the same points where the normal stress component was measured (Figure 4.21). The measurement points are shown in Figure 4.22. Like the measurements for the normal stress component, transverse stress was also measured at seven depths on line 3-4 (at $z = 0$ mm) and at three depths on line 5-6 (at $z = 133$ mm). The measurements along the weld centreline were only taken at one depth (at $N = X = 8.9$ mm) because it was found that the transverse stress component does not change much through the thickness of the plate and the depth closest to the welded stiffener is of most interest in this study. However, the stress value changes at locations where there were inconsistencies in the weld itself (for example, at $z = 133$ mm, point 2).

One-dimensional distributions for transverse stress are shown Figures 4.25 and 4.26 for line 3-4 (at $z = 0$ mm) and line 5-6 (at $z = 133$ mm), respectively. The three-dimensional stress plots are not shown for this specimen since they do not follow any clear pattern.

The transverse stresses show a pattern with maximum positive (tensile) stress being at the centre of the weld (line 1-2 in Figure 4.21). The stress value on line 3-4 (at $z = 0$ mm) ranges from about -120 MPa to +150 MPa, showing the maximum value around the weld centreline. The stress values on line 5-6 (at $z = 133$ mm) range from roughly -170 MPa to +50 MPa. The difference found on this line as compared to line 3-4 seems to be due to the stop and start of the weld (at $z = 133$ mm, point 2). These values compared with the parent plate (Specimen 1) are nearly 50% higher.

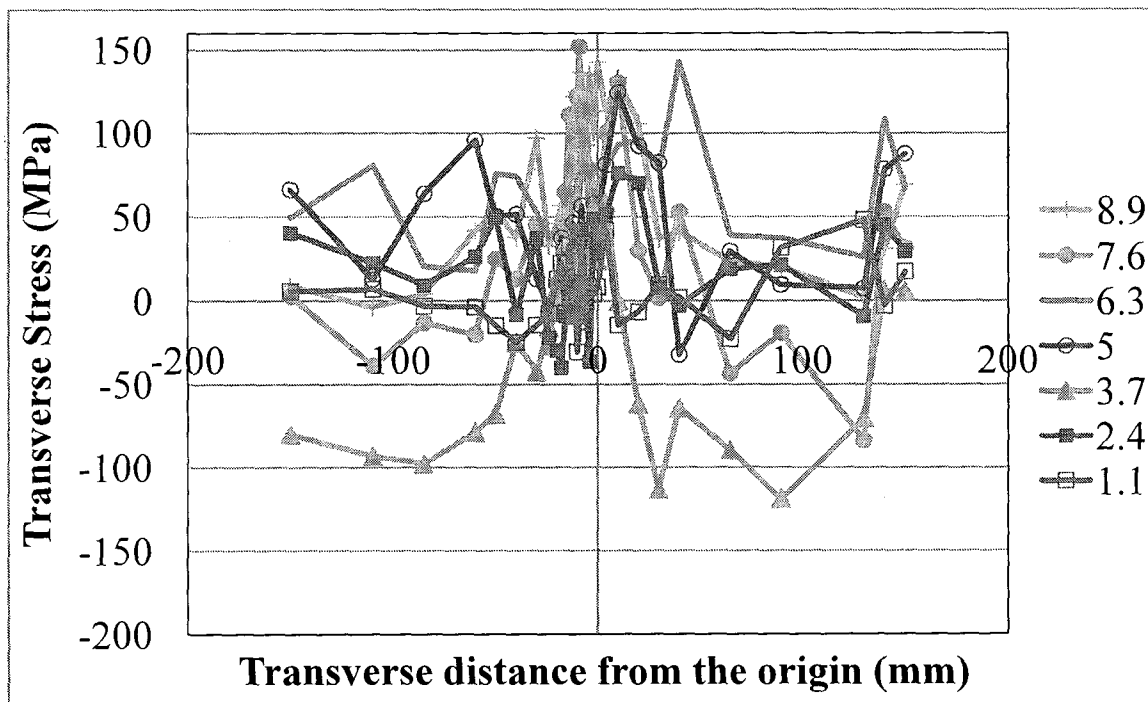


Figure 4.25: Transverse stress at various depths in transverse (T or Y) direction (at $z = 0$ mm, line 3-4)

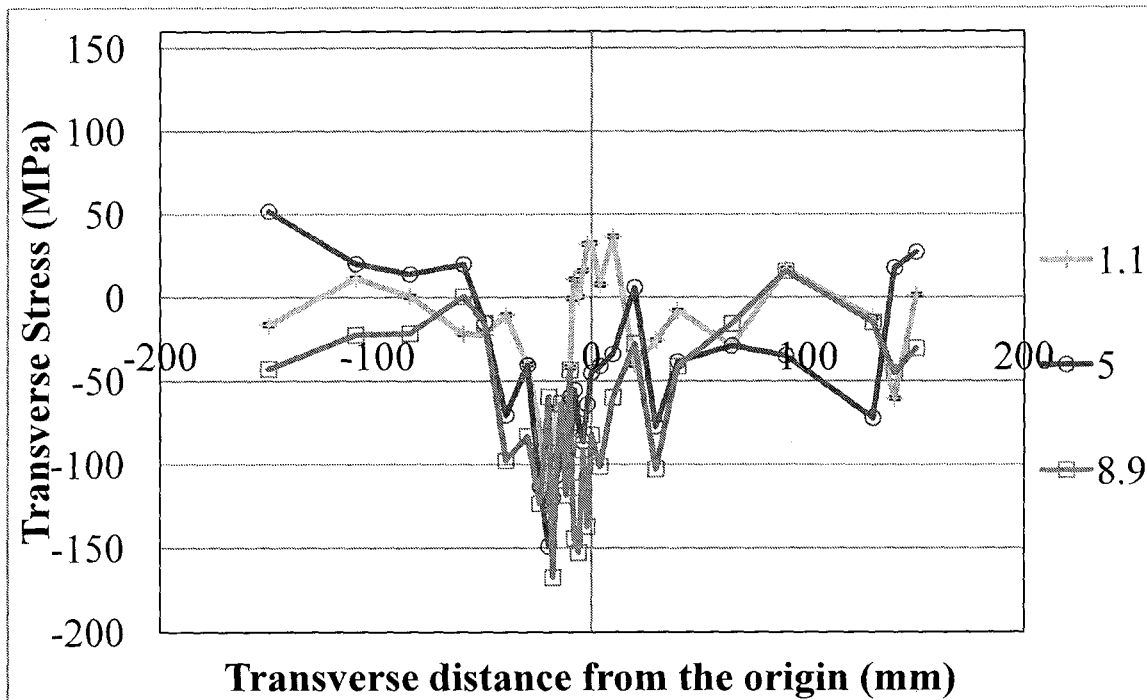


Figure 4.26: Transverse stress at various depths in transverse (T or Y) direction (at $z=133$ mm, line 5-6)

4.4.1.2.3 Longitudinal Stress for Specimen 2

The longitudinal stress (σ_z or $\sigma_{\text{longitudinal}}$) was calculated using Equation 4.7 and were measured at the same points and depths as was done for the other two stress components (Figures 4.21 and 4.22).

Figures 4.27 and 4.28 show one-dimensional distributions for the longitudinal stress for lines 3-4 (at $z = 0$ mm) and 5-6 (at $z = 133$ mm), respectively. Better and much more obvious patterns are found in the distribution of this stress component. These Figures show that the stress value remains almost unchanged even if the depth of the plate is changed. The stress value reduces as the transverse (Y or T) distance from the weld increases and finally, it becomes compressive (negative) at about 50 mm on both sides from the centre of the weld. The three-dimensional distributions for longitudinal stresses are shown in Figure 4.29 and Figure 4.30. However, these plots are not drawn to scale.

The maximum positive (tension) value is located at the centreline (line 1-2 in Figure 4.21) of the weld. The stress value on line 3-4 (at $z = 0$ mm) range from roughly -200 MPa to +450 MPa. It should be noted that the first yield stress obtained from material tests on the plate is 405 MPa. The stress value on line 5-6 (at $z = 133$ mm) range from roughly -200 MPa to +375 MPa. The reduction in longitudinal stress value on line 5-6 (at $z = 133$ mm) seems to be due to the stop and start of the weld at this location. These values compared with the parent plate (Specimen 1 which had longitudinal stress value in the range of -40 MPa to +90 MPa) are nearly five times larger. In Figure 4.29 and Figure 4.30, the three-dimensional stress distribution plots (not-to-scale) illustrate the stress level remains almost constant through the depth and transversely across the weld. A pivot table was used to organize this data and magnifies the area directly under the weld. From 10 mm on either side of the centreline of the weld, the stress measurements were taken at 1 mm or 2 mm intervals, and these measurements show in detail the even levels of stress within the weld. The stress levels do not vary more than 50 MPa from one end of the weld bead to the other.

One-dimensional distributions of the three stress components along the longitudinal direction (line 1-2) are shown in Figure 4.31. It can be seen that stress level rises within 10-15 mm from origin (point 1) and then the stress level remains unchanged until about 20 mm away from the stop and start of the weld. The stress level reduces as the stop and start weld zone is approached. Due to the limitation in the set-up and the instrument, stress measurements further away into the weld overlap zone (stop and start zone) could not be taken.

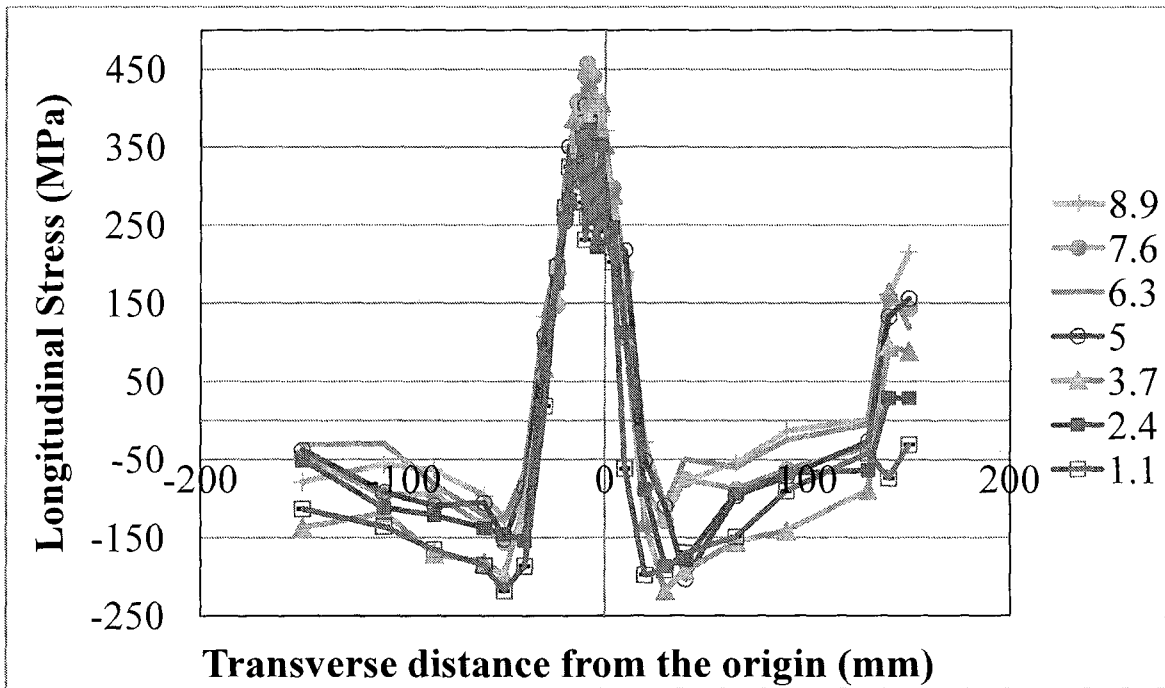


Figure 4.27: Longitudinal stress at various depths in transverse (T or Y) direction (at $z = 0$ mm, line 3-4)

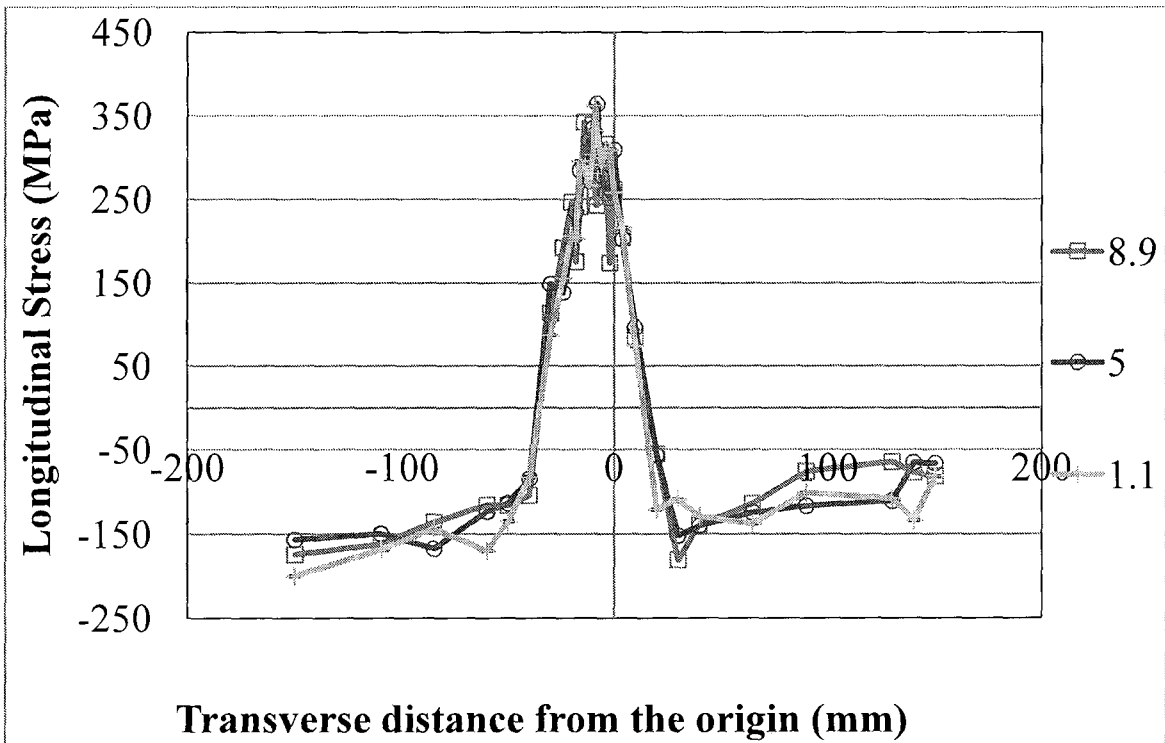


Figure 4.28: Longitudinal stress at various depths in transverse (T or Y) direction (at $z = 133$ mm, line 5-6)

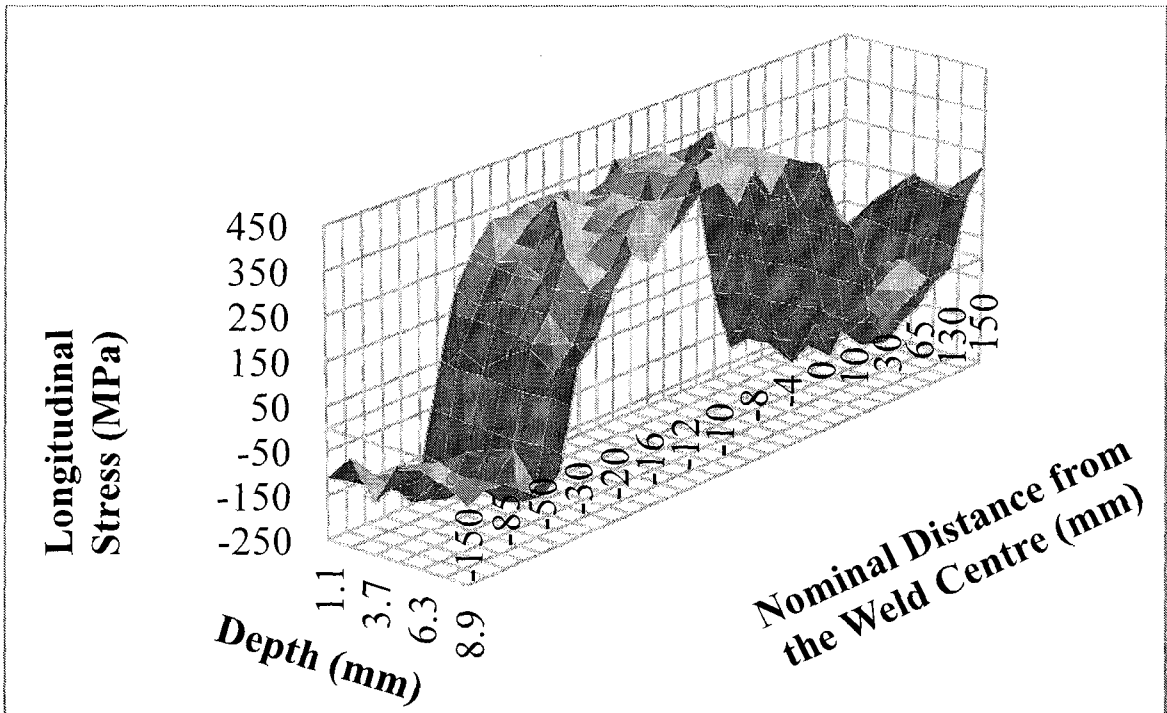


Figure 4.29: 3-D view of longitudinal stress distribution in transverse (T or Y) direction (at $z = 0$ mm, line 3-4)

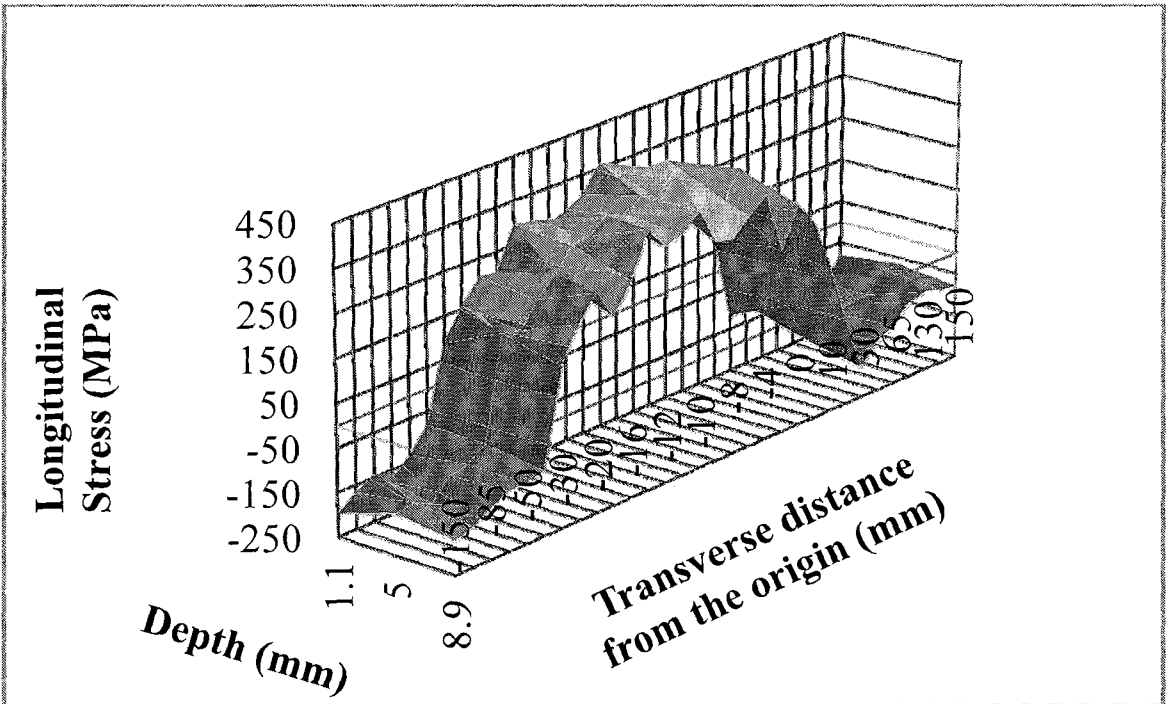


Figure 4.30: 3-D view of longitudinal stress distribution in transverse (T or Y) direction (at $z = 133$ mm, line 5-6)

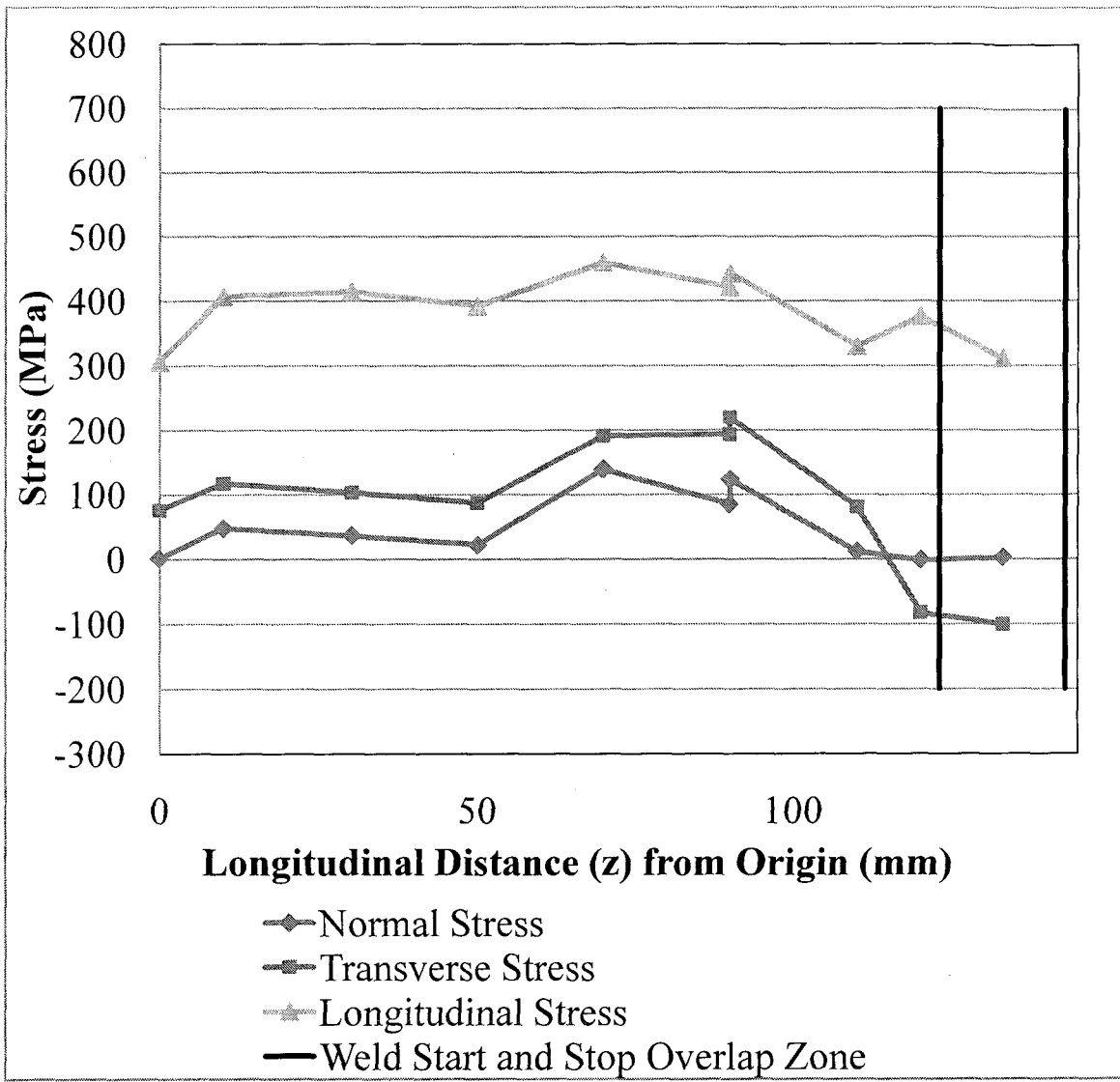


Figure 4.31: All stresses @ Transverse=-10 mm, Normal = 8.9 mm (line 1-2)

4.4.1.3 Specimen 3

Specimen 3 was a stiffened plate which was 400 mm wide (T) x 600 mm long (L) x 9.5 mm thick (N). It had two stiffeners and the primary objective was to study the effects of welding a second stiffener on the stress distribution of the first welded stiffener. The specimen was measured for residual strain along the longitudinal (L or z) and transverse (T or y) directions at seven depths through the normal direction. Figure 4.32 shows the origin (point 1) and the lines (2-1-3) on which stress measurements were taken. Point 4 shows where the inconsistency in the weld occurs (stop and start in the welding process) and therefore how the location of the measurement line was chosen. Line 2-1-3 is located halfway between the inconsistency in the weld (point 4) and the edge of the plate. Figure 4.33 shows the spacing of the measurements in the transverse direction of the plate.

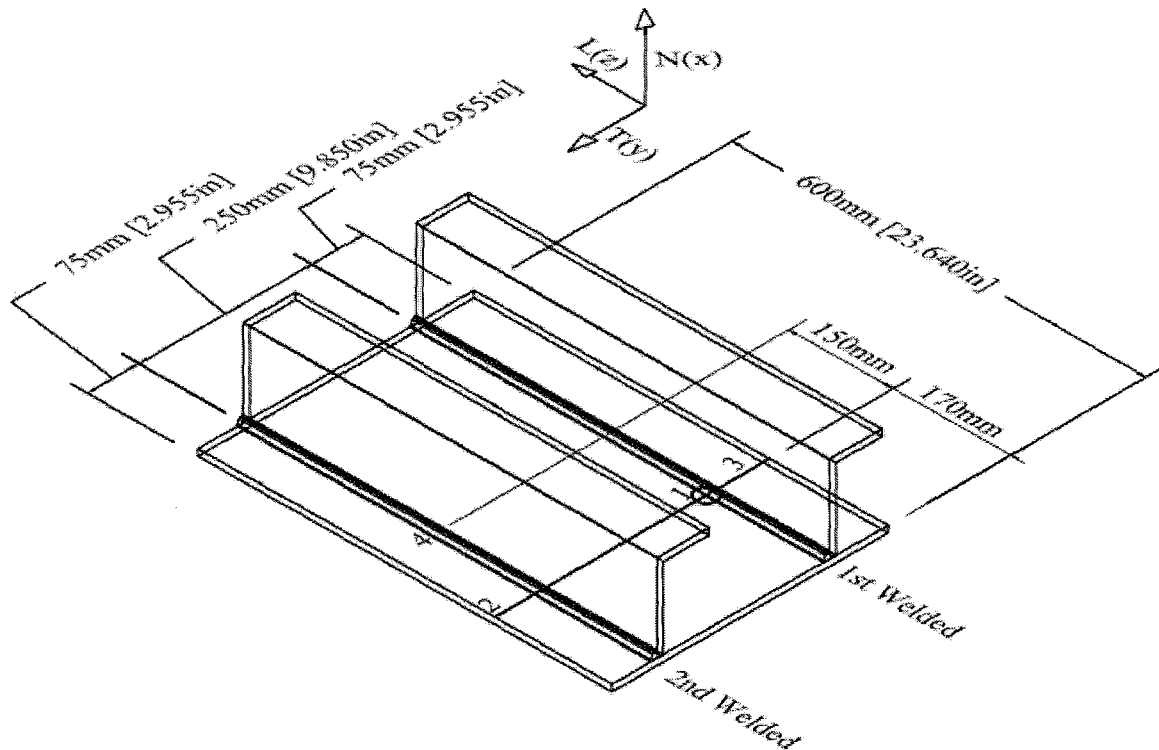


Figure 4.32: Detail for measurement points in Specimen 3

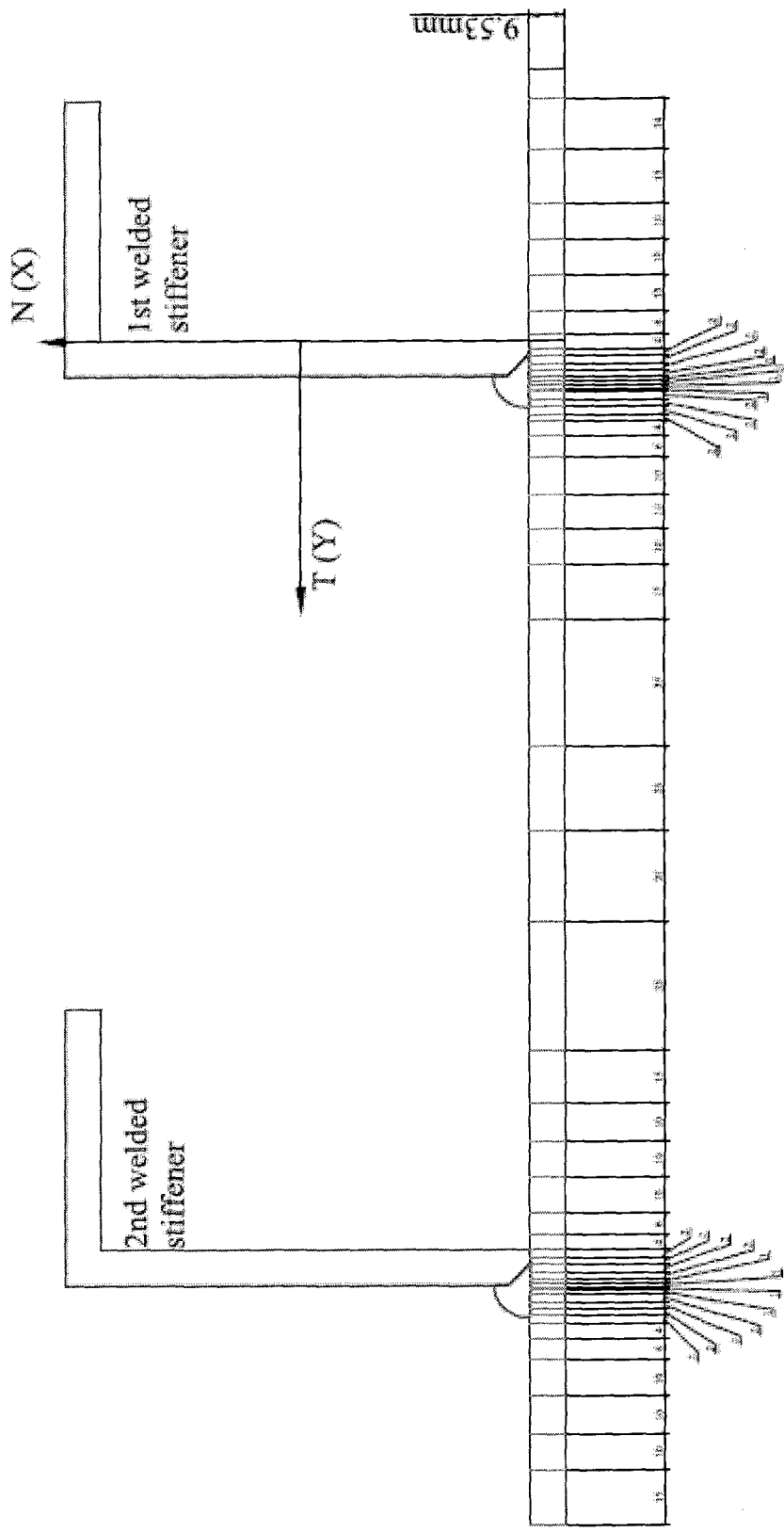


Figure 4.33: Measurement spacing in the transverse direction (mm)

4.4.1.3.1 Normal Stress for Specimen 3

The normal stresses (σ_x or σ_{normal}) are calculated using all three strain components as shown in Equation 4.5. The normal stresses were measured along the entire transverse direction (on line 2-1-3) of 400 mm (Figure 4.32).

As previously mentioned in Section 3.3 (Table 3-C) and for Specimen 2, the welding of the second stiffener for this specimen could not be completed in a single non-stop run. The welding was stopped once and restarted at point 4 after one minute on the second welded stiffener 150 mm from line 2-1-3 in Figure 4.32. The stop and start caused the weld overlap at that point. The position of line 2-1-3 was chosen, as was done for Specimen 2, based on the location of a stop and start in the welding process. The location of the origin (point 1 in Figure 4.32) was chosen at the mid-length between the stop and start of the weld of the second welded stiffener and the edge of the plate such that edge effects and weld inconsistencies (stop and start in welding) are minimized. The spacing of the measurements was similar to those of Specimen 2. Near the centre of the weld where the focus of this study is, spacing was as small as 1 mm and gradually increased up to 40 mm further away from the weld, as shown in Figure 4.33. The measurements were taken at three depths in the transverse (T or Y) direction (on line 2-1-3) at 54 locations, for a total of 162 points (= 54 x 3) and at seven depths in 11 locations (on same line 2-1-3) for a total of 44 points (= 11 x 4) to verify whether or not the strain values through the thickness of the plate changes. Therefore, the total number of measurements taken on this specimen is 206 points (= 162 + 44).

The one-dimensional distribution for normal stresses (σ_x or σ_{normal}) for line 2-1-3 is shown in Figure 4.34. Each line shows the normal stress through the cross-section of the plate at specific transverse distance from the origin (point 1 in Figure 4.32). It should be noted that a different graphical representation is shown for this stress component, as compared to the Figures for Specimen 1. The lines at 8.9 mm, 5 mm, and 1.1 mm were depths where the three measurements were taken across the entire transverse direction and provide the most comprehensive picture of the normal stresses. The additional points collected at the four other depths (7.6 mm, 6.3 mm, 3.7 mm, and 2.4 mm) complete the picture of the stresses

through the thickness of the plate (depth, N) to confirm the consistency of the stresses in this direction. The results show that three depths were sufficient to show the residual stress pattern in this specimen. For example in Figure 4.34, the line with the crosses shows the stress levels at 8.9 mm from the bottom face of the plate (measurements closest to the welded stiffener side) with a minimum value of -119 MPa to a maximum value of 32 MPa. These values compared to those found in Specimen 2 for the same normal stress component ranging from -5 MPa to 147 MPa, show the range is roughly equal at 150 MPa of change, though the absolute values are shifted down in Specimen 3. This possibly shows that the stress balance for this specimen is located elsewhere. The three-dimensional stress plots are not shown for this stress component since they do not provide any valuable information.

Similar to both Specimen 1 and Specimen 2, the normal stress component does not show any clear pattern and this is again due to the presence of the locked-in normal stresses evident in the parent plate that likely developed during the rolling process. The normal stress values range from -150 MPa to +32 MPa, with the maximum value close to the weld centreline. These values are slightly lower than the range found on Specimen 2 (-75 MPa to +150 MPa) and roughly 50% higher than the range found in Specimen 1 (-40 MPa to +80 MPa).

4.4.1.3.2 Transverse Stress for Specimen 3

The transverse stresses (σ_y or $\sigma_{\text{transverse}}$) are calculated using Equation 4.6 and measured at the same points where the normal stress component was measured (Figure 4.32). The measurement points are shown in Figure 4.33. Similar to the measurements for the normal stress component, the transverse stress was also measured at three depths at 54 locations for a total of 162 (= 54 x 3) points. However, due to beam time constraints, only nine locations were measured through the thickness to verify stress value, hence an additional 36 points (= 9 x 4) were measured. Therefore, the total number of measurements that were taken on this plate was 198 points (= 162 + 36).

The one-dimensional distributions for transverse stress are shown Figure 4.35 for line 2-1-3. The three-dimensional stress plots are not shown for this specimen since they do not follow any clear pattern.

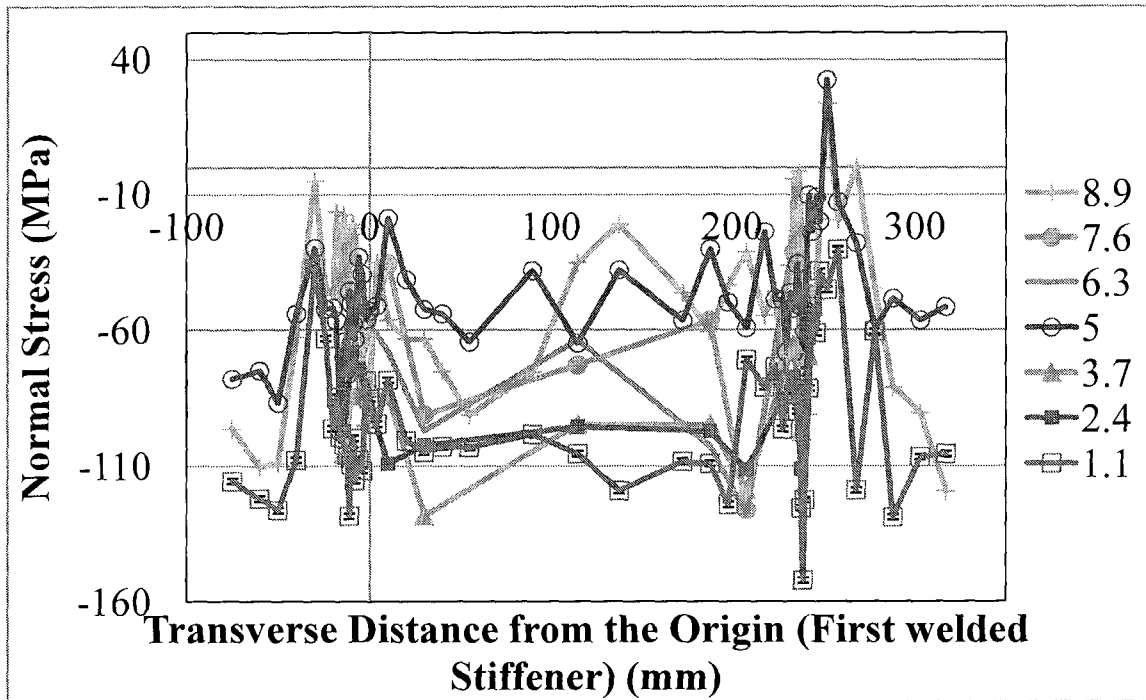


Figure 4.34: Normal Stress at various depths in transverse (T or Y) direction (line 2-1-3)

The stress values on line 2-1-3 range from about -240 MPa to +50 MPa. The values at a depth of 3.7 mm show a difference of approximately -100 MPa from the other depths through the thickness. This difference is best explained by the inherent locked-in stresses found in the parent plate, where at a depth of 3.7 mm the values were at the minimum. For example, at the distance 115 mm from the origin the change in stress levels between a depth of 2.4 mm and 3.7 mm is roughly -90 MPa. In Specimen 1, the change in transverse stress levels between 2.4 mm and 3.7 mm depths is similar at -100 MPa. As was shown in Specimen 1 as well, the maximum peak is found between the depths of 5 mm and 6.3 mm, which is also apparent in Specimen 3.

4.4.1.3.3 Longitudinal Stress for Specimen 3

The longitudinal stress (σ_z or $\sigma_{\text{longitudinal}}$) was calculated using Equation 4.7 and were measured at the same points and depths as was done for the normal and transverse stress components (Figures 4.32 and 4.33). The longitudinal strain component was collected using two different set-ups and therefore, two different sets of constants. The second set-up was similar to the longitudinal set-up for Specimens 1 and 2, and was completed in October 2008. The first set-up had the plate positioned at 45° and was used to collect the difficult points that were under the stiffeners.

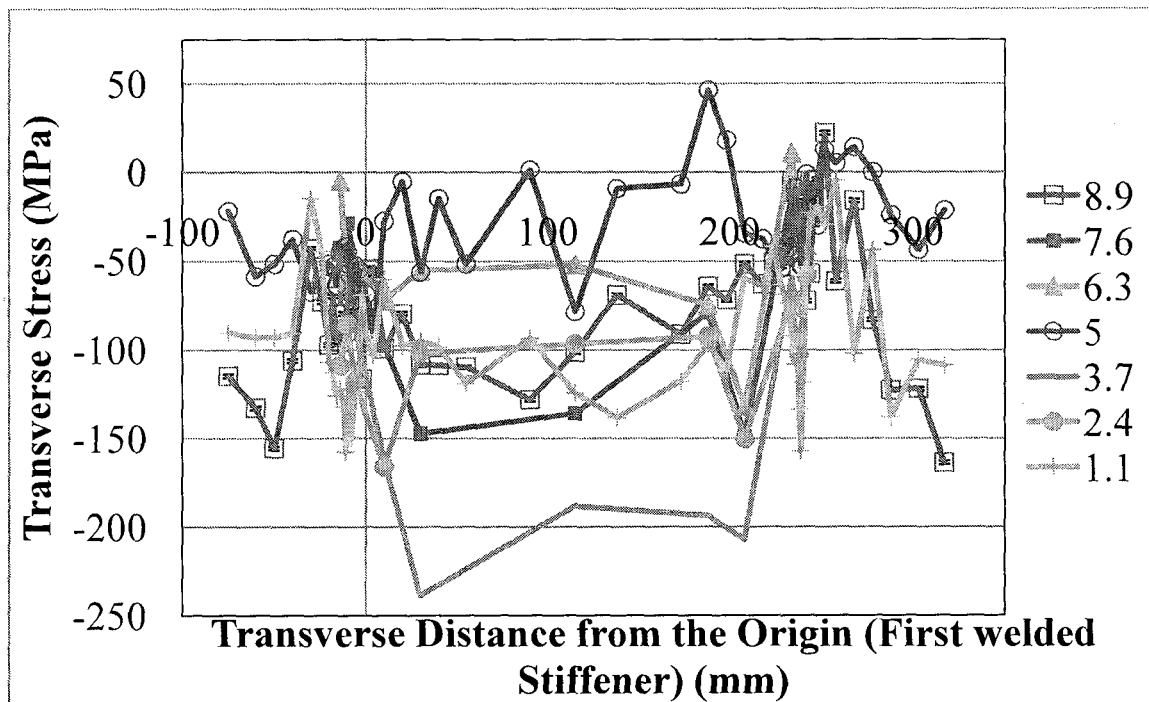


Figure 4.35: Transverse Stresses through the depth in transverse (T or Y) direction (line 2-1-3)

Figure 4.36 shows the one-dimensional distribution for the longitudinal stress for line 2-1-3. The sought after distribution of the stress values is more evident in this component. This figure shows how the depth does not affect the stress levels as severely as the transverse component. This figure shows the peak in tensile (positive) stresses occurs at the weld and as the transverse (Y or T) distance from the weld increases the stresses reduce to a

compressive (negative) stresses and plateau at roughly -150 MPa between the two stiffeners. The three-dimensional view (not-to-scale) of these stresses is shown in Figure 4.37 for the three depths (8.9 mm, 5 mm, and 1.1 mm).

The maximum tension (positive) stresses are at the centreline of the weld at a depth of 8.9 mm (that is, close to the welded surface of the plate), equal to 430 MPa with an error of plus or minus 15 MPa, which is higher than the yield stress obtained from material tests on the plate at 405 MPa. The peak stress values are only slightly higher on the second welded stiffener (max = +430 MPa) than the first welded stiffener (max = +386 MPa), with stress error levels of approximately ± 10 MPa to ± 30 MPa. The majority of the peak values at the weld centreline are about 400 MPa, just below the yield stress level. The stress values on line 2-1-3 range from -360 MPa to +430 MPa. These values compared with Specimen 2 at $z = 0$ mm (-200 MPa to +450 MPa) are more compressive. The same values compared with the parent plate (Specimen 1 which had longitudinal stress value in the range of -40 MPa to +90 MPa) the range is roughly six times greater in Specimen 3.

The plateau between the two stiffeners shows that once at a certain distance from the centreline of the weld the stress levels stabilize and show little variation. The plateau between roughly 20 mm and 208 mm from the origin, shows a range of longitudinal stress values from -220 MPa to -100 MPa, with stress error levels of approximately ± 10 MPa to ± 30 MPa.

In Figure 4.37, the three-dimensional stress distribution plot (not-to-scale) illustrates the stress level remains almost constant through the depth of the plate and transversely under the weld and in the weld area. A pivot table was used to organize this data and magnifies the area directly under the weld. From 10 mm on either side of the centreline of the weld, the stress measurements were taken at 1 mm or 2 mm intervals, and these measurements show in detail the even levels of stress within the weld. The stress levels do not vary more than 50 MPa from one edge of the weld bead to the other.

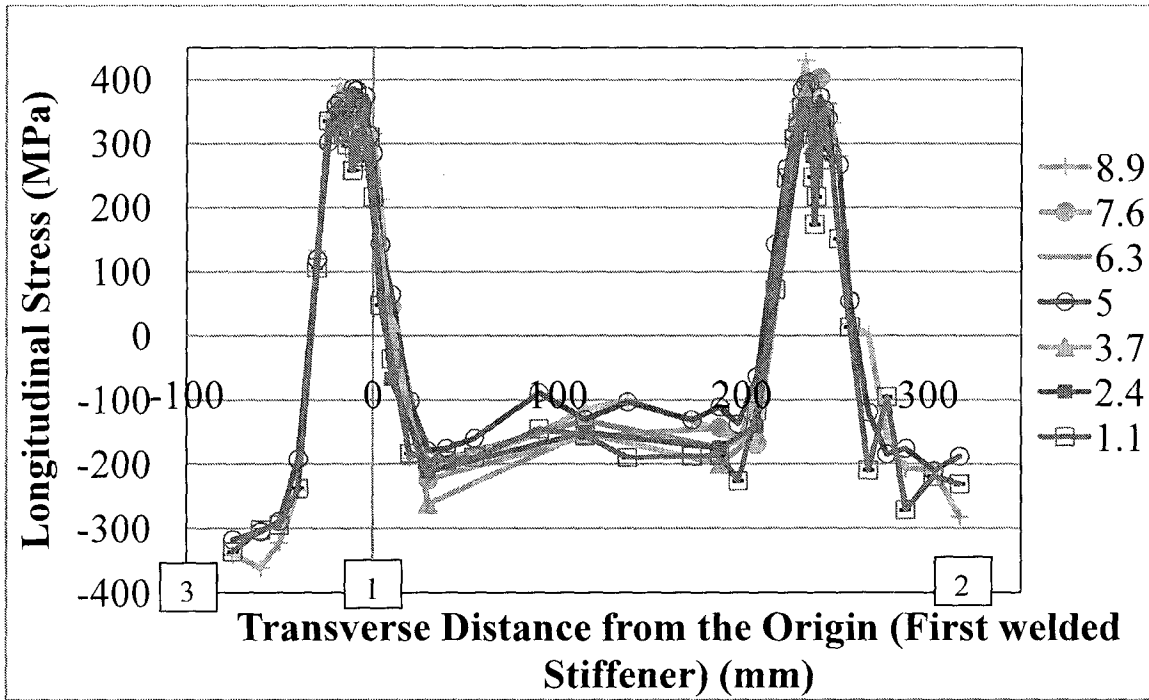


Figure 4.36: Longitudinal stress at various depths in transverse (T or Y) direction (line 2-1-3)

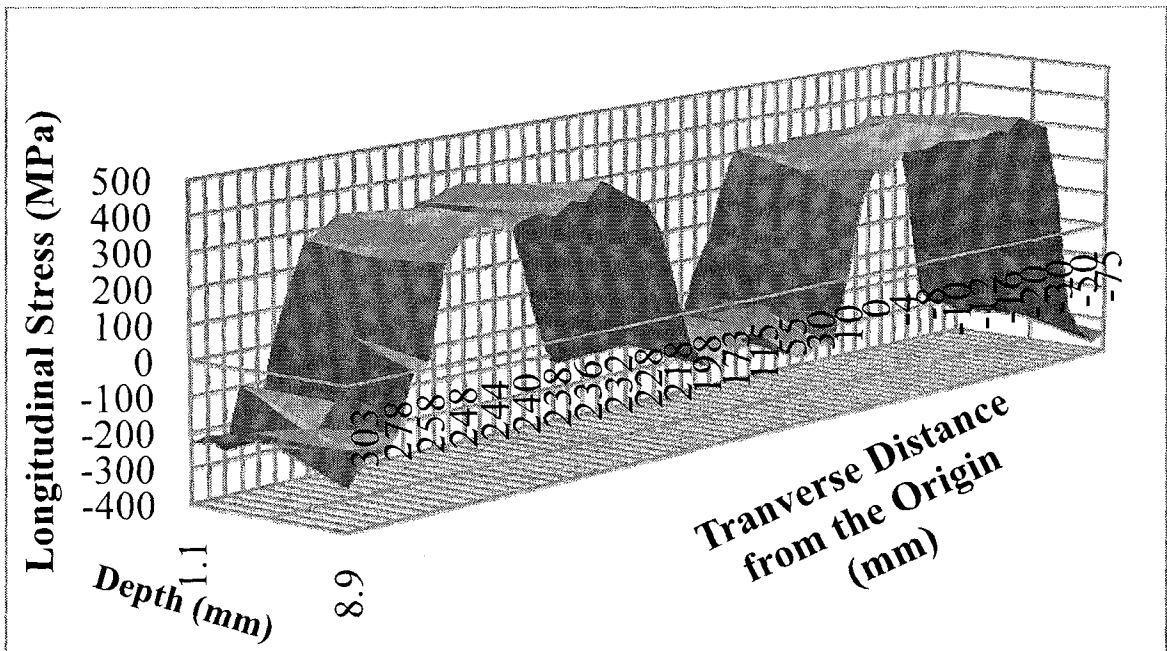


Figure 4.37: 3-D view of longitudinal stress distribution in transverse (T or Y) direction (line 2-1-3)

5 Summary and Conclusions

This study provided a very accurate representation of the stress distribution in the three specimens. The testing completed shows detailed information on the residual stress distribution through the thickness of a plate. All three strain components were collected to calculate the true residual stress distributions in the specimens. Whereas, most previous work focused only on surface stresses due to the limitations of testing methods and only focused on collecting one or two strain components and assuming a plane strain problem.

Specimen 1 provided the information necessary to have a basis to compare the stress results from the welded specimens. Most previous studies conducted did not assess the residual stresses present in the parent plate due to manufacturing and cutting processes. The bending stress found through the thickness of the plate in Specimen 1 was most prevalent in the transverse and longitudinal stresses.

Specimen 2 is the benchmark specimen for comparing stress distributions in Specimen 3 and for future studies. However, the stop and start in the weld of Specimen 2 shows some interesting information on what can happen if the welding is stopped and restarted for some reason. The study shows that stop and start decreases the maximum tensile longitudinal stress and possibly can be beneficial in ship design. Specimen 2 showed the expected stress distribution with the maximum stress at the weld centre and the eventual stress plateau away from the weld in the transverse direction.

Specimen 3 presented a first look at the effect of welding a second stiffener on the stress distribution. The effect that one stress distribution from welding has on another weld has not been extensively examined in previous work. The maximum stress values of the second welded stiffener are slightly higher than those of the first welded stiffener. There is a plateau in the stress levels for roughly 190 mm in between the two stiffeners. Overall the longitudinal stress values were more compressive in Specimen 3 than in Specimen 2.

Overall the results from these three specimens provide an excellent basis for future studies. In general, both for Specimens 2 and 3, it was found that the maximum tensile stress can be slightly higher than the yield stress.

5.1 Future Work

The data collected and analyzed for this thesis will be beneficial in the planning and execution of any future testing. Further study with uniform welds with less inconsistencies and no stop and starts is required. An automatic welding system will be tested to see if it generates acceptable welds.

A change in the spacing of the stiffeners needs to be explored to find the optimum spacing of stiffener for production. The heat input used during welding will also need to be changed to find the change in residual stress distributions with the change in heat input. A more in depth look may also be taken at the effects of the stop and start of the welding process on the residual stress distribution, expanding on the minimal data that was collected in these experiments. Another area of interest may also be the residual stress distribution when the stiffener is shorter than the parent plate and the stress patterns in the plate past the end of the stiffener and weld.

A semi-destructive method, such as hole-drilling, may be used to verify the results found here. As well, computer modelling may be used for a detailed parametric study.

Appendix A – Raw Data and Checks

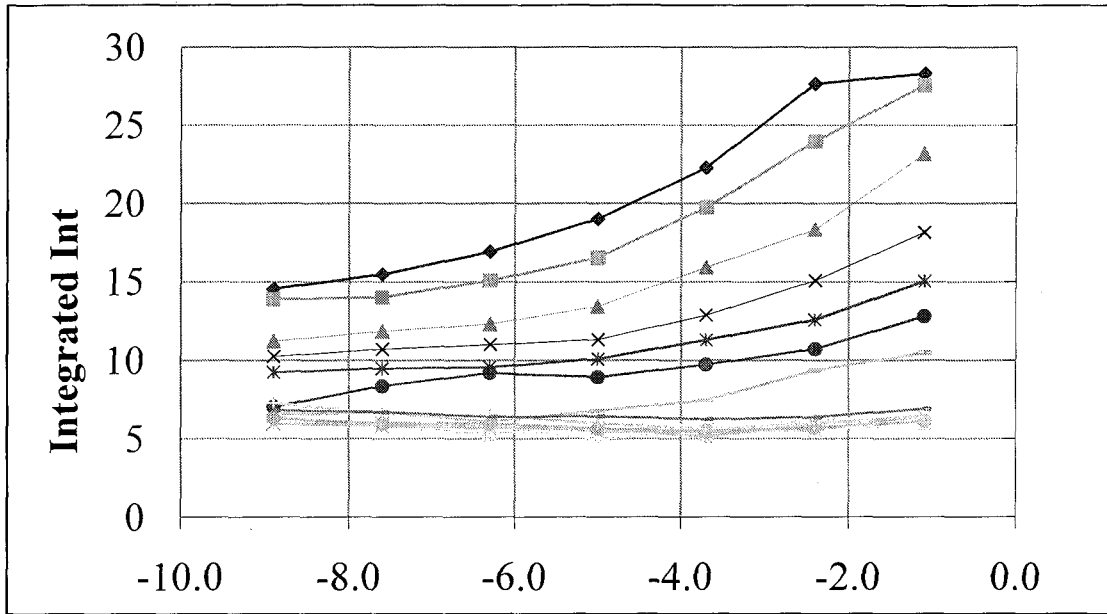


Figure 0.1: Integrated intensity check – good raw data

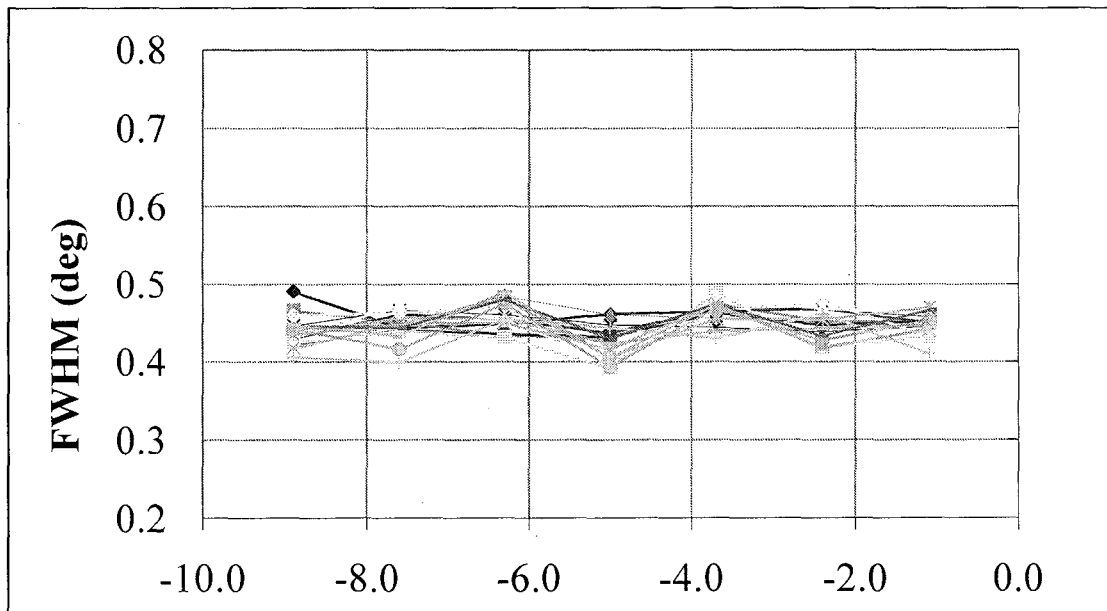


Figure 0.2: Full Width Half Maximum (FWHM) check – good raw data

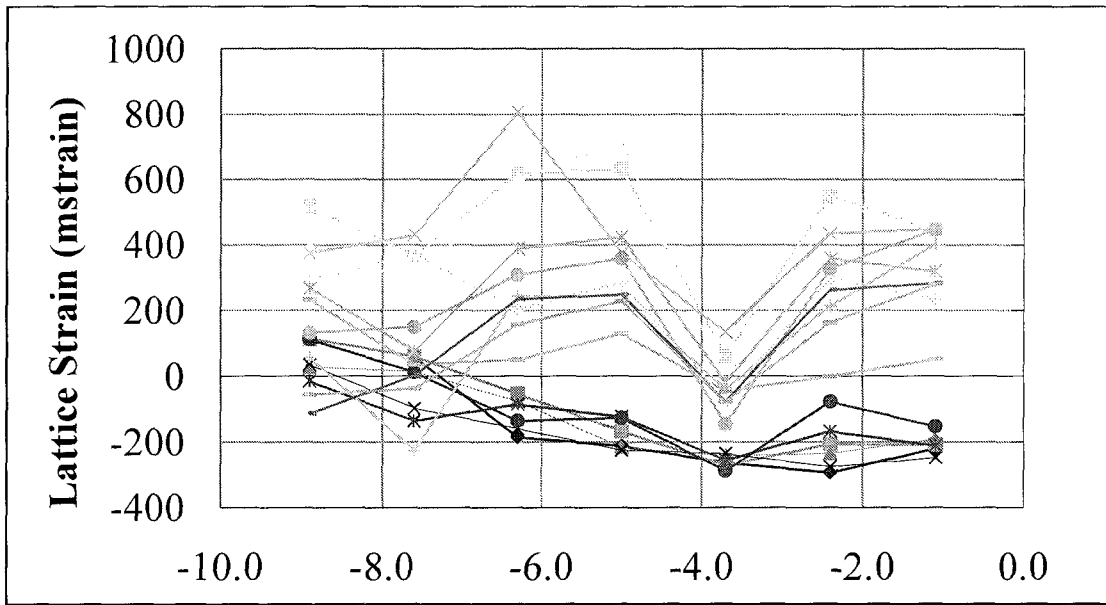


Figure 0.3: Lattice strain check - good raw data

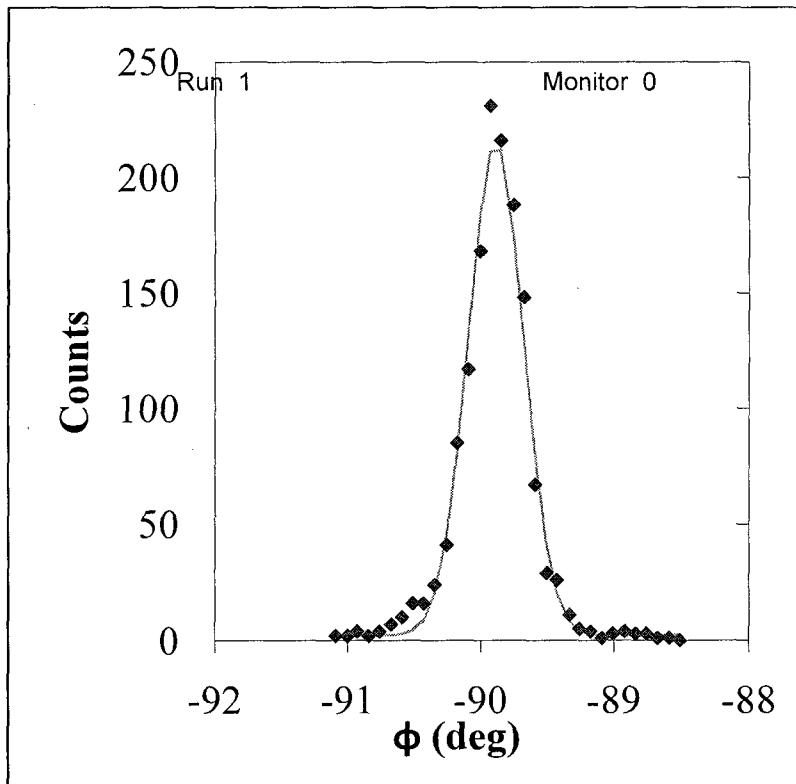


Figure 0.4: Example of good raw data with ϕ peak counts, $\phi = -89.89^\circ$

Table 0-A : Sample of raw data from computer

Run	2TM	PSI	PHI	XPOS	YPOS	ZPOS	--- Fit	Integrated Intensity	ϕ	$\mu\phi$	FWHM		
190	98.93	-44.9	-89.8	-7.96	65	0	5.8412	0.3513	-89.8823	0.01	0.4482	0.0221	0.6525
191	98.93	-44.9	-89.8	-9.26	65	0	5.9487	0.2254	-89.8603	0.0062	0.4349	0.0134	0.6301
192	98.93	-44.9	-89.8	-1.58	90	0	6.113	0.2241	-89.8397	0.0062	0.453	0.0135	0.6121
193	98.93	-44.9	-89.8	-2.88	90	0	5.7128	0.3037	-89.8536	0.0085	0.4272	0.0183	0.6563
194	98.93	-44.9	-89.8	-4.18	90	0	5.4953	0.2895	-89.9077	0.0095	0.4688	0.0206	0.687
195	98.93	-44.9	-89.8	-5.48	90	0	5.6628	0.3015	-89.8499	0.0077	0.3936	0.0168	0.6043
196	98.93	-44.9	-89.8	-6.78	90	0	5.9753	0.2721	-89.8556	0.0082	0.4747	0.0176	0.6355
197	98.93	-44.9	-89.8	-8.08	90	0	5.9664	0.2642	-89.8738	0.0069	0.4163	0.0147	0.6055
198	98.93	-44.9	-89.8	-9.38	90	0	6.3273	0.3112	-89.8759	0.0081	0.4422	0.0173	0.6215
199	98.93	-44.9	-89.8	-1.82	130	0	6.3771	0.3099	-89.845	0.0073	0.4101	0.0155	0.5374
200	98.93	-44.9	-89.8	-3.12	130	0	5.9943	0.2864	-89.8665	0.0082	0.4615	0.0179	0.6384
201	98.93	-44.9	-89.8	-4.42	130	0	5.6212	0.3155	-89.8954	0.0091	0.4302	0.0193	0.5862
202	98.93	-44.9	-89.8	-5.72	130	0	5.9951	0.3433	-89.8632	0.0094	0.4438	0.0208	0.6827
203	98.93	-44.9	-89.8	-7.02	130	0	6.4744	0.3745	-89.8631	0.01	0.4549	0.0213	0.6391
204	98.93	-44.9	-89.8	-8.32	130	0	6.6012	0.406	-89.9169	0.0092	0.3991	0.0191	0.5764
205	98.93	-44.9	-89.8	-9.62	130	0	7.2867	0.2932	-89.8844	0.0061	0.4061	0.0127	0.5735
206	98.93	-44.9	-89.8	-8.79	-10	10	17.204	0.7407	-89.886	0.0078	0.4876	0.0174	1.9597
207	98.93	-44.9	-89.8	-8.71	-10	30	16.7464	0.7378	-89.893	0.0082	0.496	0.0182	2.017
208	98.93	-44.9	-89.8	-8.64	-10	50	16.0804	0.5898	-89.8959	0.0067	0.479	0.0147	2.1074

Appendix B - Permissions

ELSEVIER LICENSE TERMS AND CONDITIONS

Jan 12, 2009

This is a License Agreement between Sara Y Kenno ("You") and Elsevier ("Elsevier"). The license consists of your order details, the terms and conditions provided by Elsevier, and the payment terms and conditions.

Supplier	Elsevier The Boulevard, Langford Kidlington, Oxford, OX5 1GB, UK	Limited Lane
Registered Company Number	1982084	
Customer name	Sara Y Kenno	
Customer address	3228 Randolph Ave Windsor, ON N9E3E7	
License Number	2106560794834	
License date	Jan 12, 2009	
Licensed content publisher	Elsevier	
Licensed content publication	Marine Structures	
Licensed content title	A finite element simulation of the test procedure of stiffened panels	
Licensed content author	S. Z. Hu and L. Jiang	
Licensed content date	April 1998	
Volume number	11	
Issue number	3	
Pages	25	
Type of Use	Thesis / Dissertation	
Portion	Figures/table/illustration/abstracts	
Portion Quantity	2	
Format	Both print and electronic	
You are an author of the Elsevier article	No	
Are you translating?	No	
Purchase order number		
Expected publication date	Jan 2009	
Elsevier VAT number	GB 494 6272 12	
Permissions price	0.00 USD	
Value added tax 0.0%	0.00 USD	
Total	0.00 USD	
Terms and Conditions		

**SPRINGER LICENSE
TERMS AND CONDITIONS**

Jan 12, 2009

This is a License Agreement between Sara Y Kenno ("You") and Springer ("Springer"). Please note that you are liable to account for Value Added Tax (VAT). The license consists of your order details, the terms and conditions provided by Springer, and the payment terms and conditions.

License Number	2106561250741
License date	Jan 12, 2009
Licensed content publisher	Springer
Licensed content publication	Experimental Mechanics
Licensed content title	Laser surface-contouring and spline data-smoothing for residual stress measurement
Licensed content author	M. B. Prime
Licensed content date	Apr 1, 2004
Volume number	44
Issue number	2
Pages	176 - 184
Type of Use	Thesis / Dissertation
Details of use	Print
Requestor Type	Individual
Portion of the article	Figures
Title of your thesis / dissertation	/ Effect of One and Two Stiffeners on Residual Stresses of Ship Hull
Expected completion date	Jan 2009
Billing Type	Invoice
Company	Sara Y Kenno
Billing Address	3228 Randolph Ave Windsor, ON N9E3E7 Canada
Customer reference info	
Total	0.00 USD
Terms and Conditions	

**ELSEVIER LICENSE
TERMS AND CONDITIONS**

Jan 12, 2009

This is a License Agreement between Sara Y Kenno ("You") and Elsevier ("Elsevier"). The license consists of your order details, the terms and conditions provided by Elsevier, and the payment terms and conditions.

Supplier	Elsevier The Boulevard, Langford Kidlington, Oxford, OX5 1GB, UK	Limited Lane
Registered Company Number	1982084	
Customer name	Sara Y Kenno	
Customer address	3228 Randolph Ave Windsor, ON N9E3E7	
License Number	2106561473062	
License date	Jan 12, 2009	
Licensed content publisher	Elsevier	
Licensed content publication	Journal of Materials Processing Technology	
Licensed content title	Investigation of residual stress and post weld heat treatment of multi-pass welds by finite element method and experiments	
Licensed content author	J. R. Cho, B. Y. Lee, Y. H. Moon and C. J. Van Tyne	
Licensed content date	30 November 2004	
Volume number	155-156	
Issue number		
Pages	6	
Type of Use	Thesis / Dissertation	
Portion	Figures/table/illustration/abstracts	
Portion Quantity	1	
Format	Both print and electronic	
You are an author of the Elsevier article	No	
Are you translating?	No	
Purchase order number		
Expected publication date	Jan 2009	
Elsevier VAT number	GB 494 6272 12	
Permissions price	0.00 USD	
Value added tax 0.0%	0.00 USD	
Total	0.00 USD	
Terms and Conditions		

**ELSEVIER LICENSE
TERMS AND CONDITIONS**

Jan 12, 2009

This is a License Agreement between Sara Y Kenno ("You") and Elsevier ("Elsevier"). The license consists of your order details, the terms and conditions provided by Elsevier, and the payment terms and conditions.

Supplier	Elsevier The Boulevard, Langford Kidlington, Oxford, OX5 1GB, UK	Limited Lane
Registered Company Number	1982084	
Customer name	Sara Y Kenno	
Customer address	3228 Randolph Ave Windsor, ON N9E3E7	
License Number	2106580375751	
License date	Jan 12, 2009	
Licensed content publisher	Elsevier	
Licensed content publication	Materials Science and Engineering: A	
Licensed content title	Correlating weld process conditions, residual strain and stress, microstructure and mechanical properties for high strength steel—the role of neutron diffraction strain scanning	
Licensed content author	M.N. James, P.J. Webster, D.J. Hughes, Z. Chen, N. Ratel, S.-P. Ting, G. Bruno and A. Steuer	
Licensed content date	15 July 2006	
Volume number	427	
Issue number	1-2	
Pages	11	
Type of Use	Thesis / Dissertation	
Portion	Figures/table/illustration/abstracts	
Portion Quantity	2	
Format	Both print and electronic	
You are an author of the Elsevier article	No	
Are you translating?	No	
Purchase order number		
Expected publication date	Jan 2009	
Elsevier VAT number	GB 494 6272 12	
Permissions price	0.00 USD	
Value added tax 0.0%	0.00 USD	
Total	0.00 USD	
Terms and Conditions		

**ELSEVIER LICENSE
TERMS AND CONDITIONS**

Jan 12, 2009

This is a License Agreement between Sara Y Kenno ("You") and Elsevier ("Elsevier"). The license consists of your order details, the terms and conditions provided by Elsevier, and the payment terms and conditions.

Supplier	Elsevier The Boulevard, Langford Kidlington, Oxford, OX5 1GB, UK	Limited Lane
Registered Company Number	1982084	
Customer name	Sara Y Kenno	
Customer address	3228 Randolph Ave Windsor, ON N9E3E7	
License Number	2106580657836	
License date	Jan 12, 2009	
Licensed content publisher	Elsevier	
Licensed content publication	Physica B: Condensed Matter	
Licensed content title	Investigation of reference samples for residual strain measurements in a welded specimen by neutron and synchrotron X-ray diffraction	
Licensed content author	A. Paradowska, T.R. Finlayson, J.W.H. Price, R. Ibrahim, A. Steuwer and M. Ripley	
Licensed content date	15 November 2006	
Volume number	385-386	
Issue number	1-2	
Pages	4	
Type of Use	Thesis / Dissertation	
Portion	Figures/table/illustration/abstracts	
Portion Quantity	3	
Format	Both print and electronic	
You are an author of the Elsevier article	No	
Are you translating?	No	
Purchase order number		
Expected publication date	Jan 2009	
Elsevier VAT number	GB 494 6272 12	
Permissions price	0.00 USD	
Value added tax 0.0%	0.00 USD	
Total	0.00 USD	
Terms and Conditions		

**ELSEVIER LICENSE
TERMS AND CONDITIONS**

Jan 12, 2009

This is a License Agreement between Sara Y Kenno ("You") and Elsevier ("Elsevier"). The license consists of your order details, the terms and conditions provided by Elsevier, and the payment terms and conditions.

Supplier	Elsevier The Boulevard, Langford Kidlington, Oxford, OX5 1GB, UK	Limited Lane
Registered Company Number	1982084	
Customer name	Sara Y Kenno	
Customer address	3228 Randolph Ave Windsor, ON N9E3E7	
License Number	2106600526618	
License date	Jan 12, 2009	
Licensed content publisher	Elsevier	
Licensed content publication	Physica B: Condensed Matter	
Licensed content title	Neutron diffraction measurement of residual stress in high strength, highly restrained, thick section steel welds	
Licensed content author	S.V. Pearce and V.M. Linton	
Licensed content date	15 November 2006	
Volume number	385-386	
Issue number	1-2	
Pages	4	
Type of Use	Thesis / Dissertation	
Portion	Figures/table/illustration/abstracts	
Portion Quantity	1	
Format	Both print and electronic	
You are an author of the Elsevier article	No	
Are you translating?	No	
Purchase order number		
Expected publication date	Jan 2009	
Elsevier VAT number	GB 494 6272 12	
Permissions price	0.00 USD	
Value added tax 0.0%	0.00 USD	
Total	0.00 USD	
Terms and Conditions		

**ELSEVIER LICENSE
TERMS AND CONDITIONS**

Jan 12, 2009

This is a License Agreement between Sara Y Kenno ("You") and Elsevier ("Elsevier"). The license consists of your order details, the terms and conditions provided by Elsevier, and the payment terms and conditions.

Supplier	Elsevier The Boulevard, Langford Kidlington, Oxford, OX5 1GB, UK	Limited Lane
Registered Company Number	1982084	
Customer name	Sara Y Kenno	
Customer address	3228 Randolph Ave Windsor, ON N9E3E7	
License Number	2106600665348	
License date	Jan 12, 2009	
Licensed content publisher	Elsevier	
Licensed content publication	International Journal of Pressure Vessels and Piping	
Licensed content title	Residual stresses measurement by neutron diffraction and theoretical estimation in a single weld bead	
Licensed content author	John W.H. Price, Anna Paradowska, Suraj Joshi and Trevor Finlayson	
Licensed content date	May 2006	
Volume number	83	
Issue number	5	
Pages	7	
Type of Use	Thesis / Dissertation	
Portion	Figures/table/illustration/abstracts	
Portion Quantity	3	
Format	Both print and electronic	
You are an author of the Elsevier article	No	
Are you translating?	No	
Purchase order number		
Expected publication date	Jan 2009	
Elsevier VAT number	GB 494 6272 12	
Permissions price	0.00 USD	
Total	0.00 USD	
Terms and Conditions		

**ELSEVIER LICENSE
TERMS AND CONDITIONS**

Jan 12, 2009

This is a License Agreement between Sara Y Kenno ("You") and Elsevier ("Elsevier"). The license consists of your order details, the terms and conditions provided by Elsevier, and the payment terms and conditions.

Supplier	Elsevier The Boulevard, Langford Kidlington, Oxford, OX5 1GB, UK	Limited Lane
Registered Company Number	1982084	
Customer name	Sara Y Kenno	
Customer address	3228 Randolph Ave Windsor, ON N9E3E7	
License Number	2106600847545	
License date	Jan 12, 2009	
Licensed content publisher	Elsevier	
Licensed content publication	Materials Science and Engineering: A	
Licensed content title	Stress measurements in welds: Problem areas	
Licensed content author	T.M. Holden, H. Suzuki, D.G. Carr, M.I. Ripley and B. Clausen	
Licensed content date	10 November 2006	
Volume number	437	
Issue number	1	
Pages	5	
Type of Use	Thesis / Dissertation	
Portion	Figures/table/illustration/abstracts	
Portion Quantity	1	
Format	Both print and electronic	
You are an author of the Elsevier article	No	
Are you translating?	No	
Purchase order number		
Expected publication date	Jan 2009	
Elsevier VAT number	GB 494 6272 12	
Permissions price	0.00 USD	
Value added tax 0.0%	0.00 USD	
Total	0.00 USD	
Terms and Conditions		

TERMS AND CONDITIONS

INTRODUCTION

1. The publisher for this copyrighted material is Elsevier. By clicking "accept" in connection with completing this licensing transaction, you agree that the following terms and conditions apply to this transaction (along with the Billing and Payment terms and conditions established by Copyright Clearance Center, Inc. ("CCC"), at the time that you opened your Rightslink account and that are available at any time at <http://myaccount.copyright.com>).

GENERAL TERMS

2. Elsevier hereby grants you permission to reproduce the aforementioned material subject to the terms and conditions indicated.

3. Acknowledgement: If any part of the material to be used (for example, figures) has appeared in our publication with credit or acknowledgement to another source, permission must also be sought from that source. If such permission is not obtained then that material may not be included in your publication/copies. Suitable acknowledgement to the source must be made, either as a footnote or in a reference list at the end of your publication, as follows:

"Reprinted from Publication title, Vol /edition number, Author(s), Title of article / title of chapter, Pages No., Copyright (Year), with permission from Elsevier [OR APPLICABLE SOCIETY COPYRIGHT OWNER]." Also Lancet special credit - "Reprinted from The Lancet, Vol. number, Author(s), Title of article, Pages No., Copyright (Year), with permission from Elsevier."

4. Reproduction of this material is confined to the purpose and/or media for which permission is hereby given.

5. Altering/Modifying Material: Not Permitted. However figures and illustrations may be altered/adapted minimally to serve your work. Any other abbreviations, additions, deletions and/or any other alterations shall be made only with prior written authorization of Elsevier Ltd. (Please contact Elsevier at permissions@elsevier.com)

6. If the permission fee for the requested use of our material is waived in this instance, please be advised that your future requests for Elsevier materials may attract a fee.

7. Reservation of Rights: Publisher reserves all rights not specifically granted in the combination of (i) the license details provided by you and accepted in the course of this licensing transaction, (ii) these terms and conditions and (iii) CCC's Billing and Payment terms and conditions.

8. License Contingent Upon Payment: While you may exercise the rights licensed immediately upon issuance of the license at the end of the licensing process for the transaction, provided that you have disclosed complete and accurate details of your proposed use, no license is finally effective unless and until full payment is received from you (either by publisher or by CCC) as provided in CCC's Billing and Payment terms and conditions. If full payment is not received on a timely basis, then any license preliminarily granted shall be deemed automatically revoked and shall be void as if never granted. Further, in the event that you breach any of these terms and conditions or any of CCC's Billing and Payment terms and conditions, the license is automatically revoked and shall be void as if never granted. Use of materials as described in a revoked license, as well as any use of the materials beyond the scope of an unrevoked license, may constitute copyright infringement and publisher reserves the right to take any and all action to protect its copyright in the materials.

9. Warranties: Publisher makes no representations or warranties with respect to the licensed material.

10. Indemnity: You hereby indemnify and agree to hold harmless publisher and CCC, and their respective officers, directors, employees and agents, from and against any and all claims arising out of your use of the licensed material other than as specifically authorized pursuant to this license.

11. No Transfer of License: This license is personal to you and may not be sublicensed, assigned, or transferred by you to any other person without publisher's written permission.

12. No Amendment Except in Writing: This license may not be amended except in a writing signed by both parties (or, in the case of publisher, by CCC on publisher's behalf).

13. Objection to Contrary Terms: Publisher hereby objects to any terms contained in any purchase order, acknowledgment, check endorsement or other writing prepared by you, which terms are inconsistent with these terms and conditions or CCC's Billing and Payment terms and conditions. These terms and conditions, together with CCC's Billing and Payment terms and conditions (which

are incorporated herein), comprise the entire agreement between you and publisher (and CCC) concerning this licensing transaction. In the event of any conflict between your obligations established by these terms and conditions and those established by CCC's Billing and Payment terms and conditions, these terms and conditions shall control.

14. **Revocation:** Elsevier or Copyright Clearance Center may deny the permissions described in this License at their sole discretion, for any reason or no reason, with a full refund payable to you. Notice of such denial will be made using the contact information provided by you. Failure to receive such notice will not alter or invalidate the denial. In no event will Elsevier or Copyright Clearance Center be responsible or liable for any costs, expenses or damage incurred by you as a result of a denial of your permission request, other than a refund of the amount(s) paid by you to Elsevier and/or Copyright Clearance Center for denied permissions.

LIMITED LICENSE

The following terms and conditions apply to specific license types:

15. **Translation:** This permission is granted for non-exclusive world **English** rights only unless your license was granted for translation rights. If you licensed translation rights you may only translate this content into the languages you requested. A professional translator must perform all translations and reproduce the content word for word preserving the integrity of the article. If this license is to re-use 1 or 2 figures then permission is granted for non-exclusive world rights in all languages.

16. **Website:** The following terms and conditions apply to electronic reserve and author websites:
Electronic reserve: If licensed material is to be posted to website, the web site is to be password-protected and made available only to bona fide students registered on a relevant course if: This license was made in connection with a course, This permission is granted for 1 year only. You may obtain a license for future website posting, All content posted to the web site must maintain the copyright information line on the bottom of each image, A hyper-text must be included to the Homepage of the journal from which you are licensing at <http://www.sciencedirect.com/science/journal/xxxxx>, or, for books, to the Elsevier homepage at <http://www.elsevier.com>,
Central Storage: This license does not include permission for a scanned version of the material to be stored in a central repository such as that provided by Heron/XanEdu.

17. **Author website** for journals with the following additional clauses:

All content posted to the web site must maintain the copyright information line on the bottom of each image, and The permission granted is limited to the personal version of your paper. You are not allowed to download and post the published electronic version of your article (whether PDF or HTML, proof or final version), nor may you scan the printed edition to create an electronic version, A hyper-text must be included to the Homepage of the journal from which you are licensing at <http://www.sciencedirect.com/science/journal/xxxxx>,
Central Storage: This license does not include permission for a scanned version of the material to be stored in a central repository such as that provided by Heron/XanEdu.

18. **Author website** for books with the following additional clauses:
Authors are permitted to place a brief summary of their work online only. A hyper-text must be included to the Elsevier homepage at <http://www.elsevier.com>. All content posted to the web site must maintain the copyright information line on the bottom of each image You are not allowed to download and post the published electronic version of your chapter, nor may you scan the printed edition to create an electronic version.
Central Storage: This license does not include permission for a scanned version of the material to be stored in a central repository such as that provided by Heron/XanEdu.

19. **Website** (regular and for author): A hyper-text must be included to the Homepage of the journal from which you are licensing at <http://www.sciencedirect.com/science/journal/xxxxx>, or, for books, to the Elsevier homepage at <http://www.elsevier.com>.

20. **Thesis/Dissertation:** If your license is for use in a thesis/dissertation your thesis may be submitted to your institution in either print or electronic form. Should your thesis be published commercially, please reapply for permission. These requirements include permission for the Library and Archives of Canada to supply single copies, on demand, of the complete thesis and include permission for UMI to supply single copies, on demand, of the complete thesis. Should your thesis be published commercially, please reapply for permission.

21. **Other conditions:** None

Sara Kenno
M.A.Sc. Candidate
Civil Engineering
University of Windsor
kenno2@uwindsor.ca

16th January 2009

Dear Sara Kenno,

RE: C. C. Weng and S. C. Lo “Measurement of residual stresses in welded steel joints using hole drilling method” *Materials Science and Technology* 8, March 1992 pages 213 – 218
Figure 6 only

I am writing to you in response to your request for permission to use the above figures in thesis to be titled *Effect of One and Two Stiffeners on Residual Stresses of Ship Hull* as part of your masters at the University of Windsor, Windsor, ON, Canada. We happy for you to use this material in your thesis only, subject to the proper acknowledgement of the copyright holder and the original publication of the material listed above.

We would also be grateful if you could include links to the online version of the journal and the journal’s homepage as follows:

Online journal: <http://www.ingentaconnect.com/content/maney/mst>
Journal homepage: www.maney.co.uk/journals/mst.

Please do contact me here with any further requirements or requests that you may have with regard to this matter.

Yours sincerely

Lisa Johnstone
Publishing Executive

Dear Madam,

With reference to your request (copy herewith) to reprint material on which Springer Science and Business Media controls the copyright, our permission is granted, free of charge, for the use indicated in your enquiry.

This permission

- allows you non-exclusive reproduction rights throughout the World.
- permission includes use in an electronic form, provided that content is
 - * password protected;
 - * at intranet;
- excludes use in any other electronic form. Should you have a specific project in mind, please reapply for permission.
- requires a full credit (Springer/Kluwer Academic Publishers book/journal title, volume, year of publication, page, chapter/article title, name(s) of author(s), figure number(s), original copyright notice) to the publication in which the material was originally published, by adding: with kind permission of Springer Science and Business Media. The material can only be used for the purpose of defending your dissertation, and with a maximum of **100** extra copies in paper.

Permission free of charge on this occasion does not prejudice any rights we might have to charge for reproduction of our copyrighted material in the future.

Best wishes,

Nel van der Werf (Ms)

Rights and Permissions/Springer

Van Godewijkstraat 30 | P.O. Box 17
3300 AA Dordrecht | The Netherlands
tel +31 (0) 78 6576 298
fax +31 (0)78 65 76-300
Nel.vanderwerf@springer.com
www.springer.com

From: Sara Kenno [mailto:kenno2@uwindsor.ca]

Sent: woensdag 14 januari 2009 18:20

To: Permissions Europe/NL

Subject: Re: FW: Rightslink/ Springer Redirected Order Request

Importance: High

Dear Estella Jap A Joe,

Thank you for your prompt response. For the following article, I wish to use *Figure 11 - Centreline longitudinal strain measured in the two as-welded 12-mm-thick plates using neutrons and synchrotron X-rays* on page 417. I will be using the figure in my M.A.Sc. thesis in the literature review chapter. I will be defending my thesis in the last weeks of January and print copies of the final draft of my thesis will be available through the University of Windsor, Windsor, ON, Canada and my department - Department of Civil and Environmental Engineering.

Publication: Metallurgical and Materials Transactions A

Pages: 411 - 420

Volume number: 37

Issue number: 2

Publication date: 02/01/2006

Title: Use of neutron and synchrotron X-ray diffraction for evaluation of residual stresses in a 2024-T351 aluminum alloy variable-polarity plasma-arc weld

Author: S. Ganguly, M.E. Fitzpatrick, and L. Edwards

Sorry for the late notification. Since I am defending in the next couple of weeks, I hope to hear from you soon.

Thanks for your help,

Sara Kenno

M.A.Sc. Candidate

Civil Engineering

University of Windsor

kenno2@uwindsor.ca

Dear Sara

Thank you for your Email of 12th January detailed below seeking permission to use material published in one of our journals within your M.A.Sc. Thesis. I am pleased to inform you that permission is granted.

Could you please ensure that a full reference is given:

Article: Mean Compressive Stresses - Experimental and Theoretical Investigations Into Their Influence on the Fatigue Strength of Welded Structures

Author(s): Rorup

Journal: The Journal of Strain Analysis for Engineering Design

Publisher: Professional Engineering Publishing

ISSN: 0309-3247

Issue: Volume 40, Number 7 / 2005

DOI: 10.1243/030932405X30902

Pages: 631-642

With kind regards

Peter

Peter Williams
Academic Director
Professional Engineering Publishing
1 Birdcage Walk
London SW1H 9JJ
UK
Registered in England No. 1103638

Tel: +44 (0) 207 304 6852

Fax: +44 (0) 207 304 6926

E-Mail: peterw@pepublishing.com

Web: www.pepublishing.com

PE Publishing can also be found on www.scitopia.org: Integrating Trusted Science + Technology Research.

Search through more than three million documents from the world's leading science and technology societies

Dear Sara

Thank you for your Email of 12th January detailed below seeking permission to use material published in one of our journals within your work on Residual Stresses of Ship Hull. I am pleased to inform you that permission is granted.

Could you please ensure that a full reference is given:

Article: Measurement of residual stresses in T-plate weldments
Author(s): Wimpory, May, O'Dowd, Webster, Smith, Kingston
Journal: The Journal of Strain Analysis for Engineering Design
Publisher: Professional Engineering Publishing
ISSN: 0309-3247
Issue: Volume 38, Number 4 / 2003
DOI: 10.1243/03093240360692931
Pages: 349-365

With kind regards

Peter

Peter Williams
Academic Director
Professional Engineering Publishing
1 Birdcage Walk
London SW1H 9JJ
UK
Registered in England No. 1103638

Tel: +44 (0) 207 304 6852
Fax: +44 (0) 207 304 6926
EMail: peterw@pepublishing.com
Web: www.pepublishing.com

PE Publishing can also be found on www.scitopia.org
<<http://www.scitopia.org/>> : Integrating Trusted Science + Technology
Research.

Search through more than three million documents from the world's
leading science and technology societies

References

ADINA R & D, I. (2008). *Automatic Dynamic Incremental Nonlinear Analysis*. Retrieved 2008, from The Finite Element System for Structures, Heat Transfer, and CFD: www.adina.com

Akhras, G., Gibson, S., Yang, S., & Morchat, R. (1998). Ultimate strength of a box girder simulating the hull of a ship. *Canadian Journal of Civil Engineering* , 25, 829-843.

ANSYS. (2008). *ANSYS*. Retrieved 2008, from www.ansys.com

ASTM. (2008). ASTM A370-08B. *American Society for Testing and Materials , Standard Test Methods and Definitions for Mechanical Testing of Steel Products* . West Conshohocken, PA, USA: ASTM International.

ASTM. (2007). ASTM A568 / A568M - 07a. *American Society for Testing and Materials , Standard Specification for Steel, Sheet, Carbon, Structural, and High-Strength, Low-Alloy, Hot-Rolled and Cold-Rolled, General Requirements for* . West Conshohocken, PA, USA: ASTM International.

ASTM. (2008). ASTM E 837-92. *American Society for Testing and Materials , Determining Residual Stresses by the Hole-Drilling Strain-Gage Method* . West Conshohocken: ASTM International.

ASTM. (2008). ASTM E837-08. *American Society for Testing and Materials , Standard Test Method for Determining Residual Stresses by the Hole-Drilling Strain-Gage Method* . West Conshohocken, PA, USA: ASTM International.

ASTM. (2008). ASTM E8M. *American Society for Testing and Materials , Standard Test Methods for Tension Testing of Metallic Materials* . West Conshohocken: ASTM International.

Ayala-Uraga, E., & Moan, T. (2007). Time-Variant Reliability Assessment of FPSO Hull Girder With Long Cracks. *Journal of Offshore Mechanics and Arctic Engineering* , 129, 81-89.

Canada, N. R. (2008, January 31). *The Canadian Neutron Beam Centre*. Retrieved January 2008, from www.neutron.nrc-cnrc.gc.ca

Cho, J. R., Lee, B. Y., Moon, Y. H., & Van Tyne, C. J. (2004). Investigation of residual stress and post weld heat treatment of multi-pass welds by finite element method and experiments. *Journal of Materials Processing Technology* , 155-156, 1690-1695.

CSA. (2004, February). General Requirements for Rolled or Welded Structural Quality Steel/Structural Quality Steel. *CSA G40.20-04 / CSA G40.21-04* . Canadian Standards Association.

Ganguly, S., Fitzpatrick, M. E., & Edwards, L. (2006). Use of neutron and synchrotron X-ray diffraction for evaluation of residual stresses in a 2024-T351 Aluminum alloy variable-polarity plasma-arc weld. *Metallurgical and Materials Transactions A (Physical Metallurgy and Materials Science)* , 37A, 411-420.

Gao, H., Guo, H., Blackburn, J. M., & Hendricks, R. W. (1997). Determination of residual stress by X-ray diffraction in HSLA-100 steel weldments. *Fifth International Conference on Residual Stress* (pp. 320-325). Linkoping, Sweden: Linkopings Universitet.

Gauthier, J., Krause, T. W., & Atherton, D. L. (1998). Measurement of residual stress in steel using the magnetic Barkhausen noise technique. *NDT&E International* , 31 (1), 23-31.

Holden, T. M., Powell, B. M., & Dolling, G. (1995). Neutron scattering facilities at Chalk River. *Neutron Scattering in Materials Science II Symposium* (pp. 7-12). Pittsburgh, PA, USA: Materials Research Society.

Holden, T. M., Suzuki, H., Carr, D. G., Ripley, M. I., & Clausen, B. (2006). Stress measurements in welds: Problem areas. *Materials Science and Engineering A* , 437, 33-37.

Hu, S. Z., & Jiang, L. (1998). A finite element simulation of the test procedure of stiffened panels. *Marine Structures* (11), 75-99.

Hutchings, M. T., Withers, P. J., Holden, T. M., & Lorentzen, T. (2005). *Introduction to the characterization of residual stress by neutron diffraction*. Boca Raton, FL, USA: Taylor & Francis Group.

International Organization for Standardization, G. S. (2001). Technology Trends Assessment. *Polycrystalline materials - Determination of residual stresses by neutron diffraction (ISO/TTA 3:2001, 1-48)*. Gaithersburg, Maryland, USA: Versailles Project on Advanced Materials and Standards, National Institute of Standards and Technology.

James, M. N., Webster, P. J., Hughes, D. J., Chen, Z., Ratel, N., Ting, S. -P., et al. (2006). Correlating weld process conditions, residual strain and stress, microstructure and mechanical properties for high strength steel - the role of neutron diffraction strain scanning. *Material Science and Engineering A*, 427, 16-26.

Krawitz, A. D. (2001). *Introduction to diffraction in materials science and engineering*. Toronto, Ontario, Canada: John Wiley & Sons Inc.

Lorentzen, T., & Ibsø, J. B. (1995). Neutron diffraction measurements of residual strains in offshore welds. *Materials Science and Engineering A*, A197, 209-214.

Paradowska, A., Finlayson, T. R., Price, J. W., Ibrahim, R., Steuwer, A., & Ripley, M. (2006). Investigation of reference samples for residual strain measurements in a welded specimen by neutron and synchrotron X-ray diffraction. *Physica B*, 385-386, 904-907.

Paradowska, A., Price, J. W., Ibrahim, R., Finlayson, T. R., Ripley, M., & Blevins, R. (2005). Residual stress evaluation in multi-beads steel weldments using neutron diffraction. *Proceedings of the IIW International Conference on Benefits of New Methods and Trends in Welding to Economy, Productivity and Quality*, (pp. 40-51). Prague, Czech Republic.

Pearce, S. V., & Linton, V. M. (2006). Neutron diffraction measurement of residual stress in high strength, highly restrained, thick section steel welds. *Physica B*, 385-386, 590-593.

- Price, J. W., Paradowska, A., Joshi, S., & Finlayson, T. (2006). Residual stresses measurement by neutron diffraction and theoretical estimation in a single weld bead. *International Journal of Pressure Vessels and Piping* , 83, 381-387.
- Prime, M. B., Sebring, R. J., Edwards, J. M., Hughes, D. J., & Webster, P. J. (2004). Laser surface-contouring and spline data-smoothing for residual stress measurement. *Experimental Mechanics* , 44 (2), 176-184.
- Rörup, J. (2005). Mean compressive stresses - Experimental and theoretical investigations into their influence on the fatigue strength of welded structures. *Journal of Strain Analysis for Engineering Design* , 40 (7), 631-642.
- Simulia. (2008). *Simulia*. Retrieved 2008, from www.simulia.com
- Somerville, W. L., Swan, J. W., & Clarke, J. D. (1977). Measurement of residual stresses and distortions in stiffened panels. *Journal of Strain Analysis* , 12 (2), 107-116.
- Sumi, Y., Mohri, M., & Kawamura, Y. (2004). Computational prediction of fatigue crack paths in ship structural details. *Fatigue and Fracture of Engineering Materials and Structures* , 28, 107-115.
- Totten, G., Howes, M., & Inoue, T. (2002). *Handbook of residual stress and deformation of steel*. Materials Park, OH: ASM International.
- Webster, G. A., & Wimpory, R. C. (2001). Non-destructive measurement of residual stress by neutron diffraction. *Journal of Materials Processing Technology* , 117, 395-399.
- Weng, C. C., & Lo, S. C. (1992). Measurement of residual stresses in welded steel joints using hole drilling method. (<http://www.ingentaconnect.com/content/maney/mst>, Ed.) *Materials Science and Technology* , 8, 213-218.
- Wilken, K. (1976). The measurement of residual stresses in welded ship structure and their effect on the strength of the structure. *International Conference of Structural Des and Fabr in Shipbuild. 1*, pp. 169-177. London, England: Weld Institute, Abington, Cambridge, England.

Wimpory, R. C., May, P. S., O'Dowd, N. P., Webster, G. A., Smith, D. J., & Kingston, E. (2003). Measurement of residual stresses in T-plate weldments. *Journal of Strain Analysis* , 38, 349-365.

Withers, P. J., & Bhadeshia, H. D. (2001). Residual Stress Part 2 - Nature and origins. *Materials Science and Technology* , 17, 366-375.

Vita Auctoris

Name: Sara Kenno

Place of Birth: Calgary, Alberta

Education: Honourable Vincent Massey Secondary School, Windsor, ON
1996 – 2002
University of Windsor, Windsor, ON
2003 – 2007, B.A.Sc.
University of Windsor, Windsor, ON
2007 – 2009, M.A.Sc.